Title
Targeting oncogenic K-Ras G12C and G13C via covalent drug design

Author
Nnadi, Chimno

Publication Date
2019

Peer reviewed|Thesis/dissertation

Targeting oncogenic K-Ras G12C and G13C via covalent drug design

by
Chimno Nnadi

DISSERTATION
Submitted in partial satisfaction of the requirements for degree of
DOCTOR OF PHILOSOPHY

in

Chemistry and Chemical Biology

in the

GRADUATE DIVISION
of the
UNIVERSITY OF CALIFORNIA, SAN FRANCISCO

Approved:

DocuSigned by:
Kevan Shokat
8FDF47C586EF40D...
Kevan Shokat
Chair

DocuSigned by:
Brian K. Shoichet
Brian K. Shoichet

DocuSigned by:
Jack Taunton
Jack Taunton

DocuSigned by:
Kevin Mark Shannon
6F9DD324E1BF466...
Kevin Mark Shannon

Committee Members

Acknowledgements

I would like to thank several influential members of the scientific community for which I would not have gotten this far. Kevan Shokat has been instrumental in the vision of this project and its realization. Brian Shoichet and Nir London have been wonderful collaborators over the years. I would also like to thank Kevin Shannon and Jack Taunton for their discussion and ideas. I have also received tremendous support from the members of the Shokat, Taunton, and Shoichet labs. Furthermore, I would like to thank my family who have supported me every step of the way. It takes a village.

Targeting oncogenic K-Ras G12C and G13C via covalent drug design

by

Chimno Nnadi

Abstract

Ras proteins are part of a large superfamily of small monomeric GTPases that act as molecular switches to regulate cell signaling. Dysfunctional Ras signaling is implicated in 30% of human cancers. Of the 3 protein isoforms, H-, K-, and N-Ras, K-Ras is the most commonly mutated, particularly at residues 12 and 13. K-Ras(G12C) and K-Ras(G13C) are acquired mutations in lung and colorectal cancer, which are among the most common and deadly malignancies worldwide. Furthermore, G12C and G13C are potentially druggable mutations that are close to the switch II pocket of K-Ras. Biochemical studies reveal that K-Ras(G13C) is a fast exchanging mutant, with a potentially destabilized nucleotide binding pocket, indicating that G13C is structurally different from G12C. Despite these differences, K-Ras(G12C) and K-Ras(G13C) are both amenable to covalent drug design via computational and empirical screening methods.

Table of contents

List of Figures

List of Tables

CHAPTER 1

Establishment of K-Ras as an important drug target

1.0 Gloss

Oncogene specificity represents the future of cancer therapy. Targeted drug development rests on the belief that, since cancer cells are very similar to self, promiscuous chemotherapy agents have a narrow therapeutic window and therefore selectivity is paramount to achieving cures. Moreover, certain classes of cancer are resilient to some targeted therapies that are upstream or downstream of the cellular signaling pathway. For example, many K-Ras-driven cancers are resistant to treatment with EGFR inhibitors such as cetuximab. Also, despite the availability of clinically approved inhibitors of RAF and MEK, which are immediately downstream of Ras, these agents are ineffective on Ras-driven cancers. Efficacious chemotherapy regimens rely on determining the oncogenic driver through genetic sequencing and treating the patients for the identified target.

For acquired cysteine mutations in cancer, covalent inhibitors are an effective strategy to achieve oncogene specificity. Cysteine is the most nucleophilic amino acid, rendering it amenable to covalent labeling by electrophilic warheads. These cysteine-selective warheads can allow the small molecule a long residence time within a nearby binding pocket and render the protein target inactive until it is cellularly recycled. Also because cysteine is a rare amino acid with a prevalence of 1.36%, electrophilic warheads lead to more selective targeting.

1.1 Introduction to Ras biology

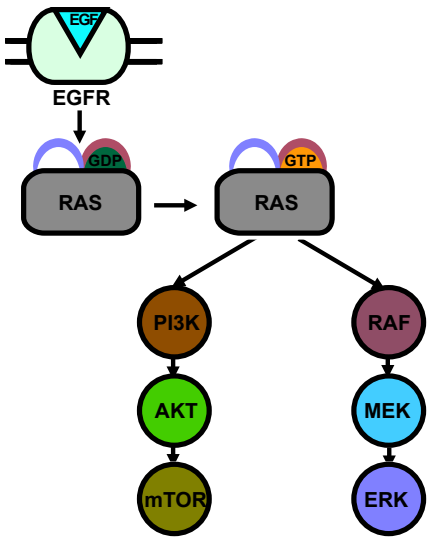

Figure 1.1: Schematic of Ras signaling pathway

Ras proteins are part of a large superfamily of small monomeric GTPases (20-25 kDa) that act as a molecular switch to regulate cell growth and proliferation. Ras is activated in response to growth factors binding to the receptor tyrosine kinases, stimulating the autophosphorylation of tyrosine residues on that receptor which bind to the adaptor protein GRB2 to recruit SOS to activate Ras. Anchored by a lipid tail to the cellular membrane, Ras cycles between an inactive GDP-bound state, and an active GTP-bound state, in response to the cellular environment. Ras activation is positively regulated by Son of Sevenless (SOS) and negatively regulated by GTPase-activating protein (GAP), with a key role being played by the 10:1 GTP:GDP nucleotide ratio within the cell. Ras signaling is dysregulated in 30% of human cancers[1], rendering it the most common oncogenic driver.

Ras is a small globular protein and consists of a core G domain and a flexible C-terminal tail that is farnesylated or geranylgeranylated and anchored to the cellular membrane. Its G

domain consists of several B-folds connected by a flexible P loop (residues 10-17) and two flexible switch I- (residues 30-40) and II loops (residues 60-76) that reside above the nucleotide binding pocket and the allosteric switch II pocket.

Of the 3 protein isoforms, H-, K-, and N-Ras, of which are near identical at the G domain, K-Ras is the most frequently mutated, particularly at residues 12 and 13[1,2]. Mutations at either codon 12 or 13 are canonically considered to prevent productive alignment of the GAP arginine finger, which completes the Ras active site[3]. Although these codon 12 and 13 mutations appear biochemically similar in their constitutive activation of Ras, several biochemical studies have shown unexpected differences between mutants, leading to allelic variation in K-Ras driven tumors[4,5]. To date, no biochemical studies have identified what distinguishes G12C from G13C.

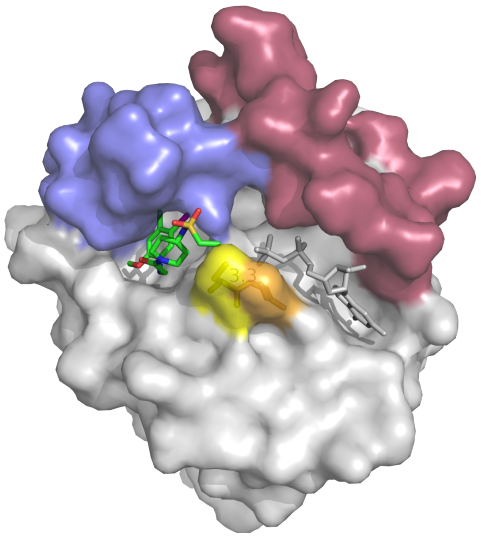

Figure 1.2: Crystal structure of K-Ras G12C GDP with switch II pocket inhibitor (green). The distance between G12C (yellow) and G13C (orange) is 3.3 angstroms.

1.2 G12C oncogene is a necessary proof of principle that Ras can be targeted

K-Ras(G12C) is a TGG→ TGT transversion mutation that resides on the flexible p-loop of Ras. K-Ras(G12C) occurs in 40% of lung adenocarcinoma, making it a highly important target. Despite the lack of biochemical data, selective targeting of K-Ras(G12C) has been achieved, driving more interest in the biochemical characterization of this oncogene. Ostrem and Peters demonstrated that K-Ras(G12C) can react irreversibly with covalent ligands that bind to a transient pocket under the switch-II loop[6] and developed G12C inhibitors using fragment-based disulfide tethering[7].

Through characterization of these early generation switch II pocket inhibitors, it was discovered that G12C still participates in nucleotide cycling. Therefore, although the switch II pocket inhibitors bind preferentially to the GDP-bound state, they disrupt nucleotide cycling and sequester Ras in the inactive state until it is targeted for degradation. It was shown that K-Ras mutants such as K-Ras(G12C) can be inhibited by an allosteric trapping mechanism in order to kill patient derived K-Ras(G12C) lung adenocarcinoma cells[6,8-10]. Since then, Wellspring Biosciences has optimized switch II pocket inhibitors (ARS-1620) that can selectively target K-Ras(G12C) within the cysteinome and shrink K-Ras(G12C) patient-derived xenografts in mice[10]. Furthermore, Amgen has developed small molecules that, in phase I clinical trials, have halted tumor progression for patients with K-Ras(G12C)-driven non-small cell lung cancer[11]. Therefore, the first K-Ras inhibitors are being used to treat patients, rendering the previously "undruggable" target druggable and proving the principle that targeting Ras is instrumental as therapy for Ras-driven cancers.

1.3 G13C is an unexplored cancer target

K-Ras(G13C) is an acquired cancer mutation that was highlighted in a 2015 review by Arkin and Dansen as a feasible yet unexplored target[12]. K-Ras(G13C) is a similarly situated TGG→ TGT transversion mutation that occurs in cancer patients, that is just one amino acid away from glycine 12. The cysteine residue is surface exposed, and resides on the p-loop nearer the nucleotide binding pocket. The authors speculated that preexisting inhibitors of K-Ras(G12C) could be modified into G13C inhibitors.

K-Ras(G13C) is an acquired mutation in lung and colorectal cancer[13], which are among the most common and deadly malignancies worldwide. Every year about 100 patients in the U.S. and 1,300 worldwide die of K-Ras(G13C)-driven metastatic colorectal cancer[1]. The G13C mutation in N-Ras drives myeloid disorders such as acute myeloid leukemia (AML) and myelodysplastic syndrome[13]. Prevalence studies in the United States in 2011 suggest that there are presently 4000 colorectal cancer patients, 2000 patients with non-small cell lung cancer, and 200 patients with AML who would benefit from a potent Ras(G13C) inhibitor[14-17]**.** The design of covalent G13C inhibitors is critical for addressing the current lack of therapy for these patients. K-Ras(G13C) could be amenable to allosteric inhibition utilizing high throughput screening methods such as covalent docking, disulfide tethering, and mass spectrometry based electrophile inhibition.

There has been very little biochemical characterization of the G13C mutation to explain its differential oncogenicity and clinical phenotype to similar transforming mutations like G12C[18]. To date, there are no crystal structures of the G13C mutant to characterize this

oncogene. Modeling G13C into Ras presupposes that the cysteine rotamer is tilted from the switch II pocket, like its G12C predecessor. Comparing K-Ras(G12C) and K-Ras(G13D) shows that residue 13 is connected to the nucleotide binding pocket via a hydrogen bonding network, which could be partially disrupted by the mutation to a bulkier mutant residue. Biochemical data of G13D indicates that the codon 13 mutations may render these oncogenes as fast exchangers[5]. Like with G12C, studying the biochemical basis of the oncogenicity of G13C may be instrumental in understanding its druggability.

1.4 Optimization of covalent drug design

The design of covalent inhibitors for known drug targets remains a difficult task. To avoid hyper-reactive compounds, most high throughput screens (HTS) cautiously remove any covalent compounds, barring canonical HTS as a screening method. Disulfide-tethering has been successful for initial development and proof of principle of G12C inhibitors but requires multiple rounds of structure-activity-relationships to achieve a selective carbon-based electrophile from the tethered fragment. Carbon-based electrophile libraries are usually small in size and difficult to compare in terms of reactivity to various targets. With the advent of in silico drug screening, covalent docking is furthermore also untested as an approach against difficult drug targets such as Ras. Most of the work described in the manuscript utilizes a medium-throughput mass spectrometry based method to screen and validate selective inhibitors for Ras.

1.5 Research significance

Through the research shown in this thesis, covalent docking is applied to the traditionally undruggable target Ras and is described as a new method to find a different class of Ras binders. The vast structural and chemical data was utilized on G12C to predict new binders of the switch II pocket (S-IIP) using covalent docking[14,15,17,18]. Millions of commercially available compounds were used to dock acrylamide fragments to K-Ras(G12C). From this data arose a docking predicted class of G12C binders that accelerate nucleotide exchange. These small molecules are predicted covalent docking binders that destabilize Ras upon binding, achieving nucleotide exchange via fluorescence-based methods. These binders label G12C with favorable potency and selectivity. These results prove that DOCKovalent is an appropriate strategy to develop covalent inhibitors for canonically undruggable targets such as small GTPases.

CHAPTER 2

Novel K-Ras G12C Switch-II Covalent Binders Destabilize Ras and Accelerate Nucleotide Exchange

2.0 Gloss

The success of targeted covalent inhibitors in the global pharmaceutical industry has led to a resurgence of covalent drug discovery. However, covalent inhibitor design for flexible binding sites remains a difficult task due to lack of methodological development. To avoid hyper-reactive compounds, most high throughput screens (HTS) cautiously remove any covalent compounds, barring HTS as a screening method. DOCKovalent is a novel *in silico* screening method, available through the DOCK3.7 branch of the well-tested software DOCK, that allows facile screening of covalent compounds to any target of interest with a reactive cysteine.

In the current decade, a series of small molecule inhibitors of K-Ras(G12C) have been designed to bind to a transient pocket under the switch II loop of K-Ras(G12C) called the switch II pocket (S-IIP). Using these K-Ras(G12C) inhibitors, we have learned that K-Ras mutants, such as K-Ras(G12C), can still cycle through inactive GDP bound state and can be actively inhibited by an allosteric trapping mechanism in order to kill patient derived K-Ras(G12C) lung adenocarcinoma cells. This immense structural and chemical data can be utilized to predict new inhibitors of K-Ras(G12C) using covalent docking. Here, we tested DOCKovalent's ability to target a traditionally undruggable protein, such as K-Ras, that have been intractable to chemical inhibition for decades.

We drew from millions of commercially available compounds to dock acrylamide fragments to K-Ras(G12C) and utilized our laboratory's intimate structural knowledge of the S-IIP to validate results from covalent docking on K-Ras(G12C) Here, we compared covalent docking to empirical electrophile screening, against the highly dynamic target K-Ras(G12C).

While the overall hit-rate of both methods was comparable, we were able to rapidly progress a docking hit to a potent irreversible covalent inhibitor that modifies the inactive, GDP-bound state of K-Ras(G12C). Hydrogen-deuterium exchange mass spectrometry was used to probe the protein dynamics of compound binding to the switch-II pocket and subsequent destabilization of the nucleotide-binding region. SOS-mediated nucleotide exchange assays showed that, contrary to prior switch-II pocket inhibitors, these compounds appear to accelerate nucleotide exchange. This study highlights the efficiency of covalent docking as a tool for the discovery of chemically novel hits against challenging targets. Upon developing covalent docking with K-Ras (G12C), the methodology can be extended to G13C, an understudied mutant with an unmet clinical need.

2.1 Introduction

Covalent drugs have long been part of the pharmaceutical medicine, from inadvertent ones like the P2Y12 drugs to beta-lactams to fosfomycin to aspirin[19]. Despite this, covalent inhibitors were specifically avoided by the pharmaceutical industry until recently, due to concerns of off-target toxicity.[20,21] The recent approval of afatinib, ibrutinib, and osimertinib, which target non-conserved cysteines in the ATP binding site of kinases, has accelerated interest in covalent drug discovery. These irreversible kinase inhibitors were developed using potent reversible ATP binding-site ligands as a starting scaffold, which are then endowed with an acrylamide-based electrophile (“warhead”). This approach allows the use of a mild electrophile, while relying on the potent reversible binding affinity of the inhibitor to “present” the warhead to the active site cysteine.[22]

A much more challenging target is exemplified by K-Ras which has no high affinity reversible ligands except the endogenous GDP/GTP nucleotides (K_D ~ pM).[23] K-Ras is a small G protein that acts as molecular switch to activate mitogenic signaling pathways in the presence of growth factors. Somatic *KRAS* mutations, including G12C induce resistance to GTPase activating proteins (GAPs) and impair intrinsic GTP hydrolysis. This results in constitutively elevated levels of K-Ras-GTP and leading to aberrant cell growth. Approximately 25% of lung adenocarcinomas harbor *KRAS* mutations, including 40% that result in G12C substitutions. In order to discover the first K-Ras(G12C) allosteric inhibitor, a fragment-based tethering screen was used.[6] Tethering is carried out with reversible covalent disulfides to identify thermodynamically favorable interactions with the protein target. Covalent bond formation in this screen can be attenuated with a stringency factor (usually by adjusting the levels of 2-mercaptoethanol).[7] Following hit discovery, further medicinal chemistry is required to convert disulfide hits from the screen to carbon-based electrophiles that are compatible with the cellular environment. This conversion can be challenging.

The optimization of the K-Ras(G12C) irreversible ligands has yielded two important insights: (1) The determination of multiple co-crystal structures revealed a highly flexible ligand binding pocket (termed switch-II pocket; S-IIP) beneath the switch-II loop; and, (2) even the best irreversible inhibitors show only weak (>200μM) binding in the absence of the warhead.[6,8-10] These findings were initially thought to limit the druggability of K-Ras(G12C). Recently however, potent on-target inhibition of K-Ras(G12C) has been validated extensively. [6,8-10] These molecules allosterically trap K-Ras(G12C) in the inactive GDP-bound state by preventing SOS-mediated nucleotide exchange. Covalent inhibition by modification of G12C allows oncogene specific

inhibition, sparing the wild-type protein from inhibition, which is predicted to contribute to the ultimate therapeutic index in patients.

Recognizing the growing importance of covalent drug discovery and the unique features of flexible protein targets like K-Ras(G12C), we set out to compare one empirical screening approach and a virtual screening approach to discovering new K-Ras(G12C) binders. There is little information on how covalent electrophile libraries fare in comparison to other screening approaches.[24] We tested a fragment-based acrylamide library using mass spectrometry in conjunction with covalent virtual screening via DOCKovalent, a structure-based virtual screening algorithm that predicts covalent ligand binding to a target receptor.[25,26] Unlike disulfide tethering, the latter two approaches directly screen compounds containing the reactive warheads (e.g. acrylamides) for optimal ligand-receptor geometry, thereby simplifying downstream medicinal chemistry.

Simulating protein flexibility is a major challenge for molecular docking.[27] K-Ras is a highly dynamic target. Many of the available 24 inhibitor-bound K-Ras(G12C) crystal structures that were available at the start of this study showed altered pocket topology due to switch-II loop flexibility and induced fit around structurally diverse ligands. Accounting for flexibility is a challenge in docking and many methods have been explored in the literature.[28-36] However, these methods can often reduce predictive success by increasing false positives, demonstrated in retrospective calculations that confirm the loss of enrichment of known ligands over decoys.[37-42] Here, we utilize the enrichment of a known ligand as the selection criteria for picking the best receptor structure for molecular docking.

Previously, DOCKovalent was used to discover *reversible* covalent inhibitors. This is the first prospective study using DOCKovalent to find *irreversible* inhibitors of a target, specifically K-Ras(G12C). We show that covalent docking is comparable to screening a small library of electrophilic fragments in terms of hit rate and off-target reactivity. We find that covalent docking in combination with orthogonal biophysical methods such as thermal stability assays and hydrogen-deuterium exchange mass spectrometry can successfully identify novel irreversible compounds with favorable potency and specificity for K-Ras(G12C). Furthermore, covalent docking produced compounds that are structurally diverse and which exert dramatically different biochemical effects from compounds discovered using disulfide tethering approaches previously applied to the same target.

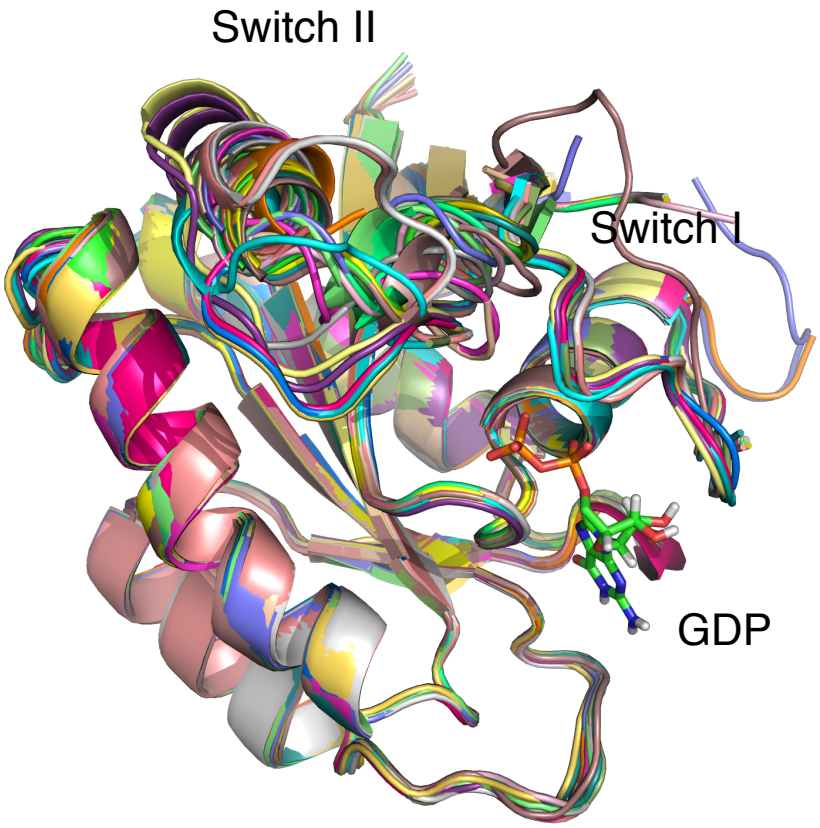

Figure 2.2.1. Structural alignment of 24 ligand-bound monomers of K-Ras(G12C). The PDB IDs for the individual structures can be found in Table 2.10.1.

2.2 Docking guided template selection

Structures of twenty-four distinct monomers of K-Ras(G12C) in complex with a covalent compound were available for docking (**Table 2.10.1**). Superimposing all of the different structures illustrates the significant flexibility of the switch II region and the caveats of docking to a static structure (**Figure 2.2.1**).

In order to select a suitable structure for the docking screen, we first attempted to computationally recapitulate the previous empirical tethering screen results from Ostrem *et al.*[6] The original tethering library of 480 compounds has since doubled in size. We covalently docked this library of 960 disulfide containing compounds as a more stringent test for enriching known binders. We identified the best candidate for docking (PDB: 4M1S chain B) as the structure that enriches for compound 6H05, the best reported K-Ras(G12C) tethering hit (94 ± 1% modification of K-Ras(G12C)**, Figure 2.2.2**). Compound 6H05 ranked 15/960 for this structure (top 1.5%). The docking pose placed the *p*-chloro-benzene in the hydrophobic region of S-IIP (Figure **2.2.2b**) as observed in the co-crystal structure of a 6H05-analogue in complex with K- Ras(G12C) (PDB: 4LUC).

We then used 4M1S chain B to dock a test set of 110 previously synthesized vinylsulfonamide-based compounds in structure-activity relationship (SAR) efforts to find more potent S-IIP binders. Vinylsulfonamide 13, the crystallographic ligand in 4M1S, ranked 4 out of this library, closely recapitulating the crystallographic binding mode (1.35Å r.m.s.d.; **Figure 2.2.2c-d**). These results in which both disulfide hits and carbon based electrophiles were

correctly selected by the program encouraged us to use 4M1S chain B for a large-scale virtual screen against K-Ras(G12C).

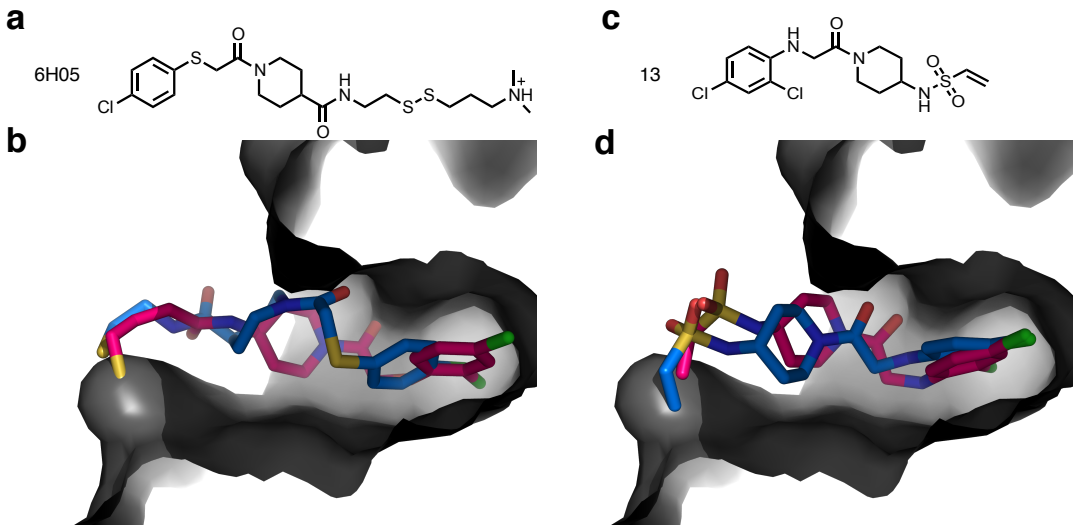

Figure 2.2.2. Docking pose of disulfide tethering hit, 6H05 a. Structure of disulfide tethering hit, 6H05. **b.** Docking pose of 6H05 (blue) in docking model (PDB: 4M1S chain B) aligned to co-crystal structure of tethering analogue (magenta) (PDB: 4LUC). **c.** Structure of ligand 13. **d.** Docking pose of 13 (blue) aligned to co-crystal structure of 13 (magenta; PDB: 4M1S chain B).

2.3 Covalent library design and docking

Prior efforts to generate K-Ras(G12C)compounds have relied on disulfide-tethering as a starting point to generate the high affinity reversible binding element.[6,7] However, conversion of a disulfide to a carbon-based electrophile requires iterative optimization of electrophile geometry and linker length to successfully engage the target cysteine. DOCKovalent directly screens carbon electrophiles and, in doing so, optimizes ligand orientation and electrophile position.

In addition to electrophile orientation, the tuning of electrophile reactivity also represents a challenge to the design of covalent inhibitors.[43] Overly reactive electrophiles may have promiscuous off-target effects, while non-reactive electrophiles may not be able to form a covalent bond with the target. Unsubstituted acrylamides are found in clinically approved agents and are considered mild electrophiles that react with nucleophilic cysteines when receptor and ligand geometry is optimized.[44]

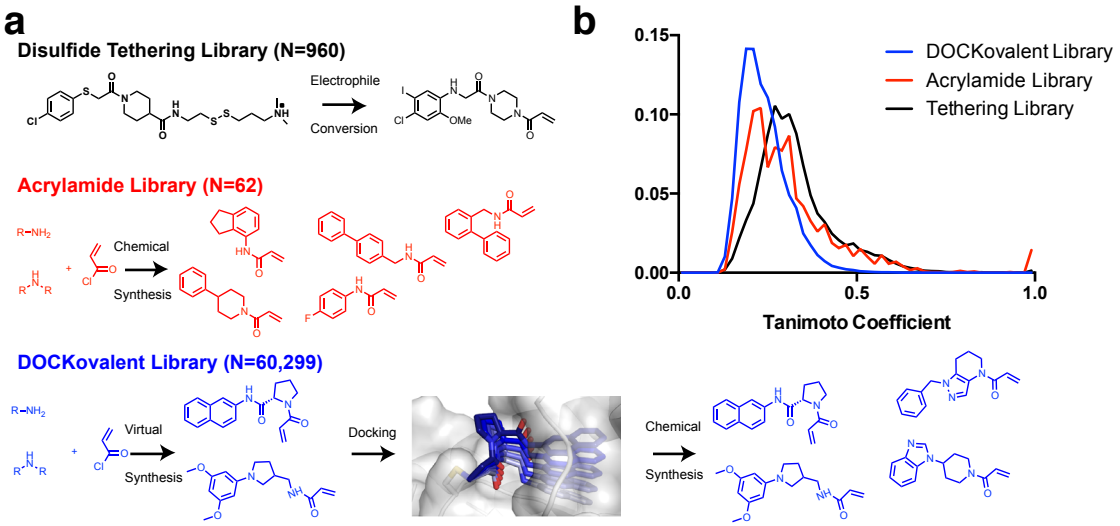

Figure 2.3. Analysis of ligand diversity in DOCKovalent and empirical screening libraries a. Summary of screening methods for covalent ligand discovery. **b**. Pairwise Tanimoto scores for each library were generated using ECFP4 fingerprints and clustered into a 50-bin histogram**.**

To computationally explore a diverse set of acrylamides, we constructed two virtual libraries based on fragment-like (xLogP <= 3.5, Molecular Weight <= 250, Number of rotatable bonds <= 5) primary (N=28,350) and secondary (N=31,949) aliphatic amines (**Figure 2.3a**).[45] Pairwise Tanimoto scores for all the compounds in the DOCKovalent virtual library, the acrylamide physical library and the disulfide-tethering library showed increased ligand diversity in the covalent docking library (**Figure 2.3b**). Acrylamides were generated *in silico* from the amine building blocks. The ligands' conformations, stereoisomers, and protonation states were then pre-computed to allow for rapid docking.

In K-Ras(G12C)crystal structures, cysteine 12 usually samples two favored rotamers: (1) facing the nucleotide binding site, often seen in apo structures; and, (2) towards the switch-II pocket observed in ligand-bound G12C structures. These rotamers have been observed in structures with different space groups and unit cell dimensions, suggesting that they are not

predetermined by crystallographic conditions. Using DOCKovalent 3.6[25], we docked the two libraries to both putative rotamers of cysteine 12 (χ1=-169.9°, -69.8°) in 4M1S chain B. The top 500 compounds (top 1.5% of each library) from each screen were manually inspected and filtered for criteria that are not assessed by the docking energy function such as internal ligand strain, unlikely protonation states, correct representation of the ligand in the docking pose, and synthetic accessibility and commercial availability of the amine-based building blocks.

2.4 Docking and empirical screening show similar hit rates

Twenty-nine compounds from the covalent docking library were selected, synthesized and experimentally tested against Cys-light K-Ras(G12C) (a truncated construct, residues 1-169, that contains only a single cysteine at position 12). For the empirical screening set, we screened an acrylamide subset

Table 2.4.2. Results of mass-spectrometry based screen of acrylamide library and DOCKovalent library.

	Electrophile Library	DOCK-ovalent
Library Size	94	60,299
MW	150-300	<300
Assayed	63	29
Hits	9	2
Nonspecific Hits	7	1
Nonspecific compounds	22	7

(N=62) of a carbon electrophile library (**Table S2-3**). To assess off-target reactivity, we also tested compound engagement to full length K-Ras(WT) 1-189, which contains additional cysteines including a flexible C-terminal C185. Overall, the two libraries showed comparable hit rates (7-15%) and reactivity profile (**Table 2.4.2**). The electrophile library contained more promiscuous acrylamides overall than the docking library (**Table 2.4.2**). We highlight two examples of acrylamide hits 1-4 from each library that are moderately reactive to both G12C and the control, K-Ras(WT)1-189 (**Figure 2.4.1a-b**).

We chose to pursue acrylamide 1 from the covalent docking library based on its high reactivity to K-Ras(G12C) (**Figure 2.4.1a-b**), its novelty compared to known K-Ras(G12C)binders[6], and the chemical tractability of its scaffold. The proline linker offers only a few rotatable bonds, which may sample a few conformationally constrained orientations to produce the final binding pose in which, the linker rigidly inserts the naphthalene into the hydrophobic S-IIP (**Figure 2.4.1c)**. Analysis of the docking poses of the binders revealed that only compound 1 showed the potential for hydrogen bond formation, specifically to R67. We also investigated the potential binding pose of compound 1 using DOCK3.6 (reversible docking), which does not constrain the covalent bond. The pose produced by DOCK3.6 recapitulates the DOCKovalent pose with only a slight rotation of the electrophile amide bond (**Figure 2.4.2**).

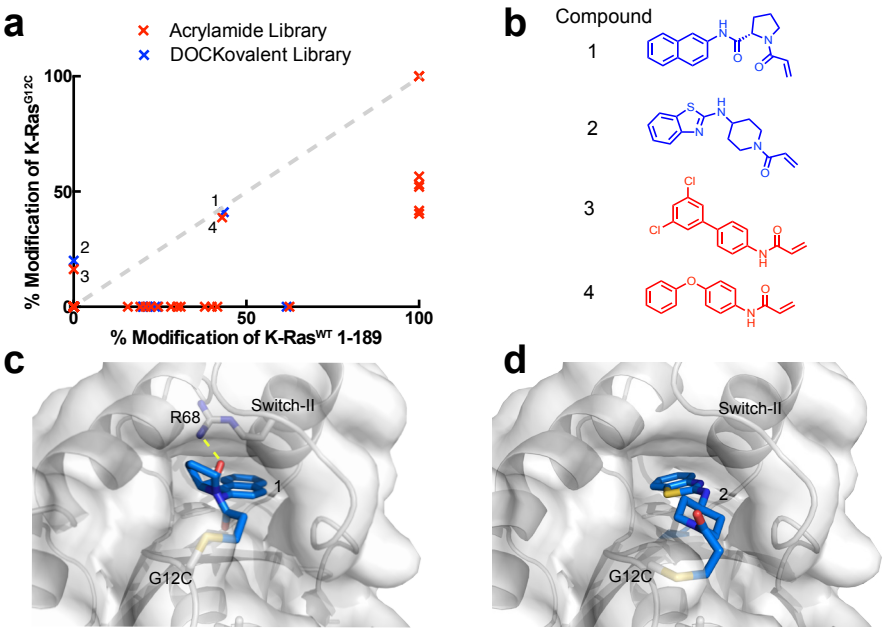

Figure 2.4.1. Docking results and poses a. The percent modification of K-Ras(WT) 1-189 *vs* Cys-light K-Ras(G12C)1-169 by compounds in the docking library (blue) or the empirical library (red) **b.** Potential hits from each library. **c.** DOCKovalent pose of compound **1** and **d.** compound **2** bound to K-Ras(G12C).

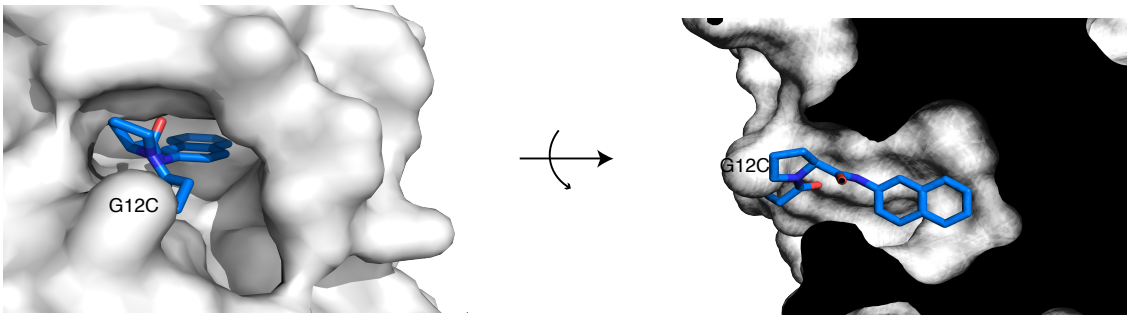

Figure 2.4.2 Surface representation of K-Ras(G12C) with the docking pose of compound 1 depicting the interior of the S-IIP.

Table 2.5. Compound 1 analogue structure-activity-relationship. Percentages represent adduct formation to Cys-light K-Ras(G12C) 1-169 or K-Ras(G12C) 1-189 with 200uM compound after 24h, 25°C by mass spectrometry. Percentages are an average of three experiments.

Compound		K-Ras^{G12C} 1-169	K-Ras^{WT} 1-189
1	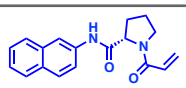	**34%** [+/-2]	**41%** [+/-1]
5	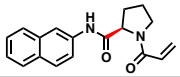	**0%** [+/-0]	**51%** [+/-2]
6	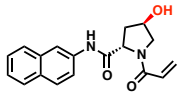	**65%** [+/-3]	**66%** [+/-1]
7	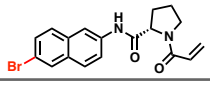	**85%** [+/-1]	**38%** [+/-3]
8	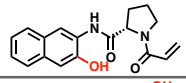	**43%** [+/-7]	**29%** [+/-2]
9	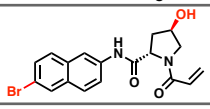	**100%** [+/-0]	**57%** [+/-1]

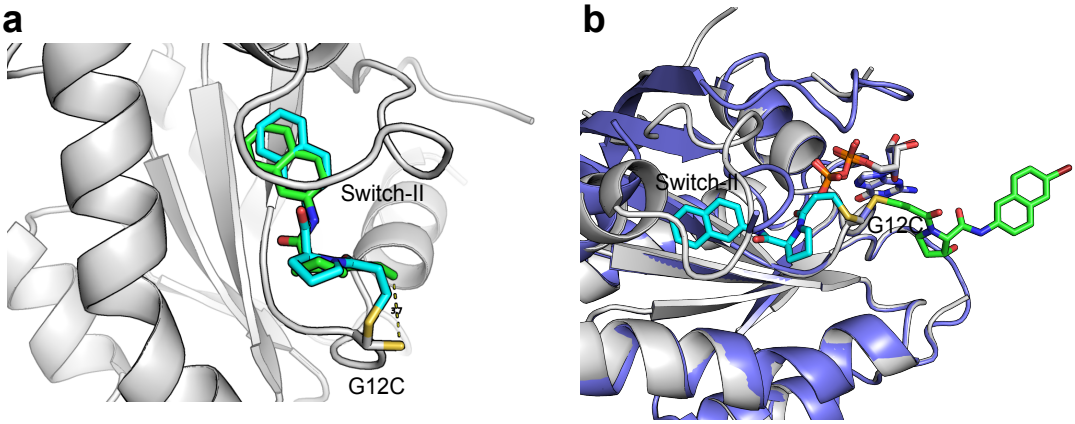

Figure 2.5.1. **DOCK and DOCKovalent poses are not recapitulated in crystallographic pose a.** DOCK pose (green) and DOCKovalent pose (cyan) of compound 1 overlay closely with only a slight rotation of the amide bond in the pyrrolidine-2-carboxamide linker. **b.** Alignment of DOCKovalent pose of compound 1 (cyan; protein in slate) to crystal structure of K-Ras(G12C) (white; PDB: 6ARK) in complex with compound 10 (green).

2.5 Docking hit could be optimized to a selective, potent, binder

We used the docking model in combination with commercially available building blocks to expedite compound optimization (**Table 2.5**). By contrast, previous efforts starting with a disulfide tethering hit required extensive medicinal chemistry to convert the disulfide fragments to acrylamides[6]. In addition to reacting to the G12C residue, acrylamide 1 exhibited nonspecific labeling of the C-terminal cysteine of K-Ras(WT) (**Table 2.5**) which was a feature important to address during the chemical optimization of the scaffold. The docking model (**Figure 2.5.1**) suggested that hydrophobic substitutions around the naphthalene moiety might be tolerated. Indeed, the testing of a series of substitutions led to the discovery of 6-bromo-naphthalene modification with improved labeling of 85% (200uM; 24h; 25°C). Structure-activity-relationship analysis of acrylamide 1 also suggested that alterations to the proline linker fine-tuned acrylamide specificity and compound affinity (**Table 2.5**). For example, substitution of D-proline for the L-proline abrogated G12C-specific reactivity but maintained comparable labeling to the wild type K-Ras. Additional modification of the proline linker to *cis*-3-hydroxy-L-proline led to the most potent acrylamide 10 (**Figure 2.5.2a**). The proline modification substantially improved the potency of 10, which was able to reach 78% labeling at 25uM (**Figure 2.5.2b**). Compound 10 also does not rely on the binding affinity of a chemically reactive phenol from the early generation G12C inhibitors, which represents an improvement in the druglikeness of the chemical scaffold.[6,8]

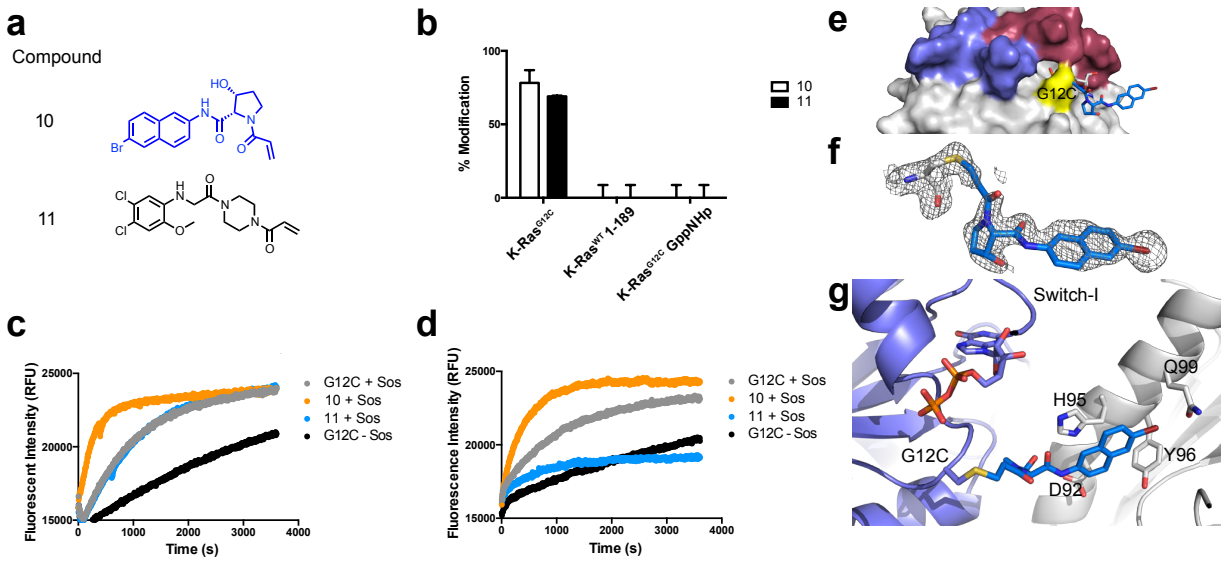

Figure 2.5.2. Compound 10 destabilizes K-Ras(G12C) a. Structures of compound 10 and switch-II inhibitor 11. **b.** Percentages represent adduct formation to K-Ras constructs with 25uM compound over 24h, 25°C. Sos-catalyzed exchange of apo and compound-labeled K-Ras(G12C) GDP with **c.** BODIPY-FL-GDP and **d.** BODIPY-FL-GTP fluorescence intensity was monitored over time. **e.** Co-crystal structure of 10 (blue) and K-Ras(G12C) GDP (grey). **f.** Fo-Fc omit map (grey mesh, 2.0σ) of 10. **g.** Cartoon representation of p-loop (slate), Cys12, and 10 (blue) with indicated residues that make hydrophobic contacts with 10 in nearby symmetry mate (white).

This compound only labels G12C in the GDP-bound state and does not label endogenous cysteines in the full K-Ras4B construct (**Figure 2.5.2b**). Compound 10 does not react with the active state of Ras, as indicated by the lack of binding to K-Ras(G12C) GppNHp. This is comparable to results using a previously reported switch II inhibitor, compound 11 (**Figure 2.5.2a**), that was discovered through tethering.

2.6 New compound accelerates nucleotide exchange

We examined the effect of these compounds on the nucleotide exchange rate of K-Ras *in vitro* using a fluorescence nucleotide exchange assay. SOS-catalyzed exchange of BODIPY-GDP and BODIPY-GTP in K-Ras(G12C) GDP constructs showed increased exchange of both fluorescent nucleotides in the presence of compound 10 but not with 11 (**Figure 2.5.2c-d**). Acrylamide inhibitors of K-Ras(G12C) have previously exhibited favored GDP binding due to strong steric clash with the γ-phosphate of GTP as well as disrupting key side chain interactions that interact with the terminal phosphate.[6,8] The mass spectrometry experiments show that compound 10 prefers to bind inactive K-Ras(G12C)as well. After binding G12C, compound 10 may destabilize the switch I region or phosphate loop and cause increased nucleotide cycling.

2.7 Structural determination of K-Ras(G12C) in complex with compound 10

We attempted to crystallize Cys-light K-Ras(G12C) bound to compound 10 using various methods including co-crystallization, soaking, and seeding using pre-formed crystals from a

different S-IIP inhibitor. Co-crystallization experiments were successful, and we determined a 1.75Å co-crystal structure of K-Ras(G12C) covalently bound to compound 10 (PDB: 6ARK). Crystallographic evidence reaffirms that the molecule is bound to G12C and suggests that the ligand interaction to the protein is weak (**Figure 2.5.2e-g**). Well defined electron density confirmed compound 10 covalently bound to G12C, however it did not occupy the switch II pocket in the crystal structure but rather was making nearby van der Waals interactions with the α2 (switch-II) helix of a nearby symmetry mate (**Figure 2.5.2f**; *Fo-Fc* at 2.0σ). This characteristic is not unique to compound 10, as other early stage switch II binders were crystallized with binding poses outside the ligand-binding site. It is unlikely that the crystallographic pose represents the in-solution binding pose. The crystallographic pose may, however, indicate that 10 is not stable in the S-IIP site following the formation of the covalent bond to G12C.

2.8 Compound binding destabilizes K-Ras

In order to assay the protein dynamics of K-Ras bound to compounds 10 and 11, we utilized hydrogen-deuterium exchange mass spectrometry (HDX-MS; **Figure 2.8**). HDX-MS is a technique that measures the exchange rate of amide hydrogens with deuterated solvent, and since the main determinant of amide exchange is their involvement in secondary structure, it is an excellent probe of protein dynamics.[46,47] Experiments were carried out for five time points of H/D exchange (0.3, 3, 30, 300, and 3000 s) in deuterated buffer at pH 7.5. HDX-MS data of K-

Ras(G12C) bound to GDP were consistent with previously published reports, confirming the flexibility of both the switch I and switch II loops.[48]

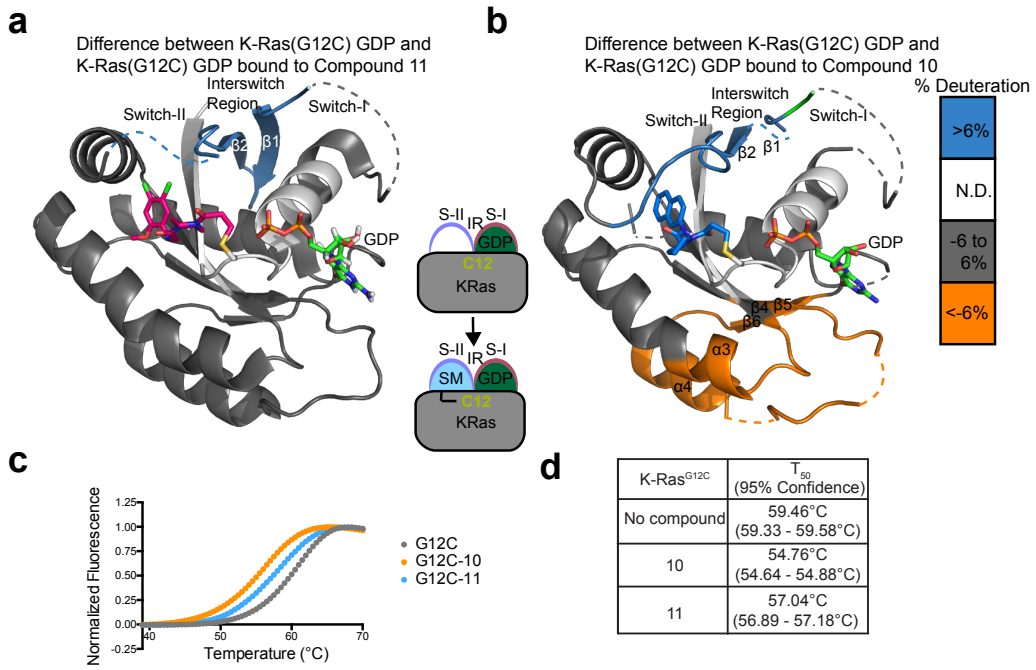

K-Ras^{G12C}	T_{50} (95% Confidence)
No compound	59.46°C (59.33 - 59.58°C)
10	54.76°C (54.64 - 54.88°C)
11	57.04°C (56.89 - 57.18°C)

Figure 2.8.1. Hydrogen-deuterium exchange on compound 10-bound K-Ras(G12C) a. Relative hydrogen-deuterium exchange differences between compound 11-bound K-Ras(G12C) GDP and apo K-Ras(G12C) GDP represented on co-crystal structure with compound 11 (PDB 4M21). Dashed lines represent disordered regions **b.** Hydrogen-deuterium exchange differences between compound 10-bound K-Ras(G12C) GDP and apo K-Ras(G12C) GDP represented on the docking pose **c.** Thermal stability assay on K-Ras(G12C) with compounds 10 and 11 and **d.** the T_{50} melting temperatures.

a

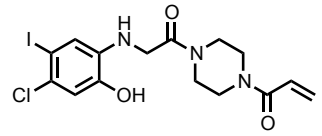

b

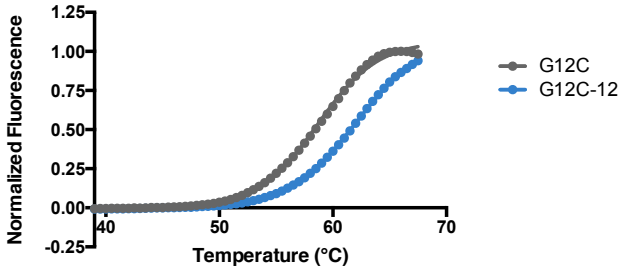

c

K-Ras^{G12C}	T_{50} (95% Confidence)
12	62.09°C (62.01 - 62.17°C)

Figure 2.8.2. Thermal stability assay on compound 12 a. Structure of compound 12. **b.** Thermal stability assay of K-Ras(G12C) labeled with compound 12 and **c.** the T_{50} melting temperature.

Numerous changes in H/D exchange were observed when comparing KRas(G12C) GDP in the presence and absence of compounds 10 or 11. Compound 11 is a confirmed switch II-binder (PDB: 4M21), and showed decreased exchange in the interswitch region (IR) composed of β2 and β3 as well as the switch II region (**Figure 2.8.1**). Comparatively, 10 also showed decreases in exchange in the IR and switch II regions, and increased exchange of the α3 and α4 helices.

To assess whether compound binding to K-Ras was in a favorable conformation after covalent bond formation, we used a thermal stability assay which measures the thermal shift associated with compound binding. Recent studies have demonstrated that compound stabilization correlates with increased potency.[49] For example, compound 12 in Ostrem *et al.* showed marked improvement in labeling of G12C (100% labeling using 10uM compound)[6] and also thermal stabilization of K-Ras(G12C) by 4°C (**Figure 2.8.2**). Compounds 10 and 11 induce 4.7 and 2.4°C destabilization of K-Ras respectively (**Figure 2.8.1c-d**), indicating they may be destabilizing core regions of the protein upon binding. For compound 10 this is consistent with

the increases in H/D exchange observed throughout large regions of the protein. Further structure-activity-relationships will be critical to increase the potency of compound 10.

2.9 Conclusion

This is the first prospective application of DOCKovalent towards finding an *irreversible* covalent inhibitor. From the results of this study, covalent docking appears to significantly accelerate early hit discovery against a very challenging and flexible target. The initial screen revealed 2 of 29 compounds could react with K-Ras(G12C) a 7% success rate. These results were comparable to an empirical electrophile library screen. DOCKovalent does not take into account the variability of the acrylamide warhead electronics at the covalent attachment point.[25] It is therefore encouraging that it was able to rank two fragments that successfully engage the protein without being overly promiscuous. Future incorporation of warhead reactivity or covalent reversible warheads may further reduce false positive hits from docking.[27] Although the hit rates were not as high as previous covalent docking campaigns[27], the success rate was still comparable to typical non-covalent virtual screening hit rates.

From the docking hit, we generated a chemically distinct G12C inhibitor which lacked the chemically reactive phenol from the original scaffold.[6,8] Early generation switch II pocket inhibitors gained potency through modifications that increased binding to the switch-II pocket region. The cis-3-hydroxy-L-proline linker used in this study increased the potency 8-fold, demonstrating that high affinity linker modifications can enhance scaffold binding.

The performance of DOCKovalent is greatly dependent on the input structure. K-Ras is a highly flexible target, particularly in the switch I and II loops, which are integral to the ligand-binding site. This study was performed using ligand enrichment of fragment disulfides and vinylsulfonamides on 24 co-crystal structures of K-Ras inhibitors. However, the recent K-Ras(G12C) inhibitor ARS-853 binds to an extended pocket, forming three hydrogen bonds[8] and may not have ranked highly in the original docking screen on the smaller K-Ras co-crystal structures. In addition to ligand enrichment, ensemble docking with consensus ranking on distinct structural subsets may improve covalent ligand design against highly flexible targets. Or, perhaps, a flexible receptor procedure, which accounts for crystallographically observed alternative states of side chains and loops, could be incorporated into covalent docking to improve the results.[27]

This study further demonstrates that the switch I and switch II loops are tightly coordinated. The S-IIP binders can communicate across the loops to affect nucleotide recognition and Ras activity. Especially in flexible proteins, the empiric validation of ligand binding needs to consider thermodynamic stability of the ligand-protein interaction. The thermal stability assay demonstrated that compound 10 was thermodynamically destabilizing to the protein. This destabilizing property was consistent with increased H/D exchange and also with increased SOS-catalyzed nucleotide exchange of both GDP and GTP. Covalent inhibitors may have destabilizing noncovalent interactions with the protein after covalent adduct formation.[34] Thus, the thermal stability assay may prove useful as a counter-screening method to measure the stabilizing noncovalent interactions during small molecule optimization. This

assay may be particularly useful for classifying K-Ras switch II compounds as allosteric inhibitors or potential nucleotide state destabilizers.

In this study, we describe a novel small molecule that destabilizes K-Ras and behaves like no other switch II pocket binder in its unique ability to accelerate SOS-mediated nucleotide exchange. We believe this will help development of novel allosteric inhibitors of K-Ras that can be used to study aspects of nucleotide exchange.

2.10 Methods

Covalent docking

Covalent docking was performed using DOCKovalent as described and implemented in DOCK3.6.[25] The covalent bond parameters were set to: length=1.8Å, bond angles=109.5°±10° (in 2.5° steps).

Protein expression and purification

K-Ras constructs were purified as previously specified.[6] Briefly, His6-tagged recombinant bacterial human K-Ras (isoform 2, residues 1-169), K-Ras Cys-light (isoform 2, residues 1-169, C51S/C80L/C118S), K-Ras (isoform 2, residues 1- 189) were transformed into Escherichia coli (BL21 (DE3)) for expression. K-Ras(G13C) was introduced into each vector using a QuikChange™ PCR protocol. Protein cultures were grown in TB with kanamycin at 37˚C. Upon an optical density (OD_{600}) reached 0.5-0.6, were induced at 18˚C with 120mg IPTG and expressed over 18

hours. The cells were pelleted at 4,5000 rpm, resuspended in lysis buffer (500 mM NaCl, 20 mM TRIS pH 8.0, 5 mM imidazole, 1 tablet of Roche cOmplete EDTA Free protease inhibitor per 50mL lysis buffer), and lysed by microfluidizer at 80psi. The lysate was spun down at 10,000g and purified by batch binding using TALON beads with elution buffer (500 mM NaCl, 20 mM TRIS pH 8.0, 250 mM imidazole). The His6-tag was cleaved with TEV overnight with cleavage buffer (300 mM NaCl, 20 mM TRIS pH 8.0, 5 mM imidazole, 1 mM DTT, 0.5 mM EDTA). The tag was removed via Nickel NTA beads and the eluate was purified by FPLC using ion exchange (buffer A: 50mM NaCl, 20 mM TRIS pH 8.0, buffer B: 500mM NaCl, 20 mM TRIS pH 8.0). The protein was concentrated to 5-20 mg/ml. If the protein was used for crystallography or hydrogen-deuterium exchange, it was subject to a subsequent size exclusion chromatography (buffer: 20 mM HEPES (pH 7.5), 150 mM NaCl) and concentrated.

X-ray crystallization, data collection and refinement

For X-ray crystallography, 1mM $MgCl_2$ and 40uM GDP (final concentration) was added to protein additionally purified through size exclusion chromatography. Hanging drop crystallization conditions were set up by mixing 1:1 protein and reservoir solutions. The reservoir contained 5% PEG400, 2M $(NH_4)_2SO_4$, 0.1M HEPES pH 7.5. After several days at 20°C, crystals were observed. The crystals were cryoprotected in crystallization solution supplemented with 28% glycerol, flash frozen, and stored in liquid nitrogen prior to obtaining diffraction data at 8.2.1 beamline at the Advanced Light Source of Lawrence Berkeley National Laboratories. Data was indexed with IMOSFLM and scaled and solved using Aimless and Phaser-

MR (ccp4i) and then subsequently refined with Phenix to the indicated statistics in **Table 2.10.4**.[35]

Compound stocks

Few unsubstituted-acrylamide fragments are available for purchase. Most acrylamide fragments were synthesized from commercially available 1° and 2° amines using 1.1-fold excess acryloyl chloride or acrylic acid as described. After purification, the compounds were made into 5mM DMSO stocks.

Mass Spectrometry Screening

50uL of 4uM K-Ras(G12C)-169 or K-Ras(WT) 1-189 was incubated with 200uM or 25uM compound (4 or 2% v/v dimethylsulfoxide respectively) for 24 hours at room temperature. The reaction was quenched with 2uL 10% v/v formic acid to yield 0.4% v/v formic acid final. Mass spectrometry experiments were performed using the Waters Acquity UPLC/ESI-TQD with a 2.1 × 50 mm Acquity UPLC BEH300 C4 column.

Nucleotide Exchange Assay

45uL of K-Ras(G12C)GDP (111nM) was prepared in assay buffer (150mM NaCl, 20mM HEPES, pH 7.5, 104 uM $MgCl_2$, 0.01% Triton X-100) was added to a 96 well Costar plate. Exchange was catalyzed by the addition of 5uL of a mixture of 2uM SOS and 2uM incoming nucleotide (200nM final; ThermoFischer™ BODIPY-FL GDP or GTP) and fluorescence intensity was monitored over 1 hour at Ex/Em: 485/520nm using a BioTek H4.

Thermal Stability Assays

The thermal denaturation of K-Ras was monitored using a fluorescence-based differential scanning fluorimetry assay. K-Ras was purified with or without compound for the use of the experiment as previously described. 8uM protein was prepared in assay buffer (150mM NaCl, 20mM Hepes, pH 7.5, 1mM $MgCl_2$) with 1/1000 Sypro Orange. The plate was heated from 25-95°C at a rate of 0.5°C /min. The fluorescence intensity was monitored at Ex/Em: 492/610nm.

Hydrogen-deuterium Exchange Mass Spectrometry

HDX reactions were conducted with 40pmol of protein, and were initiated by the addition of 46 µL of D_2O Buffer Solution (10 m*M* HEPES pH 7.5, 50 m*M* NaCl, 97% D_2O), to give a final concentration of 87% D_2O. Exchange was carried out for 0.3s, 3s, 30s, 300s and 3000s, and exchange was terminated by the addition of a quench buffer (final concentration 0.6 M guanidine HCl, 0.8% formic acid). Samples were rapidly frozen in liquid nitrogen and stored at −80°C until mass analysis.

Protein samples were rapidly thawed and injected onto a UPLC system at 2°C. The protein was run over two immobilized pepsin columns (Applied Biosystems; porosyme, 2-3131-00) at 10°C and 2°C at 200 µL/min for 3 minutes, and peptides were collected onto a VanGuard precolumn trap (Waters). The trap was subsequently eluted in line with an Acquity 1.7 µm particle, 100 × 1 mm2 C18 UPLC column (Waters), using a gradient of 5-36% B (buffer A 0.1% formic acid, buffer B 100% acetonitrile) over 16 minutes. Mass spectrometry experiments were

performed on an Impact II TOF (Bruker) acquiring over a mass range from 150 to 2200 m/z using an electrospray ionization source operated at a temperature of 200°C and a spray voltage of 4.5 kV. Peptides were identified using data-dependent acquisition methods following tandem MS/MS experiments (0.5 s precursor scan from 150-2200 m/z; twelve 0.25 s fragment scans from 150-2200 m/z). MS/MS datasets were analyzed using PEAKS7 (PEAKS), and a false discovery rate was set at 1% using a database of purified proteins and known contaminants.

Deuterium incorporation calculations were carried out as described previously.[36-38] HD-Examiner Software (Sierra Analytics) was used to automatically calculate the level of deuterium incorporation into each peptide. All peptides were manually inspected for correct charge state and presence of overlapping peptides. Deuteration levels were calculated using the centroid of the experimental isotope clusters. Full set of all H/D exchange data are shown in **Figure 2.10.1**. Significant changes between conditions were set as changes greater than 6%, 0.5 Da, and a p-value <0.05 (student t-test).

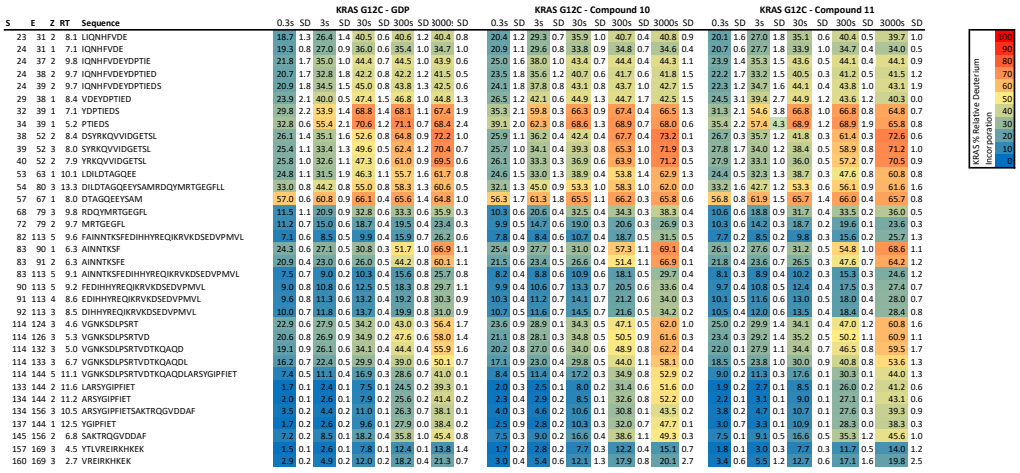

Figure 2.10.1. Relative **%**deuterium incorporation in peptides of K-Ras(G12C) with compounds 10 and 11 over time.

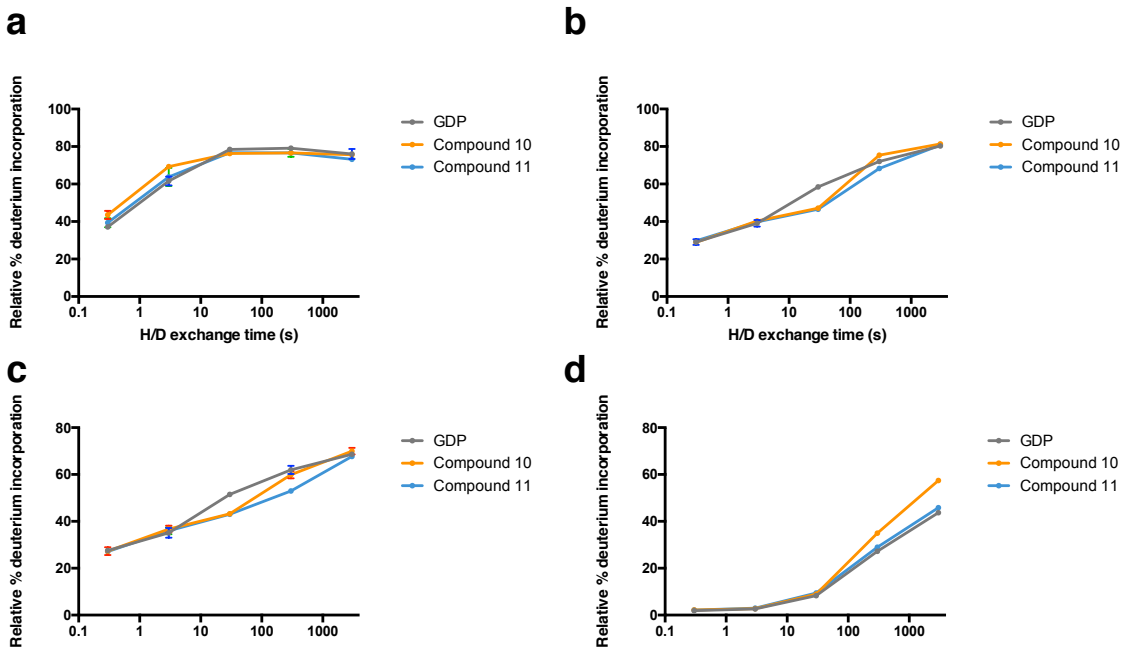

Figure 2.10.2. Relative %deuterium incorporation over time in **a.** peptides 34-39 (Switch-I region) **b.** peptides 38-52 **c.** peptides 53-63 (Switch-II region) and **d.** peptides 133-144. HDX curves are the average of three independent experiments (error bars represent SD).

Table 2.10.1. Crystal structures used for docking.

Ligand-bound K-Ras monomers used for docking studies			
4M21 chain B	4M1S chain B	4M22 chain B	56A chain B*
4LYJ	4LUC chain A	4M22 chain C	56A chain C*
4LYH chain B	4LUC chain B	4M1T chain B	56A chain D*
4LYH chain C	4LV6 chain A	59 chain B*	56A chain E*
4LYF chain B	4LV6 chain B	59 chain C*	55_P1 chain A*
4M1Y chain B	4M1O chain B	56A chain A*	55_P1 chain B*

*Crystal structures are not deposited in the Protein Data Bank.

Table 2.10.2. Percent modification of Cys-light K-Ras(G12C) 1-169 and K-Ras(WT) 1-189 by compounds in DOCKovalent Library

Compound Structure	Name	Mass	% Labeling of K-Ras(G12C)	% Labeling of K-Ras(WT) 1-189
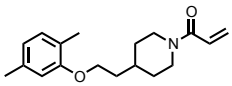	**S1-1**	287.40	0	0
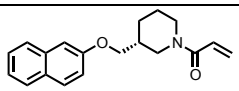	**S1-2**	295.38	0	0
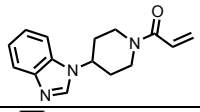	**S1-3**	255.31	0	0
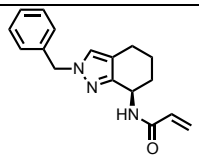	**S1-4**	281.35	0	0
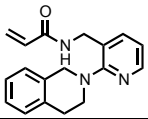	**S1-5**	293.36	0	61.7
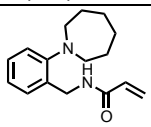	**S1-6**	258.36	0	0

Compound Structure	Name	Mass	% Labeling of K-Ras(G12C)	% Labeling of K-Ras(WT) 1-189
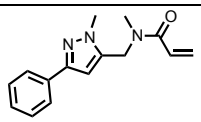	**S1-7**	255.31	0	24.2
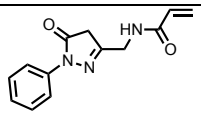	**S1-8**	243.26	0	0
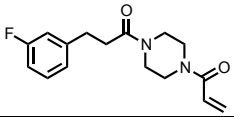	**S1-9**	290.33	0	0
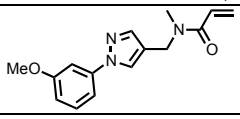	**S1-10**	271.31	0	0
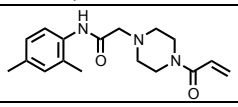	**S1-11**	301.38	0	0
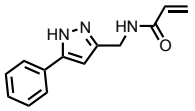	**S1-12**	227.26	0	0
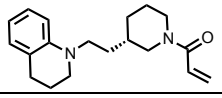	**S1-13**	298.42	0	0
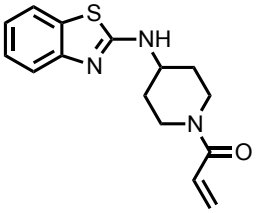	**2**	289.40	20	0
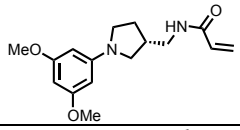	**S1-14**	290.36	0	0
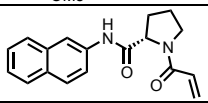	**1**	294.35	41	43.5
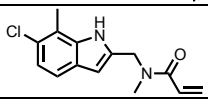	**S1-15**	262.73	0	0
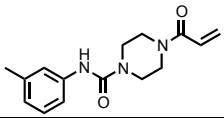	**S1-16**	273.33	0	23.6
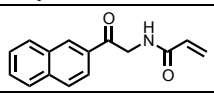	**S1-17**	239.27	0	0

Compound Structure	Name	Mass	% Labeling of K-Ras(G12C)	% Labeling of K-Ras(WT) 1-189
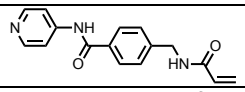	**S1-18**	281.31	0	0
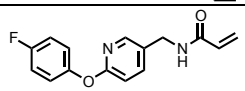	**S1-19**	272.27	0	0
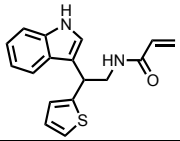	**S1-20**	296.39	0	0
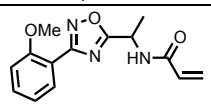	**S1-21**	273.29	0	20.2
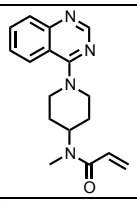	**S1-22**	296.37	0	0
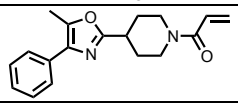	**S1-23**	296.36	0	21.4
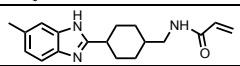	**S1-24**	297.39	0	0
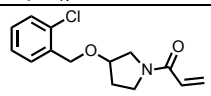	**S1-25**	265.74	0	0
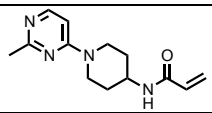	**S1-26**	246.31	0	0
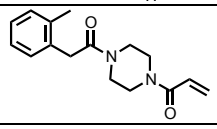	**S1-27**	272.34	0	20

Table 2.10.3. Percent modification of Cys-light K-Ras(G12C) 1-169 and K-Ras(WT) 1-189 by compounds in Acrylamide Library

Compound Structure	Name	Mass	% Labeling of K-Ras(G12C)	% Labeling of K-Ras(WT) 1-189
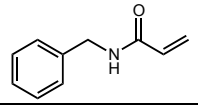	**DKM-2-31**	161.20	0	0
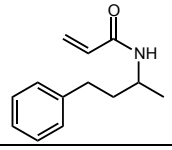	**DKM-2-32**	203.28	0	0
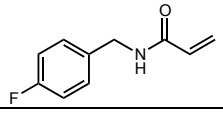	**DKM-2-34**	179.19	0	0
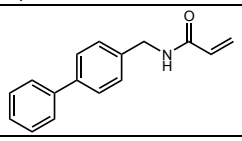	**DKM-2-37**	237.30	0	0
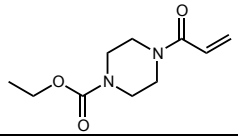	**DKM-2-39**	212.25	0	18.2
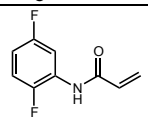	**DKM-2-40**	183.15	40.4	100
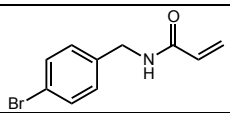	**DKM-2-43**	240.10	0	0
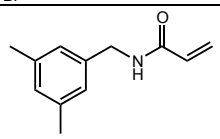	**DKM-2-47**	189.25	0	0
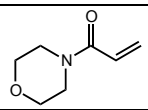	**DKM-2-49**	141.17	0	22.4
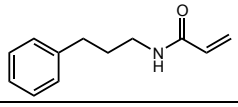	**DKM-2-50**	189.25	0	0
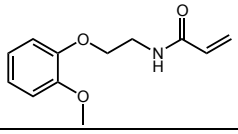	**DKM-2-58**	221.25	0	0

Compound Structure	Name	Mass	% Labeling of K-Ras(G12C)	% Labeling of K-Ras(WT) 1-189
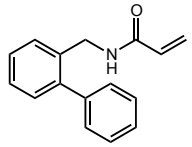	**DKM-2-59**	237.30	0	0
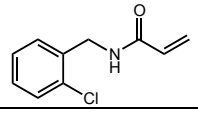	**DKM-2-60**	195.65	0	0
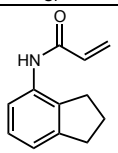	**DKM-2-84**	187.24	0	30.0
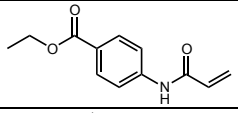	**DKM-2-85**	219.24	56.5	100
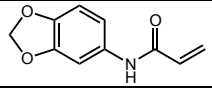	**DKM-2-86**	191.18	0	38.0
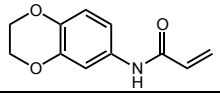	**DKM-2-87**	205.21	0	40.0
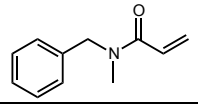	**DKM-2-95**	175.23	0	0
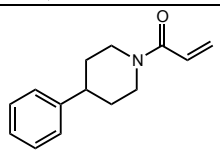	**DKM-2-97**	215.29	0	0
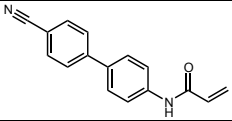	**DKM-2-98**	248.28	0	0
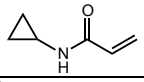	**DKM-2-99**	111.14	0	0
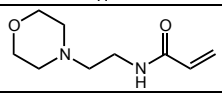	**DKM-2-100**	184.24	0	0
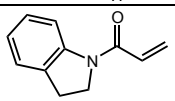	**DKM-2-101**	173.21	41.7	100
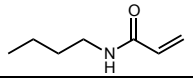	**DKM-2-102**	127.18	0	0

Compound Structure	Name	Mass	% Labeling of K-Ras(G12C)	% Labeling of K-Ras(WT) 1-189
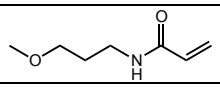	**DKM-2-103**	143.18	0	0
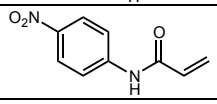	**DKM-2-104**	192.17	100	100
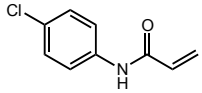	**DKM-2-107**	181.62	0	31.0
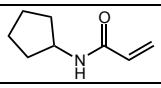	**DKM-2-108**	139.19	0	0
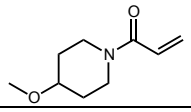	**DKM-2-109**	169.22	0	0
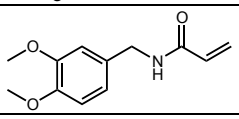	**DKM-2-110**	221.25	0	0
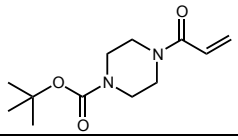	**DKM-2-111**	240.30	0	0
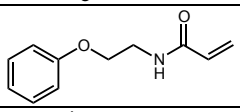	**DKM-2-113**	191.23	0	0
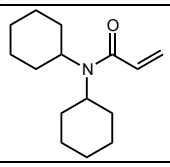	**DKM-2-114**	235.37	0	0
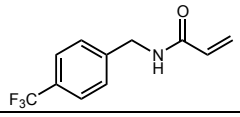	**DKM-2-116**	229.20	0	0
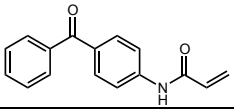	**DKM-2-117**	251.28	100	100
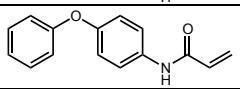	**DKM-2-119**	239.27	38.8	43
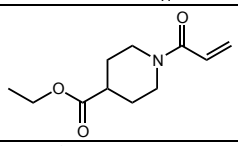	**DKM-2-120**	211.26	0	0
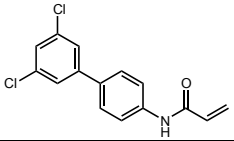	**DKM3-3**	292.16	16.3	0

Compound Structure	Name	Mass	% Labeling of K-Ras(G12C)	% Labeling of K-Ras(WT) 1-189
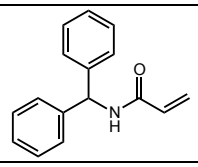	**DKM-3-4**	237.30	0	0
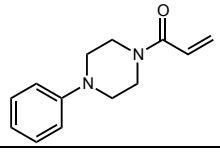	**DKM-3-5**	216.28	0	15.7
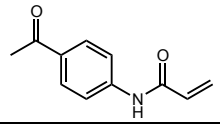	**DKM-3-7**	189.21	53	100
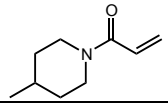	**DKM-3-8**	153.22	0	0
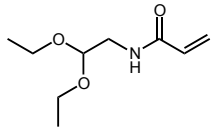	**DKM-3-9**	187.24	0	0
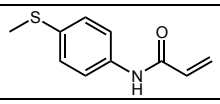	**DKM-3-10**	193.27	0	62.5
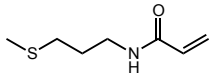	**DKM-3-12**	144.21	0	0
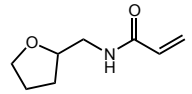	**DKM-3-15**	155.19	0	0
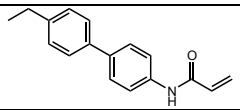	**DKM-3-16**	251.32	0	0
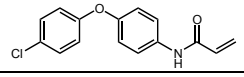	**DKM3-30**	273.71	0	0
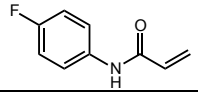	**DKM3-31**	165.16	0	41.6
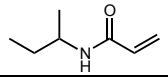	**DKM-3-32**	127.18	0	0
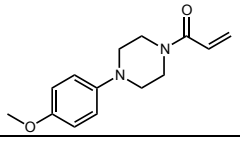	**DKM-3-36**	246.30	0	19.3

Compound Structure	Name	Mass	% Labeling of K-Ras(G12C)	% Labeling of K-Ras(WT) 1-189
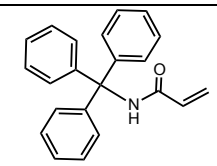	**DKM-3-41**	313.39	0	0
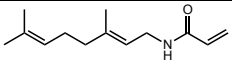	**DKM-3-42**	207.31	0	0
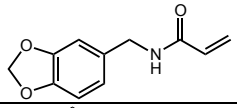	**DKM-3-43**	205.21	0	0
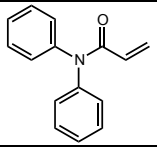	**DKM3-70**	223.27	52	100
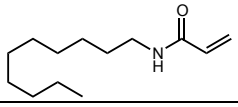	**TRH-1-12**	211.34	0	0
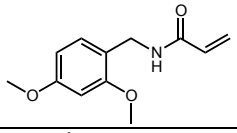	**TRH-1-13**	221.25	0	0
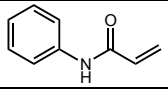	**TRH-1-19**	147.17	0	28.2
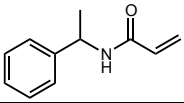	**TRH-1-20**	175.23	0	0
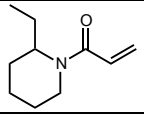	**TRH-1-27**	167.25	0	0
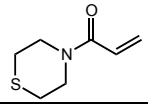	**TRH-1-30**	157.23	0	24.5
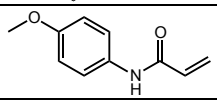	**TRH-1-32**	177.20	0	20.9

Table 2.10.4. Data collection and refinement statistics for K-Ras(G12C)-10 (PDB: 6ARK).

	K-Ras(G12C)-10
Data Collection	
Space group	H 3 2
Cell Dimension	
a, *b*, *c* (Å)	94.2799, 94.2799, 119.55
(°)	90, 90, 120
Resolution range (Å)	30.43 - 1.75 (1.78 - 1.75)
R_{merge}	0.072 (0.996)
R_{pim}	0.033 (0.451)
Mean I/σI	13.60
CC1/2	0.999 (0.702)
Completeness (%)	100.00 (100.00)
Multiplicity	2.0 (2.0)
Refinement	
Resolution (Å)	29.88 - 1.75
Reflections used in refinement	39968
R_{work}/R_{free}	0.1937/0.2314
Number of atoms	1444
Protein	1323
Ligands/ions	65
Water	56
B-factors	52.59
Protein	53.04
Ligands/ions	52.11
Water	42.50
R.m.s. deviations	
Bonds (Å)	0.006
Angles (°)	0.98

*Statistics for the highest-resolution shell are shown in parentheses.

Synthetic Methods

All commercial reagents were purchased and used without further purification. All reactions were done under argon in sealed vials with stirring. Silica gel chromatography was performed using a Combiflash Rf (Teledyne Isco) with pre-packed 4-24g silica columns and cartridges. All

reverse-phase high performance liquid chromatography (RP-HPLC) was performed using a Waters 2545 solvent delivery system equipped with an XBridge prep C18 column. Separation was achieved using a gradient between 5-95% acetonitrile (ACN) in water with 0.1% formic acid by monitoring UV absorption (λ=254 nm). For most compounds, high-resolution mass spectrometry (HRMS) was performed using a high-resolution UPLC/TOF system (Synapt G2-S, Waters) equipped with ESI source. Compounds were analyzed in positive ionization mode. Separation was done on Acquity BEH C18 column using water-methanol-formic acid gradient for elution. Elemental composition was determined using Elemental Composition module of MassLynx v.4.1 software. Liquid chromatography traces and MS (for S1-14 and S1-20) were collected with a Waters Acquity UPLC Class I/XEVO G2-XS QToF with a 2.1 x 50 mm Acquity UPLC BEH C18 column. ^{1}H NMR were recorded on a Varian Innova 400 MHz or a Bruker DRX 500 MHz spectrometer. ^{1}H chemical shifts are reported in δ (ppm) as s (singlet), d (doublet), dd (doublet of doublets), t (triplet), q (quartet), or m (multiplet) and are referenced to the residual solvent peak. Coupling constants (J) are reported as Hertz. ^{13}C NMR were recorded on a Bruker DRX 500 MHz spectrometer and the ^{13}C chemical shifts are reported in δ (ppm) and are referenced to the residual solvent peak.

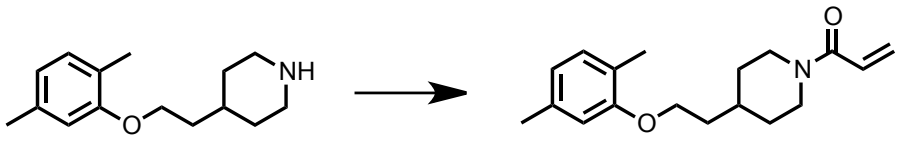

S1-1

S1-1 1-(4-(2-(2,5-dimethylphenoxy)ethyl)piperidin-1-yl)prop-2-en-1-one:

4-(2-(2,5-Dimethylphenoxy)ethyl)piperidine hydrochloride (50mg, 1 eq, 0.19 mmol) was dissolved in 2mL acetonitrile. TEA was added (150uL, 6 eq, 1.11mmol) at ambient temperature. The reaction was cooled to 0°C. Acryloyl chloride (16uL, 1.1 eq, 0.20mmol) was added and reaction was stirred for 30 minutes. The reaction was extracted with ethyl acetate (5mL x 3), dried over Na_2SO4. The compound was purified by flash chromatography on silica gel (0-15% dichloromethane: methanol gradient) and subsequently by RP-HPLC (45-95% gradient) to get the desired product the desired product (11.8mg, 22%yield) as a yellow oil. HRMS $C_{18}H_{26}NO_2$ $[M+H]^+$ expected mass: 288.1964; observed: 288.1972. ^1H NMR (400 MHz, $CDCl_3$) **δ** 7.01 (d, J=7.54, 1H), 6.67 (d, J=7.52, 1H), 6.62 (s, 1H), 6.59 (dd, J=16.96, 10.60, 1H), 6.26 (dd, J=16.86, 1.97, 1H) 5.66 (dd, J=10.59, 1.97, 1H), 4.66 (d, J=12.70, 1H), 4.00 (t, J=6.21, 2H), 3.98 (m, 1H) 3.06 (t, J=12.71, 1H), 2.65(t, J=12.63, 1H) 2.31 (s, 3H), 2.17 (s, 3H), 1.84 (m, 3H), 1.77 (q, J=6.23, 2H), 1.23 (m, 2H).

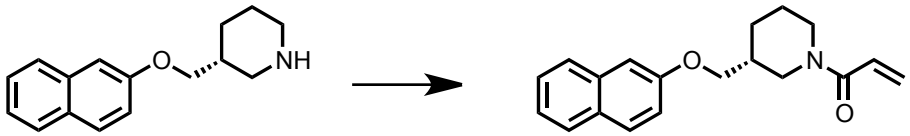

S1-2

S1-2 (*R*)-1-(3-((naphthalen-2-yloxy)methyl)piperidin-1-yl)prop-2-en-1-one:

3-[(2-Naphthyloxy)methyl]piperidine (50mg, 1 eq, 0.18 mmol) was dissolved in 2mL acetonitrile. TEA was added (250uL, 5eq, 0.9mmol) at ambient temperature. The reaction was cooled to 0°C. Acryloyl chloride (30uL, 2 eq, 0.4mmol) was added and reaction was stirred for 30 minutes. The reaction was quenched with 5mL saturated NaHCO3. The reaction was extracted with ethyl acetate (5mL x 3), dried over Na_2SO4. The compound was purified by flash chromatography on

silica gel (5-100% hexanes: ethyl acetate gradient) to get the desired product (25mg, 47%yield) as a yellow oil. HRMS $C_{19}H_{22}NO_2$ $[M+H]^+$ expected mass: 296.1651; observed: 296.1664. ^{1}H NMR (400 MHz, $CDCl_3$) **δ** 7.74 (m, 3H), 7.44 (m, 1H), 7.34 (m, 1H), 7.15 (d, J=8.92, 1H), 7.11 (s, 1H), 6.62 (m, 1H), 6.27 (t, J=16.37, 1H), 5.66 (dd, J=16.73, 10.79, 1H), 4.48 (dd, J=170.32, 13.47, 1H), 3.98 (m, 3H), 2.97 (m, 1H), 3.10 (m, 1H), 2.13 (m, 1H), 1.98 (m, 1H), 1.79 (m, 2H), 1.54 (m, 1H).

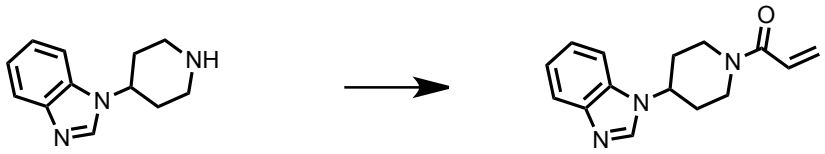

S1-3

S1-3 1-(4-(1*H*-benzo[*d*]imidazol-1-yl)piperidin-1-yl)prop-2-en-1-one:

1-(piperidin-4-yl)-1H-1,3-benzodiazole hydrochloride (27mg, 1 eq, 0.13 mmol) was dissolved in 2mL acetonitrile. TEA was added (35uL, 1.9 eq, 0.247mmol) at ambient temperature. The reaction was cooled to 0°C. Acryloyl chloride (8uL, 0.8 eq, 0.1mmol) was added. The reaction was quenched with 5mL saturated NaHCO3. The reaction was extracted with ethyl acetate (5mL x 3), dried over Na_2SO4. The compound was purified by flash chromatography on silica gel (0-15% dichloromethane: methanol) to get the desired product (15.7mg, 50%yield) as a white solid. HRMS $C_{15}H_{18}N_3O$ $[M+H]^+$ expected mass: 256.145; observed: 256.145. ^{1}H NMR (400 MHz, CD_3OD) **δ** 8.28 (s, 1H), 7.71 (m, 2H), 7.30 (m, 2H), 6.84 (dd, J=16.56,10.64, 1H), 6.24 (dd, J=16.79, 2.02, 1H), 5.78 (dd, J=10.59, 2.02, 1H), 4.73 (m, 2H), 4.34 (d, J=13.41, 1H), 3.39 (t, J=13.41, 1H), 2.97 (t, J=13.41, 1H), 2.25 (d, J=12.49), 2.09 (m, 2H).

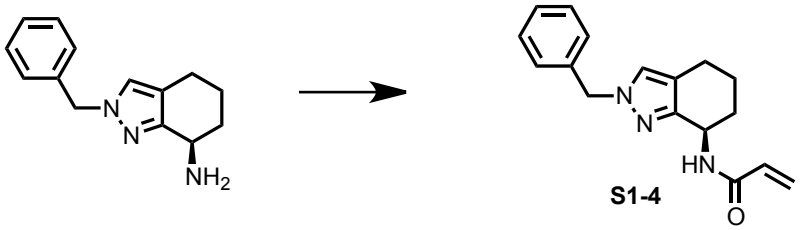

S1-4

S1-4 *N*-((2-(3,4-dihydroisoquinolin-2(1*H*)-yl)pyridin-3-yl)methyl)acrylamide:

1-benzyl-4,5,6,7-tetrahydro-1H-indazol-4-amine (75mg, 1 eq, 0.33mmol) was dissolved in 2mL acetonitrile. TEA was added (90uL, 2 eq, 0.66mmol) at ambient temperature. The reaction was cooled to 0°C. Acryloyl chloride (30uL, 1.1 eq, 0.36mmol) was added. The reaction was quenched with 5mL saturated NaHCO3. The reaction was extracted with ethyl acetate (5mL x 3), dried over Na_2SO4. The compound was purified by flash chromatography on silica gel (5-100% hexanes: ethyl acetate) to get the desired product (7mg, 8%yield) as a yellow oil. HRMS $C_{17}H_{20}N_3O$ $[M+H]^+$ expected mass: 282.1606; observed: 282.1608. ^{1}H NMR (400 MHz, CD_3OD) **δ** 7.40 (s, 1H), 7.29 (m, 3H), 7.12 (d, J=7.25, 2H), 5.65 (dd, J=6.88, 5.00, 1H), 6.25 (m, 2H), 5.26 (s, 2H), 5.04 (t, J=4.91, 1H), 2.55 (m, 2H), 1.93 (m, 2H), 1.82 (m, 1H), 1.70 (m, 1H).

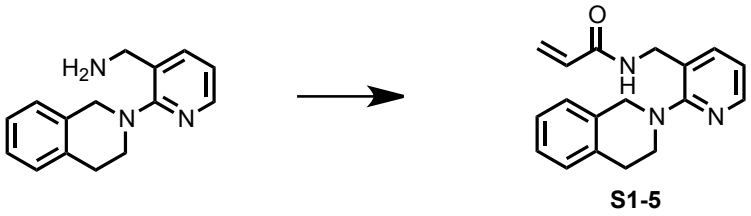

S1-5

S1-5 *N*-((2-(3,4-dihydroisoquinolin-2(1*H*)-yl)pyridin-3-yl)methyl)acrylamide:

(2-(3,4-Dihydroisoquinolin-2(1H)-yl)pyridin-3-yl)methanamine (50mg, 1 eq, 0.208mmol) was dissolved in 2mL acetonitrile. TEA was added (58uL, 2 eq, 0.416mmol) at ambient temperature. The reaction was cooled to 0°C. Acryloyl chloride (19uL, 1.1 eq, 0.229mmol) was added. The reaction was quenched with 5mL saturated NaHCO3. The reaction was extracted with ethyl

acetate (5mL x 3), dried over Na_2SO4. The compound was purified by flash chromatography on silica gel (5-100% hexanes: ethyl acetate) to get the desired product (8.2mg, 13%yield) as a white oily solid. HRMS $C_{18}H_{20}N_3O$ $[M+H]^+$ expected mass: 294.1606; observed: 294.1609. ^1H NMR (400 MHz, $CDCl_3$) **δ** 8.29 (dd, J=4.87, 1.72, 1H), 7.59 (dd, J=7.49, 1.64, 1H), 7.19 (m, 3H), 7.15 (m, 1H), 6.99 (dd, J=4.92, 7.47, 1H), 6.42 (s, 1H), 6.26 (dd, J=16.98, 1.24, 1H), 6.05 (dd, J=17.00, 10.31, 1H), 5.63 (dd, J=10.31, 1.21, 1H), 4.64 (d, J=5.91, 2H), 4.39 (s, 2H), 3.40 (t, J=5.80, 2H), 3.07 (t, J=5.72, 2H). ^{13}C NMR (400 MHz, $CDCl_3$) **δ** 165.78, 161.19, 147.05, 137.84, 134.91, 134.22, 130.71, 129.04, 127.01, 126.87, 126.55, 126.11, 125.41, 118.91, 77.39, 52.24, 49.62, 40.05, 29.84.

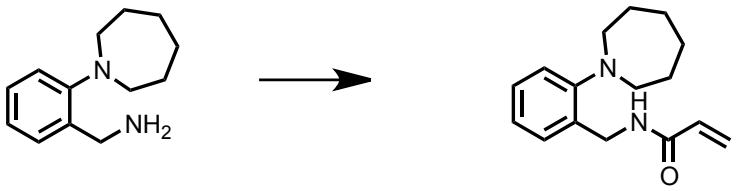

S1-6

S1-6 *N*-(2-(azepan-1-yl)benzyl)acrylamide:

[2-(1-Azepanyl)phenyl]methanamine (61mg, 1 eq, 0.3mmol) was dissolved in 2mL acetonitrile. TEA (70uL, 2eq, 0.5mmol) was added at ambient temperature. The reaction was cooled to 0°C. Acryloyl chloride (22uL, 1.1 eq, 0.27mmol) was added. The reaction was quenched with 5mL saturated NaHCO3 and left stirring for 15 minutes at ambient temperature. The reaction was extracted with ethyl acetate (5mL x 3), dried over Na_2SO4. The compound was purified by flash chromatography on silica gel (5-100% hexanes: ethyl acetate) to get the desired product (32.8mg, 42%yield) a white oily solid. HRMS $C_{16}H_{23}N_2O$ $[M+H]^+$ expected mass: 259.181; observed: 259.1819. ^1H NMR (400 MHz, $CDCl_3$) **δ** 7.24 (m, 2H), 7.16 (d, J=8.13, 1H), 7.03 (t,

J=7.04, 1H), 6.97 (s, 1H), 6.29 (dd, J=16.96, 1.25, 1H), 6.10 (dd, J=16.92, 10.25, 1H), 5.64 (dd, J=10.23, 1.24, 1H), 4.61 (d, J=5.51, 2H), 3.10 (t, J=5.31, 4H), 1.73 (m, 8H).

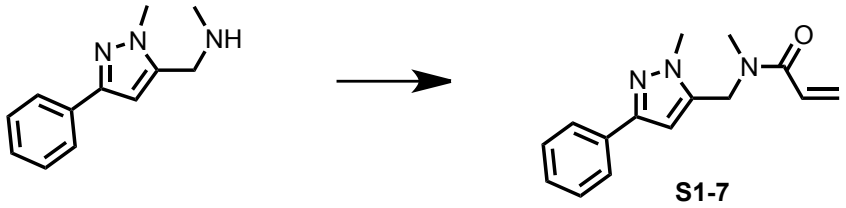

S1-7

S1-7 *N*-methyl-*N*-((1-methyl-3-phenyl-1*H*-pyrazol-5-yl)methyl)acrylamide:

N-methyl-1-(1-methyl-3-phenyl-1*H*-pyrazol-5-yl)methanamine (25mg, 1 eq, 0.124mmol) was dissolved in 2mL acetonitrile. TEA (35uL, 2 eq, 0.25mmol) was added at ambient temperature. The reaction was cooled to 0°C. Acryloyl chloride (11uL, 1.1 eq, 0.136mmol) was added. The reaction was quenched with 5mL saturated NaHCO3 and left stirring for 15 minutes at ambient temperature. The reaction was extracted with ethyl acetate (5mL x 3), dried over Na_2SO4. The compound was purified by flash chromatography on silica gel (5-100% hexanes: ethyl acetate) to get the desired product (17.6mg, 56% yield) as a white oily solid. HRMS $C_{15}H_{18}N_3O$ $[M+H]^+$ expected mass: 256.145; observed: 256.1458. ^{1}H NMR (400 MHz, $CDCl_3$) **δ** 7.76 (d, J=7.62, 2H), 7.38 (t, J=7.44, 2H), 7.30 (d, J=7.44, 1H), 6.61 (dd, J=10.40, 16.78, 1H), 6.50 (s, 1H) 6.40 (dd, J=16.78, 1.95, 1H), 5.77(d, J=10.69, 1H), 4.75 (s, 2H), 3.89 (s, 3H), 3.05 (s, 3H).

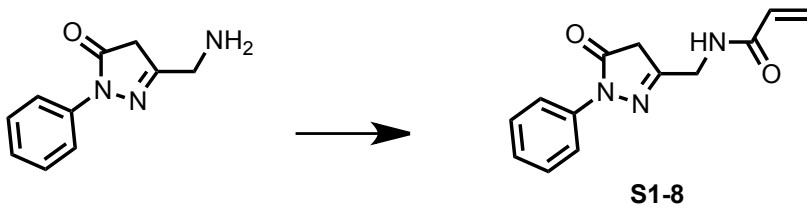

S1-8

S1-8 *N*-((5-oxo-1-phenyl-4,5-dihydro-1*H*-pyrazol-3-yl)methyl)acrylamide:

5-(Aminomethyl)-2-phenyl-1,2-dihydro-3H-pyrazol-3-one dihydrochloride (25mg, 1 eq, 0.13mmol) was dissolved in 2mL acetonitrile. TEA (37uL, 2eq, 0.26mmol) was added at ambient temperature. The reaction was cooled to 0°C. Acryloyl chloride (12uL, 1.1 eq, 0.15mmol) was added. The reaction was quenched with 5mL saturated NaHCO3 and left stirring for 15 minutes at ambient temperature. The reaction was extracted with ethyl acetate (5mL x 3), dried over Na_2SO4. The compound was purified by flash chromatography on silica gel (5-100% hexanes: ethyl acetate) to get the desired product (3mg, 9%yield) as a yellow oil. HRMS $C_{13}H_{14}N_3O_2$ $[M+H]^+$ expected mass: 244.1086; observed: 244.1089. ^{1}H NMR (400 MHz, MeOD) **δ** 7.66 (t, J=7.70, 2H), 7.44 (t, J=7.70, 2H), 7.29 (t, J=7.69, 1H), 6.29 (m, 2H), 5.69 (dd, J= 8.35, 3.65, 1H), 4.37 (s, 2H).

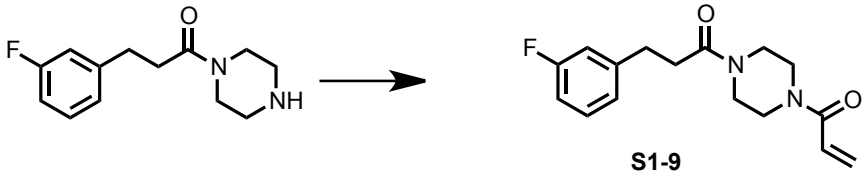

S1-9

S1-9 1-(4-(3-(3-fluorophenyl)propanoyl)piperazin-1-yl)prop-2-en-1-one:

3-(3-Fluorophenyl)-1-(piperazin-1-yl)propan-1-one hydrochloride (25mg, 1 eq, 0.11mmol) was dissolved in 2mL acetonitrile. TEA (30uL, 2eq, 0.21mmol) was added at ambient temperature. The reaction was cooled to 0°C. Acryloyl chloride (10uL, 1.1 eq, 0.11mmol) was added. The reaction was quenched with 5mL saturated NaHCO3 and left stirring for 15 minutes at ambient temperature. The reaction was extracted with ethyl acetate (5mL x 3), dried over Na_2SO4. The compound was purified by flash chromatography on silica gel (5-100% hexanes: ethyl acetate)

to get the desired product (12.8mg, 40%yield) as a clear oil. HRMS $C_{16}H_{20}FN_2O_2$ $[M+H]^+$ expected mass: 291.1509; observed: 291.1509. ^{1}H NMR (400 MHz, $CDCl_3$) **δ** 7.25 (m, 1H), 7.00 (d, J =7.61, 1H), 6.90 (m, 2H), 6.53 (m, 1H), 6.32 (dd, J=16.97, 1.70, 1H), 5.74 (dd, J=10.56, 1.57, 1H), 3.55 (m, 8H), 2.99 (t, J= 7.40, 2H), 2.64 (t, J=7.40, 2H). ^{13}C NMR (500 MHz, $CDCl_3$) **δ** 170.78, 165.74 + 164.02 (d, J=214.72), 162.06, 143.67, 130.19 + 130.12 (d, J=8.32), 129.00, 127.06, 124.28, 115.56 + 115.39 (d, J=21.09), 113.45 + 113.28 (d, J=21.09), 45.60, 45.25, 41.79, 41.44, 34.68, 31.13.

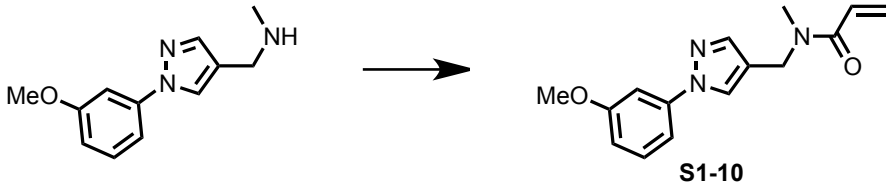

S1-10

S1-10 *N*-((1-(3-methoxyphenyl)-1*H*-pyrazol-4-yl)methyl)-*N*-methylacrylamide: 1-[1-(3-methoxyphenyl)-1H-pyrazol-4-yl]-N-methylmethanamine (57.6mg, 1 eq, 0.229mmol) was dissolved in 2mL acetonitrile. TEA (64uL, 2eq, 0.458mmol) was added at ambient temperature. The reaction was cooled to 0°C. Acryloyl chloride (20uL, 1.1 eq, 0.252mmol) was added. The reaction was quenched with 5mL saturated NaHCO3 and left stirring for 15 minutes at ambient temperature. The reaction was extracted with ethyl acetate (5mL x 3), dried over Na_2SO4. The compound was purified by flash chromatography on silica gel (5-100% hexanes: ethyl acetate) to get the desired product (29.6mg, 48%yield) as a clear oil. HRMS $C_{15}H_{18}N_3O_2$ $[M+H]^+$ expected mass: 272.1399; observed: 272.1404. ^{1}H NMR (400 MHz, $CDCl_3$) **δ** 7.32 (t, J=8.06, 1H), 7.20 (d, J=8.06, 1H), 6.82 (d, J=8.06, 1H), 6.58 (dd, J=16.83, 10.27, 1H), 6.37 (dd, J=16.74, 1.78, 1H), 5.73 (dd, J=10.40, 1.68, 1H), 4.54 (s, 2H), 3.86 (s, 3H), 3.07 (s, 3H).

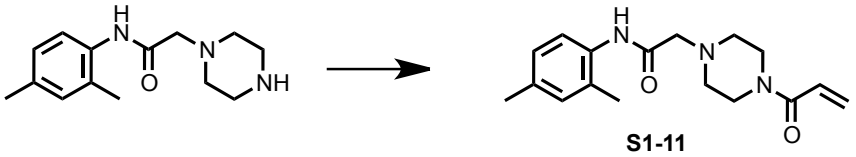

S1-11

S1-11 2-(4-acryloylpiperazin-1-yl)-*N*-(2,4-dimethylphenyl)acetamide:

N-(2,4-dimethylphenyl)-2-piperazin-1-yl-acetamide (25mg, 1 eq, 0.10mmol) was dissolved in 2mL acetonitrile. TEA (28uL, 2eq, 0.20mmol) was added at ambient temperature. The reaction was cooled to 0°C. Acryloyl chloride (9uL, 1.1 eq, 0.11mmol) was added. The reaction was quenched with 5mL saturated NaHCO3 and left stirring for 15 minutes at ambient temperature. The reaction was extracted with ethyl acetate (5mL x 3), dried over Na_2SO4. The compound was purified by flash chromatography on silica gel (0-15% dichloromethane: methanol) to get the desired product (9mg, 30% yield) a white solid. HRMS $C_{17}H_{24}N_3O_2$ $[M+H]^+$ expected mass: 302.1869; observed: 302.1874. ^{1}H NMR (400 MHz, $CDCl_3$) **δ** 9.06 (s, 1H) 7.94 (s, 1H), 7.06 (d, J=7.59, 1H), 6.88 (d, J=7.70, 1H), 6.56 (dd, J=17.09, 10.61, 1H), 6.31 (dd, J=17.05, 1.97, 1H), 5.73 (dd, J=10.68, 1.97, 1H), 3.76 (s, 2H), 3.65 (s, 2H), 3.22 (s, 2H), 2.68 (t, J=5.09, 4H), 2.33 (s, 3H), 2.24 (s, 3H). ^{13}C NMR (500 MHz, $CDCl_3$) **δ** 167.41, 165.65, 137.04, 135.43, 130.32, 128.66, 127.23, 125.49, 123.89, 121.77, 62.21, 53,73, 53.27, 46.04, 42.26, 21.39, 17.50

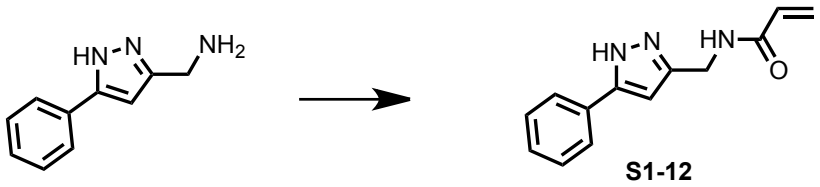

S1-12

S1-12 *N*-((5-phenyl-1*H*-pyrazol-3-yl)methyl)acrylamide:

(3-phenyl-1*H*-pyrazol-5-yl)methanamine (50mg, 1eq, 0.287mmol) was dissolved in 2mL acetonitrile. TEA (80uL, 2eq, 0.574mmol) was added at ambient temperature. The reaction

was cooled to 0°C. Acryloyl chloride (25uL, 1.1 eq, 0.316mmol) was added. The reaction was quenched with 5mL saturated NaHCO3 and left stirring for 15 minutes at ambient temperature. The reaction was extracted with ethyl acetate (5mL x 3), dried over Na_2SO4. The compound was purified by flash chromatography on silica gel (0-15% dichloromethane: methanol) and RP-HPLC (35-70% gradient) to get the desired product (13mg, 20% yield) as a white powder. HRMS $C_{13}H_{14}N_3O$ $[M+H]^+$ expected mass: 228.1137; observed: 228.1145. ^{1}H NMR (400 MHz, MeOD) **δ** 7.69 (s, 2H), 7.41 (t, J=6.96, 2H), 7.32 (t, J=6.89, 1H), 6.57 (s, 1H), 6.28 (m, 2H), 5.69 (dd, J=7.84, 4.24, 1H), 4.50 (s, 2H).

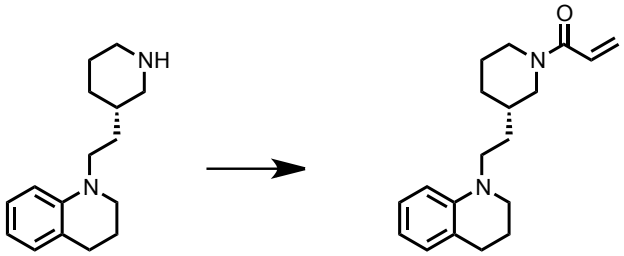

S1-13

S1-13 (*S*)-1-(3-(2-(3,4-dihydroquinolin-1(2*H*)-yl)ethyl)piperidin-1-yl)prop-2-en-1-one: (*S*)-1-(2-(piperidin-3-yl)ethyl)-1,2,3,4-tetrahydroquinoline (63.8mg, 1 eq, 0.227mmol) was dissolved in 2mL acetonitrile. TEA (57uL, 2eq, 0.408mmol) was added at ambient temperature. The reaction was cooled to 0°C. Acryloyl chloride (18uL, 1 eq, 0.224 mmol) was added. The reaction was quenched with 5mL saturated NaHCO3 and left stirring for 15 minutes at ambient temperature. The reaction was extracted with ethyl acetate (5mL x 3), dried over Na_2SO4. The compound was purified by flash chromatography on silica gel (5-95% hexanes: ethyl acetate), followed by RP-HPLC (45-95% gradient) to get the desired product (2.1mg, 3% yield) as an orange solid. HRMS $C_{19}H_{27}N_2O$ $[M+H]^+$ expected mass: 299.2123; observed: 299.2125. ^{1}H NMR

(400 MHz, $CDCl_3$) **δ** 7.03 (m, 1H), 6.93 (m, 1H), 6.55 (m, 3H), 6.25 (d, J=16.94, 1H), 5.65 (t, J=9.53, 1H), 4.45 (dd, J=31.77, 12.64, 1H), 3.87 (d, J=12.64, 1H), 3.32 (t, J=6.24, 2H), 3.26 (m, 2H), 3.08 (t, J=12.11, 1H), 2.83 (t, J=12.96, 1H), 2.74 (t, J=6.24, 2H), 2.54 (t, J=10.80, 1H), 1.94 (m, 3H), 1.75 (d, J=13.57, 1H), 1.47 (m, 3H), 1.26 (m, 1H).

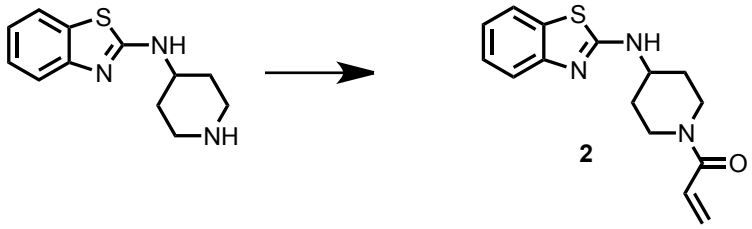

2

2 1-(4-(benzo[*d*]thiazol-2-ylamino)piperidin-1-yl)prop-2-en-1-one: *N*-(piperidin-4-yl)benzo[*d*]thiazol-2-amine (58mg, 1 eq, 0.213 mmol) was dissolved in 2mL acetonitrile at ambient temperature. TEA (60uL, 2eq, 0.427mmol) was added at ambient temperature. The reaction was cooled to 0°C. Acryloyl chloride (19uL, 1.1 eq, 0.235mmol) was added. The reaction was quenched with 5mL saturated NaHCO3 and left stirring for 15 minutes at ambient temperature. The reaction was extracted with ethyl acetate (5mL x 3), dried over Na_2SO4. The compound was purified by flash chromatography on silica gel (0-15% dichloromethane: methanol) to get the desired product (7mg, 11%yield) as a yellow oil.

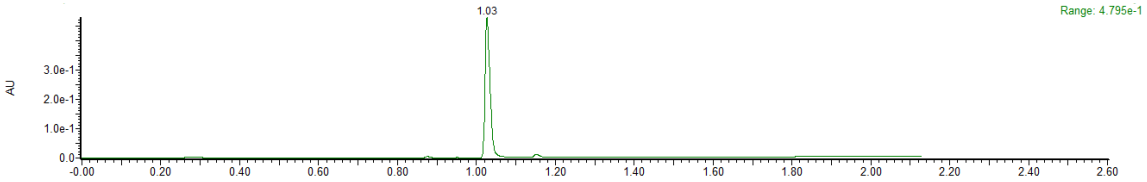

HRMS $C_{15}H_{18}N_3OS$ $[M+H]^+$ expected mass: 288.1171; observed: 288.1176. ^{1}H NMR (400 MHz, $CDCl_3$) **δ** 7.58 (d, J=8.06, 1H), 7.54 (d, J=8.08, 1H), 7.30 (t, J=8.07, 1H), 7.10 (t, J=7.75, 1H), 5.17 (s, 1H), 4.58 (s, 1H), 4.00 (s, 2H), 3.27 (t, J=12.29, 1H), 2.97 (t, J=11.96, 1H), 2.23 (m, 2H), 1.63 (s, 2H),

1.49 (s, 2H). ^{13}C NMR (500 MHz, $CDCl_3$) **δ** 165.63, 165.61, 152.44, 130.53, 128.25, 127.62, 126.16, 122.04, 120.94, 119.22, 52.16, 44.66, 41.02, 33.07, 32.08.

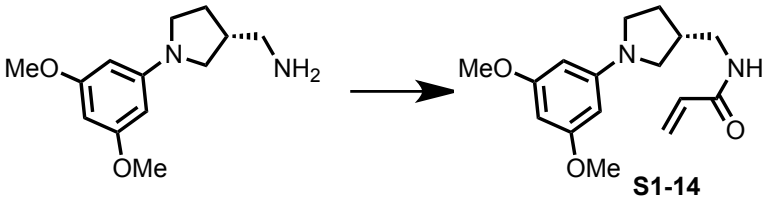

S1-14

S1-14 (*R*)-*N*-((1-(3,5-dimethoxyphenyl)pyrrolidin-3-yl)methyl)acrylamide:

1-Ethyl-3-(3-dimethylaminopropyl)carbodiimide(11mg, 1.4eq, 0.7mmol) was dissolved in 1mL dimethylformamide at ambient temperature. The reaction was cooled to 0°C. DIPEA (44uL, 5 eq, 0.25mmol), and then hydroxybenzotriazole (11mg, 1.4eq, 0.7mmol) was added. Acrylic acid (5uL, 1.4eq, 0.7mmol) was added to the reaction, and was stirred for 30 minutes. (R)-(1-(3,5-dimethoxyphenyl)pyrrolidin-3-yl)methanamine (12mg, 1 eq, 0.051mmol) was added at 0°C. The reaction was washed with 5mL saturated NaCl. The product was extracted with ethyl acetate (5mL x 3) and dried over Na_2SO4. The compound was purified by flash chromatography on silica gel (5-100% hexanes: ethyl acetate) to get the desired product (2.3mg, 16% yield) as a yellow oil. MS $C_{16}H_{22}N_2O_3$ $[M+H]^+$ expected: 291.1703, observed: 291.1732. ^{1}H NMR (400 MHz, $CDCl_3$) **δ** 6.30 (d, J=16.73, 1H), 6.09 (dd, J=16.54, 9.73, 1H), 5.89 (m, 1H), 5.74 (d, J=1.95, 2H), 5.67 (d, J=9.73, 1H), 3.78 (s, 6H), 3.40 (m, 4), 3.28 (m, 1H), 3.04 (m, 1H), 2.59 (m, 1H), 2.29 (m, 1H), 1.78 (m, 1H).

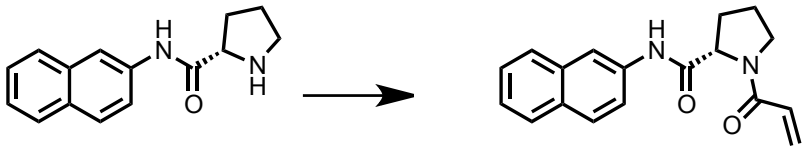

1

1 (1R)-2-acryloyl-*N*-(naphthalen-2-yl)cyclopentanecarboxamide:

L-Proline-2-naphthylamide hydrochloride (55.5mg, 1 eq, 0.20mmol) was dissolved in 2mL acetonitrile. TEA (58uL, 2eq, 0.414mmol) was added at ambient temperature. The reaction was cooled to 0°C. Acryloyl chloride (19uL, 1.1 eq, 0.228mmol) was added. The reaction was quenched with 5mL saturated NaHCO3 and left stirring for 15 minutes at ambient temperature. The reaction was extracted with ethyl acetate (5mL x 3), dried over Na_2SO4. The compound was purified by flash chromatography on silica gel (5-95% hexanes: ethyl acetate) to get the desired product (39.4mg, 67%yield) as a white, crystalline solid.

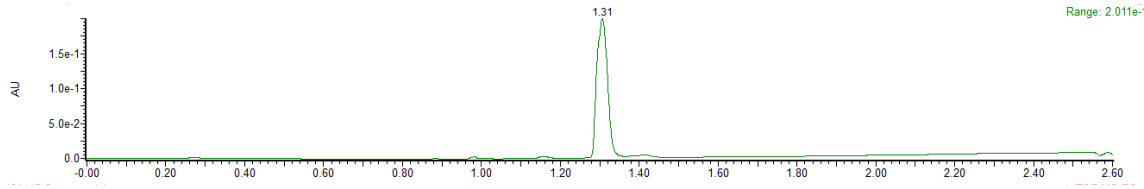

HRMS $C_{18}H_{18}N_2O_2Na$ $[M+Na]^+$ expected mass: 317.1266; observed: 317.1271. ^{1}H NMR (500MHz, $CDCl_3$) **δ** 10.02 (s, 1H), 8.23 (s, 1H), 7.73 (m, 3H), 7.45 (dd, J=8.82, 1.98, 1H), 7.41 (t, J=7.39, 1H), 7.35 (t, J=7.52, 1H), 6.52 (d, J=6.38, 2H), 5.82 (t, J=6.31, 1H), 4.94 (d, J=7.67, 1H), 3.72 (t, J=9.60, 1H), 3.57 (m, 1H), 2.66 (dd, J=12.48, 6.56, 1H), 2.22 (m, 1H), 2.09 (m, 1H), 1.88 (m, 1H). ^{13}C NMR (500MHz, $CDCl_3$) **δ** 169.06, 166.74, 135.92, 133.97, 130.57, 129.63, 128.62, 127.99, 127.74, 127.57, 126.37, 124.80, 120.21, 116.39, 60.99, 47.82, 26.54, 25.21.

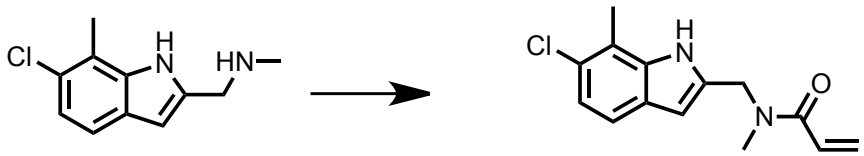

S1-15

S1-15 *N*-((6-chloro-7-methyl-1*H*-indol-2-yl)methyl)-*N*-methylacrylamide:

6-chloro-2-methyl-1H-indol-2-y methyl methylamine (50mg, 1eq, 0.24 mmol) was dissolved in 2mL acetonitrile. TEA was added (67uL, 2eq, 0.48mmol) was added at ambient temperature. The reaction was cooled to 0°C. Acryloyl chloride (21uL, 1.1 eq, 0.26mmol) was added. The reaction was quenched with 5mL saturated NaHCO3 and left stirring for 15 minutes at ambient temperature. The reaction was extracted with ethyl acetate (5mL x 3), dried over Na_2SO4. The compound was purified by flash chromatography on silica gel (5-100% hexanes: ethyl acetate) to get the desired product (14.1mg, 22%yield), as an orange oil. HRMS $C_{14}H_{15}ClN_2ONa$ $[M+Na]^+$ expected mass: 285.0771; observed: 285.0776. ^{1}H NMR (400 MHz, $CDCl_3$) **δ** 7.31 (d, J=8.45, 1H) 7.08 (d, J=8.49, 1H) 6.57 (dd, J=16.73, 10.30, 1H), 6.41 (dd, J=16.73, 1.93, 1H), 6.38 (d, J = 2.11, 1H), 5.77 (dd, J=10.45, 1.83, 1H), 4.60 (s, 2H) 3.10 (s, 3H), 2.49 (s, 3H).

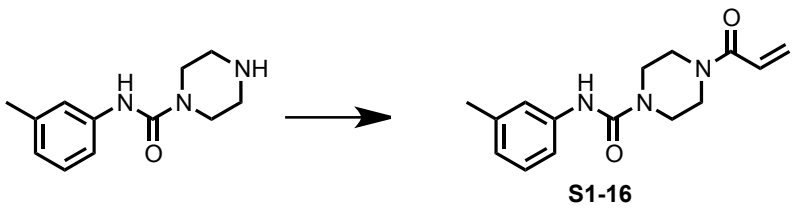

S1-16

S1-16 4-acryloyl-*N*-(*m*-tolyl)piperazine-1-carboxamide:

N-(*m*-tolyl)piperazine-1-carboxamide (35.6mg, 1 eq, 0.162 mmol) was dissolved in 2mL ACN. TEA was added (45uL, 2 eq, 0.324 mmol). The reaction was cooled to 0°C. Acryloyl chloride (13uL, 1 eq, 0.162 mmol) was added. The reaction was quenched with 5mL saturated NaHCO3

and left stirring for 15 minutes at ambient temperature. The reaction was extracted with ethyl acetate (5mL x 3), dried over Na_2SO4. The compound was purified twice by flash chromatography on silica gel (5-100% hexanes: ethyl acetate (to get the desired product (3.7mg, 8% yield) as a yellow powder. HRMS $C_{15}H_{20}N_3O_2$ $[M+H]^+$ expected mass: 274.1556; observed: 274.1563. ^{1}H NMR (500 MHz, $CDCl_3$) **δ** 7.21 (s, 1H), 7.18 (t, J=7.88, 1H), 7.11 (d, J=8.00, 1H), 6.88 (d, J=7.70, 1H), 6.57 (dd, J=16.79, 10.37, 1H), 6.35 (dd, J=16.85, 1.86), 6.34 (s, 1H), 5.76 (dd, J=10.53, 1.83, 1H), 3.64 (m, 8H), 2.33 (s, 3H)**.** ^{13}C NMR (500 MHz, $CDCl_3$) **δ** 167.72, 157.91, 140.58, 139.48, 129.47, 128.96, 128.76, 125.03, 122.82, 119.30, 46.70, 45.19, 44.93, 43.00, 21.55.

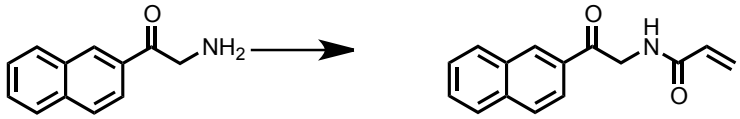

S1-17

S1-17 *N*-(2-(naphthalen-2-yl)-2-oxoethyl)acrylamide:

2-(naphthalen-2-yl)-2-oxoethanaminium chloride (25.3mg, 1 eq, 0.114 mmol) was dissolved in 2mL ACN. TEA was added (32uL, 2 eq, 0.228 mmol). The reaction was cooled to 0°C. Acryloyl chloride (9uL, 1 eq, 0.114 mmol) was added. The reaction was quenched with 5mL saturated NaHCO3 and left stirring for 15 minutes at ambient temperature. The reaction was extracted with ethyl acetate (5mL x 3), dried over Na_2SO4. The compound was purified by flash chromatography on silica gel (5-100% hexanes: ethyl acetate), followed by RP-HPLC (25-90% gradient) to get the desired product (3.7mg, 14% yield) as a white solid. HRMS $C_{15}H_{14}NO_2$ $[M+H]^+$ expected mass: 240.1025; observed: 240.1029. ^{1}H NMR (500 MHz, $CDCl_3$) **δ** 8.80 (d, J=8.66, 1H), 8.08 (d, J=8.23, 1H), 8.04 (d, J=7.35, 1H), 7.90 (d, J=8.23, 1H), 7.65 (t, J=7.66, 1H),

7.58(t, J=7.58, 1H), 7.54 (d, J=7.66, 1H), 6.78 (s, 1H), 6.39 (dd, J=17.15,1.48, 1H), 6.29 (dd, J=17.02, 10.12, 1H), 5.75 (dd, J=10.18, 1.38, 1H). 4.91 (s, 2H).

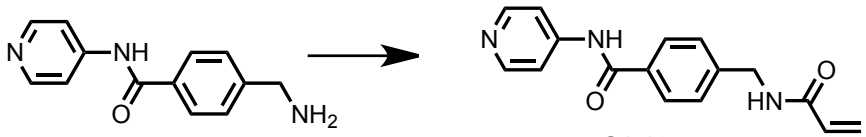

S1-18

S1-18 4-(acrylamidomethyl)-*N*-(pyridin-4-yl)benzamide:

(4-(pyridin-4-ylcarbamoyl)phenyl)methanaminium chloride hydrochloride (25.6mg, 1 eq, 0.085 mmol) was dissolved in 2mL acetonitrile. TEA was added (75 uL, 6 eq, 0.51 mmol). The reaction was cooled to 0°C. Acryloyl chloride (7uL, 1 eq, 0.085mmol) was added. The reaction was quenched with 5mL saturated NaHCO3 and left stirring for 15 minutes at ambient temperature. The reaction was extracted with ethyl acetate (5mL x 3), dried over Na_2SO4. The compound was purified by flash chromatography on silica gel (0-15% dichloromethane: methanol) followed by RP-HPLC with a gradient of 25-90% to get the desired product (1.1mg, 5% yield) as a white solid. HRMS $C_{16}H_{16}N_3O_2$ $[M+H]^+$ expected mass: 282.1243; observed: 282.1235. ^{1}H NMR (500MHz, CD_3OD) **δ** 8.44 (d, J = 6.3, 2H), 7.94(d, J=8.45, 2H), 7.84 (d, J=6.3, 2H), 6.32 (dd, J = 17.19, 9.16, 1H) 6.27 (dd, J = 17.19, 2.87, 1H), 5.71 (dd, J = 9.20, 2.83), 4.54 (s, 2H).

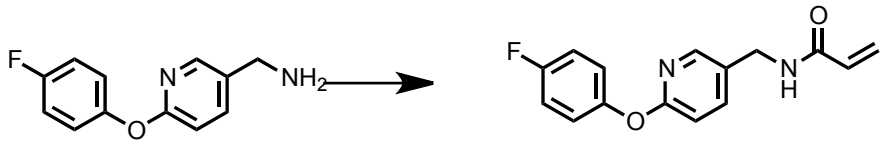

S1-19

S1-19 *N*-((6-(4-fluorophenoxy)pyridin-3-yl)methyl)acrylamide:

(6-(4-fluorophenoxy)pyridin-3-yl)methanamine hydrochloride (23.0mg, 1 eq, 0.105 mmol) was dissolved in 2mL ACN. TEA was added (29uL, 2 eq, 0.211 mmol). The reaction was cooled to 0°C. Acryloyl chloride (9uL, 1 eq, 0.105 mmol) was added. The reaction was quenched with 5mL saturated NaHCO3 and left stirring for 15 minutes at ambient temperature. The reaction was extracted with ethyl acetate (5mL x 3), dried over Na_2SO4. The compound was purified by flash chromatography on silica gel (5-100% hexanes: ethyl acetate), followed by RP-HPLC (25-90% gradient) to get the desired product (0.8 mg, 3% yield), as an opaque oil. HRMS $C_{15}H_{14}FN_2O_2$ $[M+H]^+$ expected mass: 273.1039; observed: 273.1039. ^1H NMR (400 MHz, $CDCl_3$) **δ** 8.09 (d, J=2.52, 1H), 7.69 (dd, J=8.47, 2.52, 1H), 6.89 (d, J=8.47), 7.08 (d, J=6.47, 4H), 6.33 (dd, J=16.99,1.20, 1H), 6.09 (dd, J=16.99, 10.26, 1H), 5.81 (s, 1H), 5.70 (dd, J=10.38, 1.21), 4.49 (s, 1H), 4.47 (s, 1H).

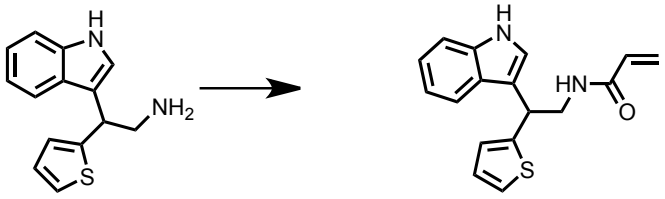

S1-20

S1-20 *N*-(2-(1*H*-indol-3-yl)-2-(thiophen-2-yl)ethyl)acrylamide:

2-(1*H*-indol-3-yl)-2-(thiophen-2-yl)ethanamine (25.1mg, 1 eq, 0.104 mmol) was dissolved in 2mL ACN. TEA was added (30uL, 2 eq, 0.208 mmol). The reaction was cooled to 0°C. Acryloyl chloride (8uL, 1 eq, 0.104 mmol) was added. The reaction was quenched with 5mL saturated NaHCO3 and left stirring for 15 minutes at ambient temperature. The reaction was extracted with ethyl acetate (5mL x 3), dried over Na_2SO4. The compound was purified by flash

chromatography on silica gel (5-100% hexanes:EtOAC), followed by RP-HPLC (25-90% gradient) to get the desired product (4.7mg, 15**%** yield) as an opaque oil. HRMS $C_{17}H_{16}N_2OS$ $[M-H]^-$ expected mass: 295.0911, observed: 295.0901. ^{1}H NMR (500 MHz, $CDCl_3$) **δ** 7.57 (d, J=8, 1H), 7.38 (d, J=8.07, 1H), 7.21 (t, J=7.62, 1H), 7.18 (m, 1H), 7.13 (d, J=2.37, 1H), 7.09 (t, J=7.62, 1H), 6.96 (m, 2H), 4.77 (t, J= 7.22, 1H), 4.14 (m, 1H), 3.97 (m, 1H). ^{13}C NMR (500 MHz, $CDCl_3$) **δ** 165.63, 146.15, 136.59, 130.86, 126.95, 126.84, 126.53, 124.93, 124.22, 122.62, 122.04, 119.93, 119.57, 116.70, 111.43, 45.03, 38.29.

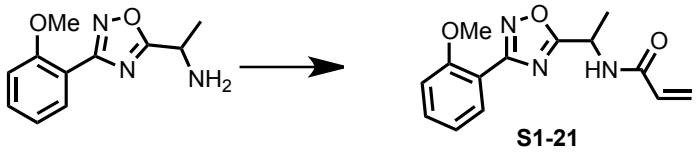

S1-21

S1-21 *N*-(1-(3-(2-methoxyphenyl)-1,2,4-oxadiazol-5-yl)ethyl)acrylamide:

1-[3-(2-methoxyphenyl)-1,2,4-oxadiazol-5-yl]ethan-1-amine hydrochloride (26.8mg, 1 eq, 0.105 mmol) was dissolved in 2mL ACN. TEA was added (30uL, 2 eq, 0.21 mmol). The reaction was cooled to 0°C. Acryloyl chloride (9uL, 1 eq, 0.105 mmol) was added. The reaction was quenched with 5mL saturated NaHCO3 and left stirring for 15 minutes at ambient temperature. The reaction was extracted with ethyl acetate (5mL x 3), dried over Na_2SO4. The compound was purified by flash chromatography on silica gel (5-100% hexanes:EtOAC), followed by RP-HPLC (25-90% gradient) to get the desired product (5.1mg, 20% yield), as an opaque oil. HRMS $C_{14}H_{16}N_3O_3$ $[M+H]^+$ expected mass: 274.1192; observed: 274.1198. ^{1}H NMR (500 MHz, $CDCl_3$) **δ** 7.97 (dd, J=7.68, 1.76, 1H), 7.49 (m, 1H), 7.07 (dd, 7.69, 14.81, 1H), 6.37 (dd, J=17.05, 1.05, 1H), 6.18 (dd, J=17.00, 10.38, 1H), 5.74 (J=10.35, 1.05, 1H), 5.59 (q, J=7.12, 1H), 3.97 (s, 3H), 1.68 (d, J=7.09, 3H).

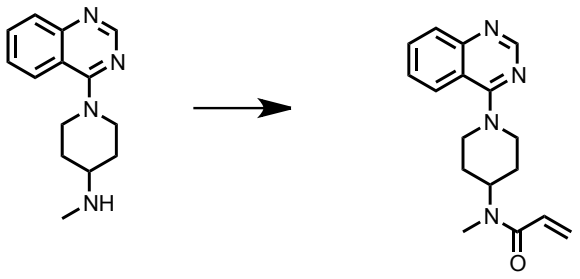

S1-22

S1-22 *N*-methyl-*N*-(1-(quinazolin-4-yl)piperidin-4-yl)acrylamide:

N-methyl-1-(quinazolin-4-yl)piperidin-4-amine (53.7mg, 1 eq, 0.222 mmol) was dissolved in 2mL ACN. TEA was added (62uL, 2 eq, 0.443 mmol). The reaction was cooled to 0°C. Acryloyl chloride (18uL, 1 eq, 0.222 mmol) was added. The reaction was quenched with 5mL saturated NaHCO3 and left stirring for 15 minutes at ambient temperature. The reaction was extracted with ethyl acetate (5mL x 3), dried over Na_2SO4. The compound was purified by flash chromatography on silica gel (0-15% DCM:methanol), followed by RP-HPLC (25-55% gradient) to get the desired product (3.1mg, 5% yield), as an opaque oil. HRMS $C_{17}H_{21}N_4O$ $[M+H]^+$ expected mass: 297.1715; observed: 297.1717. ^{1}H NMR (500 MHz, MeOD) **δ** 8.59 (d, J=4.77, 1H), 8.48 (s, 1H), 8.06 (d, J=8.41, 1H), 7.82 (m, 1H), 7.57 (m, 1H), 6.90 (dd, 16.90, 10.90, 1H), 6.75 (dd, 16.88, 10.50, 1H), 6.23 (dd, J=16.91, 10.36, 1H), 5.76 (dd, 10.65, 19.7, 1H), 4.77 (m, 1H), 4.57 (m, 1H), 4.28 (m, 1H), 3.03 (s, 1H), 2.93 (s, 1H), 2.09 (m, 3H), 1.83 (m, 2H).

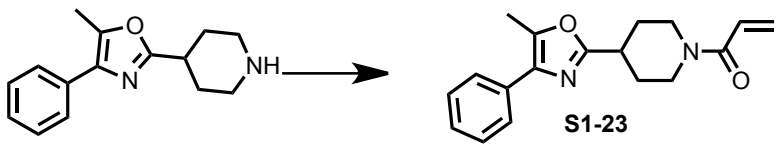

S1-23

S1-23 1-(4-(5-methyl-4-phenyloxazol-2-yl)piperidin-1-yl)prop-2-en-1-one:

5-methyl-4-phenyl-2-(piperidin-4-yl)oxazole (27.0mg, 1eq, 0.111 mmol) was dissolved in 2mL CAN. TEA was added (31uL, 2eq, 0.223 mmol). The reaction was cooled to 0°C. Acryloyl chloride (9uL, 1 eq, 0.111 mmol) was added. The reaction was quenched with 5mL saturated $NaHCO_3$ and left stirring for 15 minutes at ambient temperature. The reaction was extracted with ethyl acetate (5mL x 3), and dried over Na_2SO_4. The compound was purified by flash chromatography on silica gel (5-100% hexanes: ethyl acetate), followed by RP-HPLC (45-95% gradient) to get the desired product (3.1mg, 5% yield), as a white solid. HRMS $C_{18}H_{21}N_2O_2$ $[M+H]^+$ expected mass: 297.1603; observed: 297.1617. ^{1}H NMR (400 MHz, $CDCl_3$) **δ** 7.62 (d, J=8.06, 2H), 7.41 (t, J=7.52, 2H), 7.29 (t, J= 7.42, 1H), 6.60 (dd, J=16.87, 10.59, 1H), 6.28 (dd, J=16.82, 1.90, 1H), 5.70 (dd, J=10.56, 1.84, 1H), 3.12 (m, 1H), 3.08 (m, 2H), 2.50 (s, 3H), 2.13 (m, 2H), 1.89 (m, 2H), 1.65 (m, 2H).

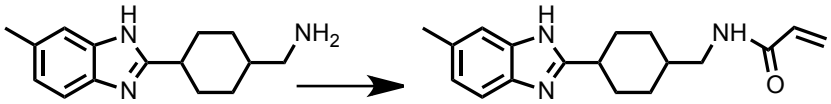

S1-24

S1-24 *N*-((4-(6-methyl-1*H*-benzo[*d*]imidazol-2-yl)cyclohexyl)methyl)acrylamide:

(4-(6-methyl-1*H*-benzo[*d*]imidazol-2-yl)cyclohexyl)methanamine (50.8mg, 1 eq, 0.209mmol) was dissolved in 2mL ACN. TEA was added (174uL, 6 eq, 1.254 mmol). The reaction was cooled to 0°C. Acryloyl chloride (17uL, 1 eq, 0.209 mmol) was added. The reaction was quenched with 5mL saturated NaHCO3 and left stirring for 15 minutes at ambient temperature. The reaction was extracted with ethyl acetate (5mL x 3), dried over Na_2SO4. The compound was purified by flash chromatography on silica gel (0-15% hexanes:EtOAC), followed by RP-HPLC (5-95%

gradient) to get the desired product (4.6mg, 7% yield), as a white solid. HRMS $C_{18}H_{24}N_3O$ $[M+H]^+$ expected mass: 298.1919; observed: 298.1925. ^{1}H NMR (500 MHz, MeOD) **δ** 7.39 (d, J=8.35, 1H), 7.31 (s, 1H), 7.07 (d, J=8.35, 1H), 6.27 (dd, J=17.05, 9.41, 1H), 6.22 (dd, J = 17.05, 2.68, 1H), 5.66 (dd, J=9.41, 2.64, 1H), 3.18 (d, J=6.80, 2H), 2.89 (m, 1H), 2.45 (s, 3H), 2.16 (d, J=13.01, 2H), 1.76 (d, J=13.01, 2H), 1.69 (m, 2H), 1.66 (m, 1H), 1.19 (d, 2H).

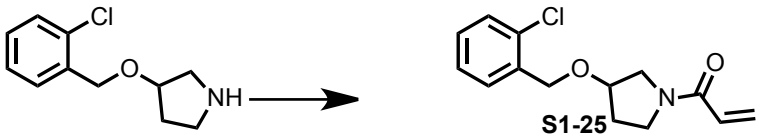

S1-25

S1-25 1-(3-((2-chlorobenzyl)oxy)pyrrolidin-1-yl)prop-2-en-1-one:

3[(2-chlorobenzyl)oxy]pyrrolidine hydrochloride (50.3mg, 1 eq, 0.203mmol) was dissolved in 2mL ACN. TEA was added (57uL, 2 eq, 0.405 mmol). The reaction was cooled to 0°C. Acryloyl chloride (16uL, 1 eq, 0.203 mmol) was added. The reaction was quenched with 5mL saturated NaHCO3 and left stirring for 15 minutes at ambient temperature. The reaction was extracted with ethyl acetate (5mL x 3), dried over Na_2SO4. The compound was purified by flash chromatography on silica gel (5-100% hexanes:EtOAc), followed by RP-HPLC (45-95% gradient) to get the desired product (1.5mg, 3% yield), as an opaque oil. HRMS $C_{14}H_{17}ClNO_2$ $[M+H]^+$ expected mass: 266.0948; observed: 266.0959. ^{1}H NMR (500 MHz, MeOD, 1:1 rotamers) **δ** 7.48 (m, 1H), 7.38 (m, 1H), 7.29 (m, 2H), (6.63 + 6.58) (rotamers dd, J=16.83, 10.51, 1H), (6.27+6.26) (dd, rotamers, J=16.86, 1.88, 1H), (5.75+5.73) (rotamers, dd, J=10.46, 1.89, 1H), 4.65 (m, 2H), 4.32 (m, 1H), 3.75 (m, 2H), 3.68 (m, 1H), 3.56 (m, 1H), 2.14 (m, 2H).

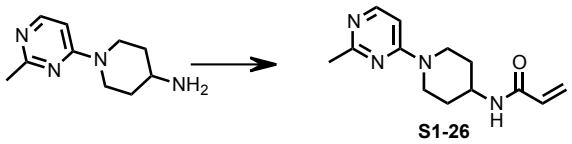

S1-26

S1-26 *N*-(1-(2-methylpyrimidin-4-yl)piperidin-4-yl)acrylamide:

1-(2-methylpyrimidin-4-yl)piperidin-4-amine (34.1mg, 1 eq, 0.177mmol) was dissolved in 2mL ACN. TEA was added (50uL, 2 eq, 0.355 mmol). The reaction was cooled to 0°C. Acryloyl chloride (14uL, 1 eq, 0.177 mmol) was added. The reaction was quenched with 5mL saturated NaHCO3 and left stirring for 15 minutes at ambient temperature. The reaction was extracted with ethyl acetate (5mL x 3), dried over Na_2SO4. The compound was purified by flash chromatography on silica gel (0-15% DCM:methanol), followed by RP-HPLC (20-55% gradient) to get the desired product (5.1mg, 12% yield), as a white solid. HRMS $C_{13}H_{19}N_4O$ $[M+H]^+$ expected mass: 247.1559; observed: 247.1561.^{1}H NMR (500 MHz, MeOD) **δ** 8.32 (s, 1H), 8.04 (d, J=7.15, 1H), 6.83 (d, J=7.14, 1H), 6.58 (dd, J=6.58, 5.52, 1H), 6.24 (m, 2H), 4.10 (m, 1H), 3.26 (m, 2H), 2.50 (s, 3H), 2.04 (m, 2H), 1.51 (m, 2H).

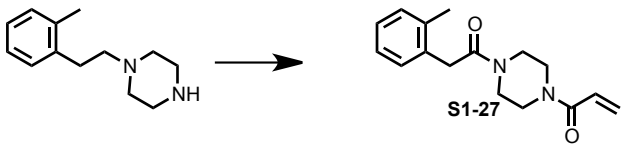

S1-27

S1-27 1-(4-(2-(*o*-tolyl)acetyl)piperazin-1-yl)prop-2-en-1-one:

1-(piperazin-1-yl)-2-(*o*-tolyl)ethanone (67mg, 1 eq, 0.307mmol) was dissolved in 2mL ACN. TEA was added (86uL, 2 eq, 0.614 mmol). The reaction was cooled to 0°C. Acryloyl chloride (25uL, 1 eq, 0.307 mmol) was added. The reaction was quenched with 5mL saturated NaHCO3 and left stirring for 15 minutes at ambient temperature. The reaction was extracted with ethyl acetate

(5mL x 3), dried over Na_2SO4. The compound was purified by RP-HPLC (5-95% gradient) to get the desired product 8.4mg, 10% yield), as an opaque oil. HRMS $C_{16}H_{21}N_2O_2$ $[M+H]^+$ expected mass: 273.1603; observed: 273.1608.^{1}H NMR (400 MHz, $CDCl_3$) **δ** 7.15 (m, 4H), 6.53 (m, 1H), 6.31 (d, J=16.75, 1H), 5.73 (d, J=9.76, 1H), 3.71 (s, 4H), 3.57 (s, 2H), 3.43 (s, 2H), 2.29 (s, 3H).

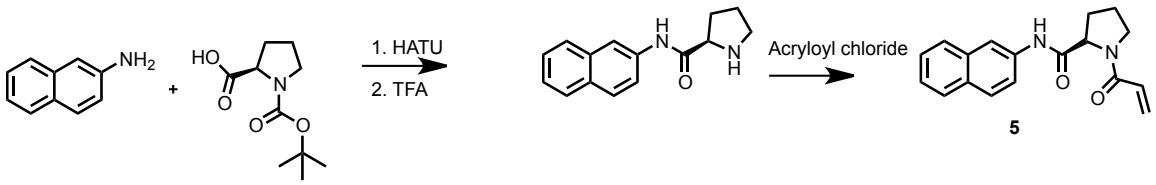

5 (*R*)-1-acryloyl-*N*-(naphthalen-2-yl)pyrrolidine-2-carboxamide:

N-Boc-L-proline (100mg, 0.465 mmol, 1 eq) was dissolved in 1mL DMF and DIPEA (324uL, 4 eq, 1.86 mmol). The solution was cooled to 0°C and HATU (194mg, 0.511 mmol, 1.1 eq) was added. The reaction was stirred for 20 minutes followed by an addition of 2-amino-naphthalene (73mg, 0.511 mmol, 1.1eq). After 2-5 hours, the solution was diluted with 10mL brine and extracted with EtOAc (3x10mL). The combined organic layers were dried over Na_2SO_4, filtered, and evaporated to dryness *in vacuo*. The residue was purified by flash chromatography on silica gel (5-100%) EtoAC:hexanes to afford the desired product, (*R*)-*tert*-butyl 2-(naphthalen-2-ylcarbamoyl)pyrrolidine-1-carboxylate.

The product was dissolved in 2mL DCM. The mixture was cooled to 0°C and 1mL TFA was added. When the reaction was complete, the mixture was quenched using 5mL NaHCO3 and the product was extracted with 3x3mL DCM. The crude product, (*R*)-*N*-(naphthalen-2-yl)pyrrolidine-2-carboxamide, was used without further purification.

(*R*)-*N*-(naphthalen-2-yl)pyrrolidine-2-carboxamide (38.6 mg, 0.161 mmol, 1 eq) was dissolved in 2mL ACN to which TEA (45uL, 0.321 mmol, 2 eq) was added. The solution was cooled to 0°C upon which acryloyl chloride (14uL, 0.177 mmol, 1.1 eq) was added. After 30 minutes, the reaction was quenched with 5mL NaHCO3. The solution was left to stir for 15 minutes. The mixture was extracted with ethyl acetate (3x5mL). The combined organic layers were dried with Na_2SO_4, filtered, and evaporated *in vacuo*. The residue was purified by flash chromatography on silica gel (5-100%) hexanes: ethyl acetate to get the desired product (*R*)-1-acryloyl-*N*-(naphthalen-2-yl)pyrrolidine-2-carboxamide (14.6mg, 31% yield), as an opaque oil.

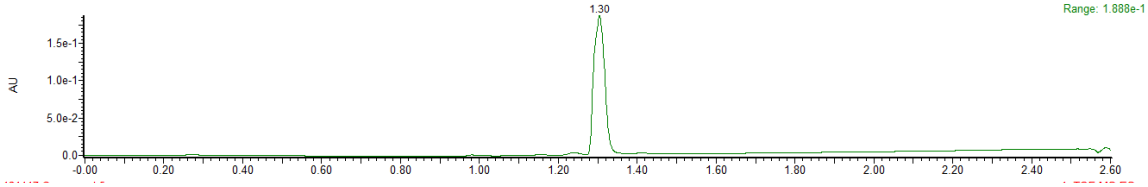

HRMS $C_{18}H_{18}N_2O_2Na$ $[M+Na]^+$ expected mass: 317.1266; observed: 317.1267. ^{1}H NMR (400 MHz, $CDCl_3$) **δ** 9.99 (s, 1H), 8.23 (s, 1H), 7.74 (m, 3H), 7.47 (dd, J=8.84, 2.12, 1H), 7.42 (t, J=6.82, 1H), 7.36 (t, J=7.44, 1H). 6.52 (J=6.10, 2H), 5.82 (t, J=6.10, 1H), 4.94 (d, J=7.82, 1H), 3.72 (m, 1H), 3.58 (m, 1H), 2.68 (dd, J=12.62, 6.50, 1H), 2.21 (m, 1H), 2.09 (m, 1H), 1.86 (m, 1H). ^{13}C NMR (500 MHz, $CDCl_3$) **δ** 169.01, 166.81, 135.92, 134.00, 130.60, 129.68, 128.66, 127.98, 127.76, 127.60, 126.42, 124.84, 120.24, 116.42, 60.99, 47.84, 26.46, 25.23.

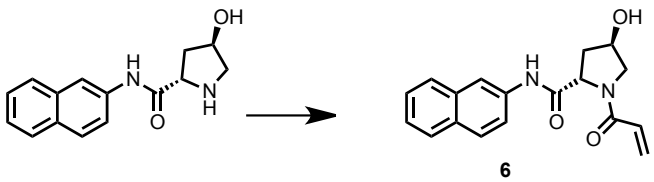

6

6 (2*S*,4*R*)-1-acryloyl-4-hydroxy-*N*-(naphthalen-2-yl)pyrrolidine-2-carboxamide:

4-hydroxy-*N*-(naphthalen-2-yl)pyrrolidine-2-carboxamide (50mg, 1 eq, 0.195 mmol) was dissolved in 4mL mixture of 1:1 ACN:DMF. TEA (164uL, 1.170 mmol, 6 eq) was added. The solution was cooled to 0°C upon which acryloyl chloride (17uL, 0.215 mmol, 1.1 eq) was added. After 30 minutes, the reaction was quenched with 5mL NaHCO3. The solution was left to stir for 15 minutes. The mixture was extracted with ethyl acetate (3x5mL). The combined organic layers were dried with Na_2SO_4, filtered, and evaporated *in vacuo*. The residue was purified by flash chromatography on silica gel (5-100%) hexanes: ethyl acetate to get the desired product (2*S*,4*R*)-1-acryloyl-4-hydroxy-*N*-(naphthalen-2-yl)pyrrolidine-2-carboxamide (10.5mg, 17% yield), as a white solid. MS

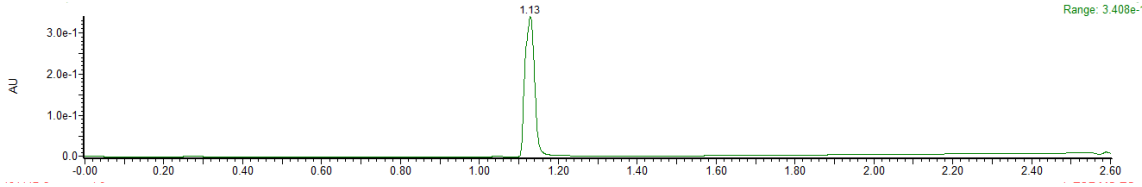

HRMS $C_{18}H_{18}N_2O_3Na$ $[M+Na]^+$ expected mass: 333.1215; observed: 333.1219. ^{1}H NMR (400 MHz, $(CD_3)_2SO$, 9:1 rotamers) **δ** (10.28+10.41) (s, 1H), 8.29 (s, 1H), 7.83 (m, 3H), 7.59 (d, J=8.85, 1H), 7.46 (t, J=6.76, 1H), 7.39 (t, 6.90, 1H), (6.63 + 6.36) (dd, J=16.67, 10.05, 1H), 6.13 (J=16.62, 2.08, 1H), (5.71 + 5.64) (J=10.15, 2.28, 1H), 5.20 (d, J=3.56, 1H), (4.62 + 4.76) (t, J=7.93, 1H), (4.43 + 4.35) (s, 1H), 3.76 (dd, J=10.69, 4.49, 1H), 3.58 (d, J=10.69, 1H), 2.16 (m, 1H), 1.99 (m, 1H). ^{13}C NMR (500 MHz, MeOD) **δ** 172.94, 167.25, 137.18, 135.21, 132.19, 129.87, 129.52, 128.88, 128.59, 127.46, 126.05, 121.29, 121.13, 118.06, 71.22, 61.38, 56.94, 39.18.

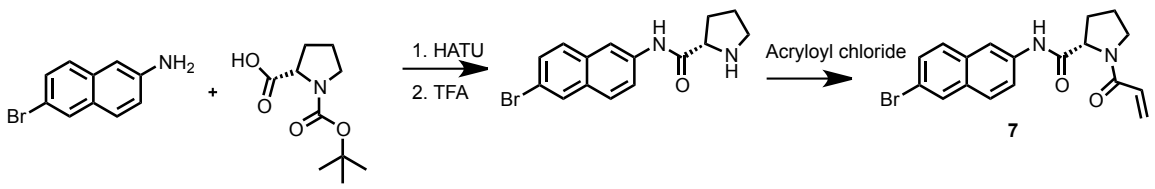

7 (*S*)-1-acryloyl-*N*-(6-bromonaphthalen-2-yl)pyrrolidine-2-carboxamide:

N-Boc-L-proline (100mg, 0.465 mmol, 1 eq) was dissolved in 1mL DMF. The solution was cooled to 0°C and HATU (582mg, 1.533 mmol, 3.3 eq) was added. The reaction was stirred for 15 minutes followed by an addition of 2-amino-6-bromo-naphthalene (114mg, 0.511 mmol, 1.1eq). After 6 hours, the solution was diluted with 10mL brine and extracted with EtOAc (3x10mL). The combined organic layers were dried over Na_2SO_4, filtered, and evaporated to dryness *in vacuo*. The residue was purified by flash chromatography on silica gel (5-100%) EtoAC:hexanes to afford the desired product, (2*S*,4*R*)-*tert*-butyl-2-((6-bromonaphthalen-2-yl)carbamoyl)-4-hydroxypyrrolidine-1-carboxylate, (217mg, yield quantitative).

The product was dissolved in 2mL DCM. The mixture was cooled to 0°C and 1mL TFA was added. When the reaction was complete, the mixture was quenched using 5mL NaHCO3 and the product was extracted with 3x3mL DCM. The crude product, (*S*)-*N*-(6-bromonaphthalen-2-yl)pyrrolidine-2-carboxamide was used without further purification.

(*S*)-*N*-(6-bromonaphthalen-2-yl)pyrrolidine-2-carboxamide (83.8 mg, 0.263 mmol, 1 eq) was dissolved in 2mL ACN to which TEA (73uL, 0.525 mmol, 2 eq) was added. The solution was cooled to 0°C upon which acryloyl chloride (8uL, 0.104 mmol, 1.1 eq) was added. After 30 minutes, the reaction was quenched with 5mL NaHCO3. The solution was left to stir for 15 minutes. The mixture was extracted with ethyl acetate (3x5mL). The combined organic layers were dried with Na_2SO_4, filtered, and evaporated *in vacuo*. The residue was purified by flash

chromatography on silica gel (5-100%) hexanes: ethyl acetate, followed by RP-HPLC gradient of 5-95% to afford the desired product (*S*)-1-acryloyl-*N*-(6-bromonaphthalen-2-yl)pyrrolidine-2-carboxamide (14.2mg, 14%yield), as an opaque oil.

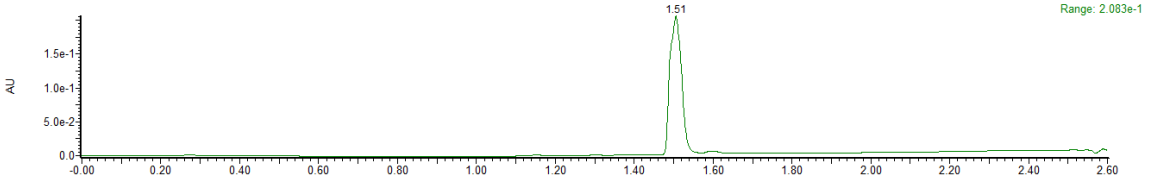

^{1}H NMR (400 MHz, $CDCl_3$). HRMS $C_{18}H_{18}BrN_2O_2$ $[M+H]^+$ expected mass: 373.0552; observed: 373.0553. **δ** 10.10 (s, 1H), 8.20 (s, 1H), 7.86 (s, 1H), 7.61 (d, J=8.78, 1H), 7.56 (d, J=8.78, 1H), 7.44 (m, 2H), 6.52 (dd, J=6.03, 1.41, 2H), 5.83 (dd, J=6.71, 5.44, 1H), 4.94 (d, J=7.68, 1H), 3.73 (m, 1H), 3.60 (m, 1H), 2.64 (m, 1H), 2.23 (m, 1H), 2.10 (m, 1H), 1.90 (m, 1H) ^{13}C NMR (400 MHz, $CDCl_3$) **δ** 169.23, 166.75, 136.38, 132.42, 131.52, 129.74, 129.70, 129.59, 129.38, 127.97, 127.70, 121.18, 118.54, 116.22, 61.04, 47.89, 26.64, 25.24.

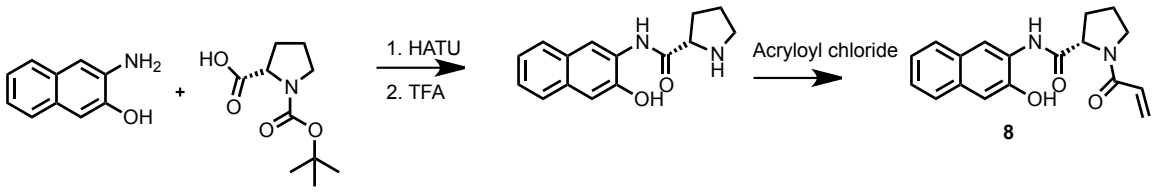

8

8 ((*S*)-1-acryloyl-*N*-(3-hydroxynaphthalen-2-yl)pyrrolidine-2-carboxamide:

N-Boc-L-proline (100mg, 0.465 mmol, 1 eq) was dissolved in 1mL DMF. The solution was cooled to 0°C and HATU (194mg, 0.511 mmol, 1.1 eq) was added. The reaction was stirred for 15 minutes followed by an addition of 3-amino-2-naphthol (81mg, 0.511 mmol, 1.1eq). After 12-18 hours, the solution was diluted with 10mL brine and extracted with EtOAc (3x10mL). The combined organic layers were dried over Na_2SO_4, filtered, and evaporated to dryness *in vacuo*.

The residue was purified by flash chromatography on silica gel (5-100%) hexanes: ethyl acetate to afford the desired product, (*S*)-*tert*-butyl 2-((3-hydroxynaphthalen-2-yl)carbamoyl)pyrrolidine-1-carboxylate, (27.3mg, 19% yield).

The product was dissolved in 2mL DCM. The mixture was cooled to 0°C and 1mL TFA was added. When the reaction was complete, the mixture was quenched using 5mL NaHCO3 and the product was extracted with 3x3mL DCM. The crude product, ((*S*)-*N*-(3-hydroxynaphthalen-2-yl)pyrrolidine-2-carboxamide, was used without further purification.

(*S*)-*N*-(3-hydroxynaphthalen-2-yl)pyrrolidine-2-carboxamide (24.3 mg, 0.095 mmol, 1 eq) was dissolved in 3mL ACN to which TEA (80uL, 0.570 mmol, 6 eq) was added. The solution was cooled to 0°C upon which acryloyl chloride (8uL, 0.104 mmol, 1.1 eq) was added. After 30 minutes, the reaction was quenched with 5mL NaHCO3. The solution was left to stir for 15 minutes. The mixture was extracted with ethyl acetate (3x5mL). The combined organic layers were dried with Na_2SO_4, filtered, and evaporated *in vacuo*. The residue was purified by flash chromatography on silica gel (5-100%) hexanes: ethyl acetate, followed by RP-HPLC gradient of 5-95% to afford the desired product ((*S*)-1-acryloyl-*N*-(3-hydroxynaphthalen-2-yl)pyrrolidine-2-carboxamide (1.7mg, 6% yield), as a white powder.

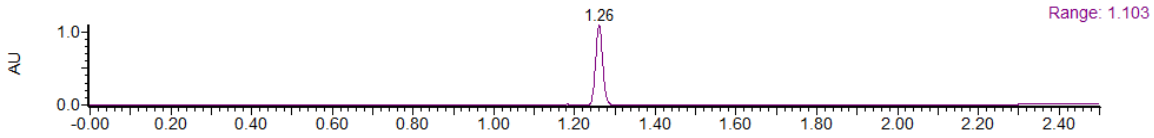

HRMS $C_{18}H_{18}N_2O_3Na$ $[M+Na]^+$ expected mass: 333.1215; observed: 333.1223. ^{1}H NMR (400 MHz, $CDCl_3$) **δ** 10.21 (s, 1H), 7.83 (s, 1H), 7.65 (d, J=7.99, 1H), 7.63 (d, J=7.99, 1H), 7.32 (m, 3H), 6.54 (d, J=5.93, 2H), 5.85 (t, J=5.92, 1H), 5.02 (d, J=7.51, 1H), 3.76 (t, J=9.13, 1H), 3.63 (q, J=9.06, 1H), 2.66 (q, J=6.21, 1H), 2.24 (m, 1H), 2.13 (m, 1H), 1.95 (m, 1H). ^{13}C NMR (500 MHz, $CDCl_3$) **δ**

170.47, 167.06, 147.27, 132.54, 130.28, 128.60, 127.75, 127.72, 127.29, 126.17, 125.14, 124.06, 119.90, 113.32, 60.72, 47.92, 26.77, 25.28.

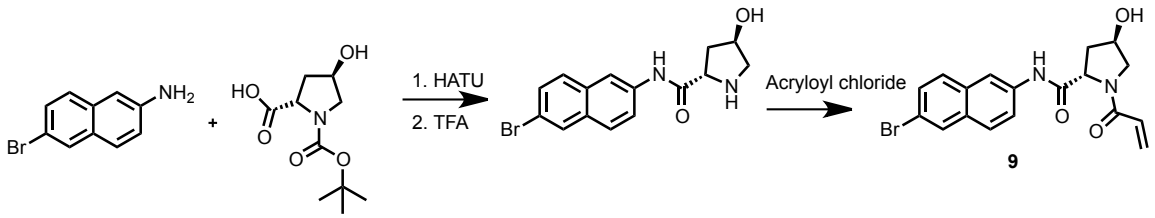

9

9 (2*S*,4*R*)-1-acryloyl-*N*-(6-bromonaphthalen-2-yl)-4-hydroxypyrrolidine-2-carboxamide: Trans-N-(tert-Butoxycarbonyl)-4-hydroxy-L-proline (100mg, 0.433 mmol, 1 eq) was dissolved in 1mL DMF. The solution was cooled to 0°C and HATU (329mg, 0.865mmol, 2 eq) was added. The reaction was stirred for 15 minutes followed by an addition of 2-amino-6-bromo-naphthalene (106mg, 0.476 mmol, 1.1eq). DMAP (5mg, 0.0433mmol, 0.1 eq) was added. After heating the solution to 50°C for 6 hours, the solution was diluted with 10mL brine and extracted with ethyl acetate (3x10mL). The combined organic layers were dried over Na_2SO_4, filtered, and evaporated to dryness *in vacuo*. The residue was purified by flash chromatography on silica gel (5-100%) hexanes: ethyl acetate to afford the desired product, (2*S*,4*R*)-*tert*-butyl 2-((6-bromonaphthalen-2-yl)carbamoyl)-4-hydroxypyrrolidine-1-carboxylate (199.8mg, yield quantitative).

The product was dissolved in 2mL DCM. The mixture was cooled to 0°C and 1mL TFA was added. After 5 hours, the solvent and excess TFA was removed *in vacuo* with 3x 5mL toluene. The crude product, (2*S*,4*R*)-*tert*-butyl 2-((6-bromonaphthalen-2-yl)carbamoyl)-4-hydroxypyrrolidine-1-carboxylate, was used without further purification.

(2*S*,4*R*)-*tert*-butyl 2-((6-bromonaphthalen-2-yl)carbamoyl)-4-hydroxypyrrolidine-1-carboxylate (37.3 mg, 0.086 mmol, 1 eq) was dissolved in 2mL ACN to which TEA (24uL, 0.172 mmol, 2 eq)

was added. The solution was cooled to 0°C upon which acryloyl chloride (8uL, 0.094 mmol, 1.1 eq) was added. After 30 minutes, the reaction was quenched with 5mL NaHCO3. The solution was left to stir for 15 minutes. The mixture was extracted with ethyl acetate (3x5mL). The combined organic layers were dried with Na_2SO_4, filtered, and evaporated *in vacuo*. The residue was purified by flash chromatography on silica gel (5-90%) hexanes: ethyl acetate to afford the desired product (2*S*,4*R*)-1-acryloyl-*N*-(6-bromonaphthalen-2-yl)-4-hydroxypyrrolidine-2-carboxamide (8.7mg, 26% yield), as a white powder.

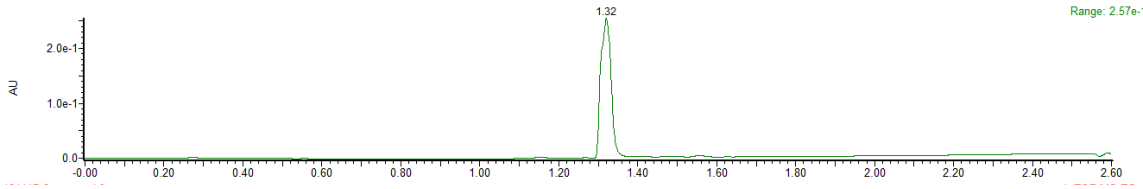

HRMS $C_{18}H_{17}BrN_2O_3Na$ $[M+Na]^+$ expected mass: 411.032; observed: 411.0333. ^{1}H NMR (400 MHz, $(CD_3)_2SO$, 4:1 rotamers) δ (10.36+10.48) (s, 1H), 8.32 (s, 1H), 8.12 (s, 1H), 7.86 (d, J=8.77, 1H), 7.77 (d, J=8.77, 1H), 7.63 (dd, J=8.86, 2.05, 1H), 7.57 (dd, J=8.81, 1.98, 1H), (6.63+6.35) (dd, J=16.73,10.30, 1H), 6.13 (dd, J=16.77, 2.05, 1H), (5.71 + 5.64) (dd, J=10.38, 2.16, 1H), (5.20 + 5.14) (d, J=3.38, 1H), (4.61+4.78) (t, J=7.94, 1H), (4.43 + 4.34) (s, 1H), 3.76 (dd, J=10.77, 4.23, 1H), 3.58 (d, J=10.94, 1H), 2.15 (m, 1H), 1.99 (m, 1H). ^{13}C NMR (500 MHz, $(CD_3)_2SO$) **δ** 170.87, 163.66, 137.25, 136.70, 131.95, 130.80, 129.52, 129.41, 129.32, 127.65, 127.38, 120.99, 117.24, 115.06, 68.92, 59.45, 55.40, 37.99.

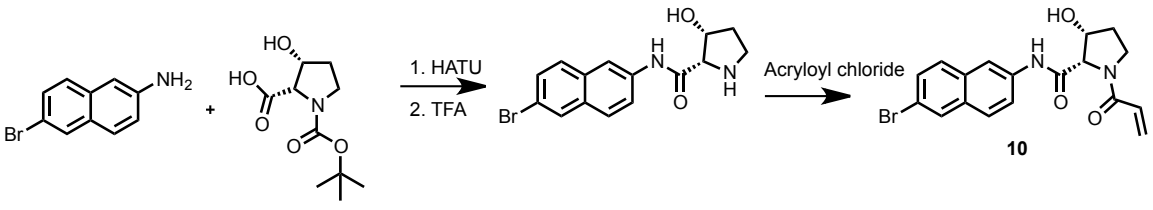

10

10 (2*S*,3*R*)-1-acryloyl-*N*-(6-bromonaphthalen-2-yl)-3-hydroxypyrrolidine-2-carboxamide:

N-boc-cis-3-hydroxy-L-proline (57mg, 0.248 mmol, 1.1eq) was dissolved in 2mL pyridine. The solution was cooled to 0°C and HATU (171mg, 2 eq, 0.450mmol) was added. The reaction was stirred for 15 minutes followed by an addition of 2-amino-6-bromo-naphthalene (50mg, 0.225 mmol, 1eq). After heating the solution to 70°C in a reflux condenser for 2.5 hours, the solution was diluted with 10mL brine and extracted with ethyl acetate (3x10mL). The combined organic layers were dried over Na_2SO_4, filtered, and evaporated to dryness *in vacuo*. The residue was purified by flash chromatography on silica gel (5-100%) hexanes: ethyl acetate to afford the desired product(2*S*,3*R*)-*tert*-butyl 2-((6-bromonaphthalen-2-yl)carbamoyl)-3-hydroxypyrrolidine- 1-carboxylate (60.5mg, 62% yield).

The product was dissolved in 2mL DCM. The mixture was cooled to 0°C and 1mL TFA was added. After 5 hours, the solvent and excess TFA was removed *in vacuo* with 3x 5mL toluene. The crude product, (2*S*,3*R*)-*N*-(6-bromonaphthalen-2-yl)-3-hydroxypyrrolidine-2-carboxamide, was used without further purification.

(2*S*,3*R*)-*N*-(6-bromonaphthalen-2-yl)-3-hydroxypyrrolidine-2-carboxamide (53.2 mg, 0.159 mmol, 1 eq) was dissolved in 2mL ACN to which TEA (44uL, 0.318 mmol, 2 eq) was added. The solution was cooled to 0°C upon which acryloyl chloride (13uL, 0.159 mmol, 1 eq) was added. After 30 minutes, the reaction was quenched with 5mL NaHCO3. The solution was left to stir for 15 minutes. The mixture was extracted with EtOAc (3x5mL). The combined organic layers were dried with Na_2SO_4, filtered, and evaporated *in vacuo*. The residue was purified by flash chromatography on silica gel (5-100%) EtoAC:hexanes, followed by (0-15%) dichloromethane: methanol, to afford the desired product, (2*S*,3*R*)-1-acryloyl-*N*-(6-bromonaphthalen-2-yl)-3-hydroxypyrrolidine-2-carboxamide (6.6mg, 11% yield), as a white powder.

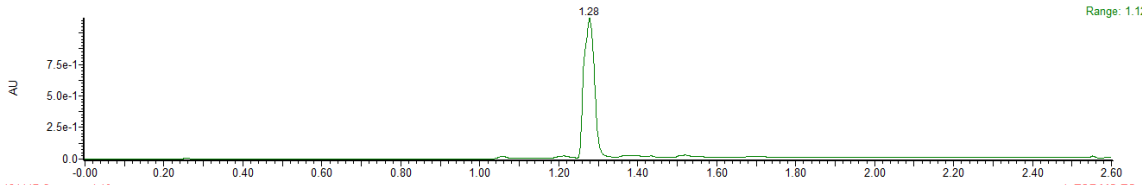

HRMS $C_{18}H_{17}BrN_2O_3Na$ $[M+Na]^+$ expected mass: 411.032; observed: 411.0328. ^{1}H NMR (400 MHz, MeOD, 75:25 rotamers) **δ** 8.25 (s, 1H), 7.99 (s, 1H), 7.76 (dd, J=9.85, 9.10, 1H), 7.69 (d, J=8.55, 1H), 7.65 (dd, J=8.55, 2.01, 1H), 7.53 (m, 1H), (6.68+6.43) (dd, J=16.93, 10.49, 1H), 6.28 (J=16.84,1.90, 1H), (5.78+5.71) (dd, J=10.51, 1.90, 1H), 4.70 (m, 1H), 4.67 (m, 1H), 3.96 (m, 1H), 3.74 (m, 2H), 2.21 (m, 1H). ^{13}C NMR (500 MHz, MeOD, 75:25 rotamers) **δ** 170.00, 167.25, 137.93, 133.70, 133.04, (130.70+130.64), (130.60+130.58), (130.45+130.50), 129.47, 128.80, 128.59, (122.64+122.46), 119.40, 117.90, (71.88+73.55), (66.03+66.21), (46.47+45.57), (34.04+31.83).

11 and **12** were synthesized and characterized as described in Ostrem *et al.*[6]

Acrylamide library (N=62) synthesis is described in Bateman *et al* and Roberts *et al*.[50,51]

CHAPTER 3

G13C is a fast exchanging mutant that is amenable to covalent binding

3.0 Gloss

K-Ras(G12C) as an oncogenic target has experienced breakthrough recently in the pharmaceutical industry with the advent of a line of covalent inhibitors such as ARS-1620 and AMG-510 that reside in the switch II pocket. Given its recent success, one must look from residue 12 to residue 13 which this merely one codon away and is also often mutated frequently in K-Ras driven cancers. K-Ras(G13C), an analogous cancer-causing mutation in Ras, is a rather understudied mutation. Little about the biochemistry of the mutant and its druggability is commonly known. Here, we hope to investigate the bio chemistry of K-Ras(G13C) via structural analysis and nucleotide exchange assays. Furthermore, we hope to probe its druggability via covalent library screening, and covalent docking technologies. Summarily, K-Ras(G13C) is a nucleophilic oncogenic cysteine that appears to be a fast exchanging activating mutant that is amenable to covalent inhibition.

3.1 Introduction

The etiology of allelic variation in K-Ras-driven cancers remains an unanswered question to date[52-54]. For example, K-Ras(G12C) is mutated in 40% of K-Ras driven lung adenocarcinomas, while K-Ras(G13C) is mutated in 1% of that patient population although codon 12 and 13 are adjacent[55,56]. Biochemical and cellular studies on other G12 and G13 mutants show that many G12 mutants appear to be more transforming than their G13 counterparts[57-59]. The G13C mutation lacks biochemical characterization to explain its difference to G12C in oncogenicity and clinical phenotype[60]. Furthermore, G12C inhibitors are unable to fully modify K-Ras(G13C), necessitating an alternative strategy to drug this oncogenic mutation. Modeling K-Ras(G13C)

and K-Ras(G13D) shows that residue 13 is connected to the nucleotide binding pocket via a hydrogen bonding network, which could be partially disrupted by the mutation to a bulkier mutant residue. Structural and biochemical data show that the K-Ras(G13C) could be amenable to both nucleotide binding inhibition or allosteric inhibition to the switch II pocket utilizing high throughput screening methods such as disulfide tethering, electrophile inhibition, and covalent docking.

K-Ras(G12C) is likely to be the first K-Ras mutation to be targeted molecularly due to the specificity of the covalent inhibitors developed from Wellspring Biosciences and Amgen[6,8-10]. We have gotten to the point where the G12C inhibitors are able to shrink patient derived mouse xenografts and reduce tumor burden in patients that carry that mutation. K-Ras(G13C) is a similarly situated oncogenic mutation. Modeling K-Ras(G12C) and K-Ras(G13D) shows that residue 13 is connected to the nucleotide binding pocket via a hydrogen bonding network, which could be partially disrupted by the mutation to a bulkier mutant residue. Structural and biochemical data show that the K-Ras(G13C) could be amenable to allosteric inhibition utilizing high throughput screening methods such as covalent docking and mass spectrometry based electrophile inhibition. The results shown in this manuscript render K-Ras(G13C) amenable to covalent drug binding.

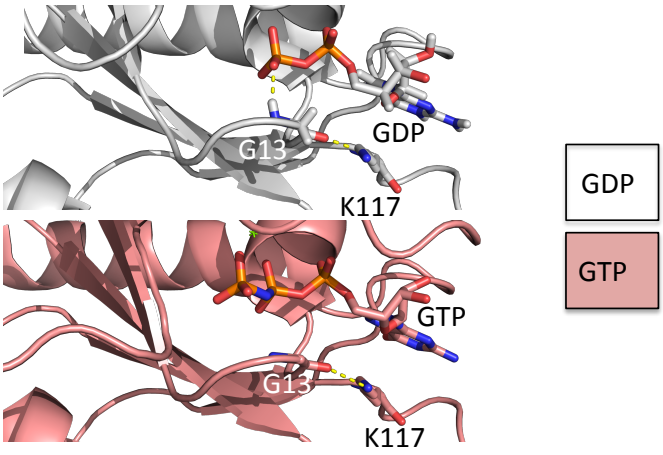

Figure 3.2.1: K-Ras(G13) participates in nucleotide recognition through a hydrogen-bond network. Structure of GDP-bound (PDB: 4OBE) and GNP-bound K-Ras (PDB: 3GFT).

3.2 K-Ras(G13C) is important for nucleotide recognition

Structural analysis of GDP- and GppnHP-bound K-Ras show that glycine 13 participates in nucleotide recognition in the p-loop (**Figure 3.2.1**). This key residue 13 is connected via a hydrogen bonding network from lysine 117 to the beta-phosphate of GDP. Lysine 117 participates in core hydrophobic interactions with the guanosine base. Modification of K117, such as ubiquitination, or mutations such as K117N alter intrinsic nucleotide exchange by drastically decreasing affinity for guanosine diphosphate or trisphosphate. It is likely that mutations to glycine 13 may also affect nucleotide exchange by destabilizing the protein's nucleotide recognition. Hunter *et al* demonstrate that K-Ras(G13D) is a fast exchanger via mant-based nucleotide exchange assays.[5]

We examined the effect of K-Ras(G13C) on nucleotide recognition *in vitro* using a fluorescent nucleotide exchange assay. EDTA-mediated nucleotide exchange of BODIPY-GDP and GTP were performed on mutant forms of K-Ras$^{1\text{-}189}$ GDP constructs. Compared to K-Ras(G12C) and wild type-Ras, K-Ras(G13C) showed increased exchange of BODIPY- labeled GDP

and GTP analogues (**Figure 3.2.2b-c**). This may indicate that G13C is may be destabilizing the nucleotide binding pocket.

We examined the melting temperatures of the mutant K-Ras$^{1-189}$ GDP constructs via a thermal stability assay (**Figure 3.2.2d**). K-Ras(G13C) demonstrated a Tm of 53.6±0.1ºC, which was markedly lower than the wild type (59.3±0.1ºC) and G12C (61.1±0.1ºC) (**Figure 3.2.2e**). This evidence indicates that K-Ras(G13C) is a destabilizing mutation.

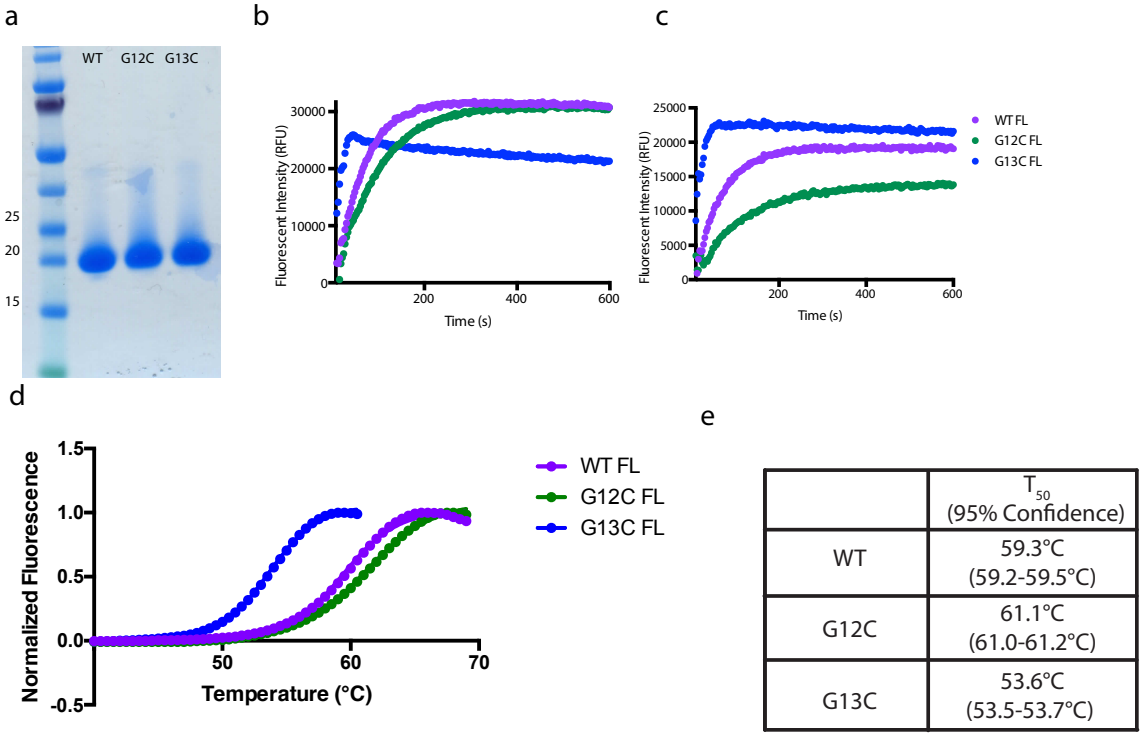

	T_{50} (95% Confidence)
WT	59.3°C (59.2-59.5°C)
G12C	61.1°C (61.0-61.2°C)
G13C	53.6°C (53.5-53.7°C)

Figure 3.2.2: K-Ras(G13C) is a destabilizing mutant a. 4-12% bis-tris Nupage polyacrylamide gel of K-Ras$^{1-189}$ constructs. EDTA-mediated nucleotide exchange of b. BODIPY-FL GDP and c. BODIPY-FL GTP into K-Ras$^{1-189}$ constructs. d. thermal stability assay on K-Ras$^{1-189}$ constructs and e. the Tm melting temperatures.

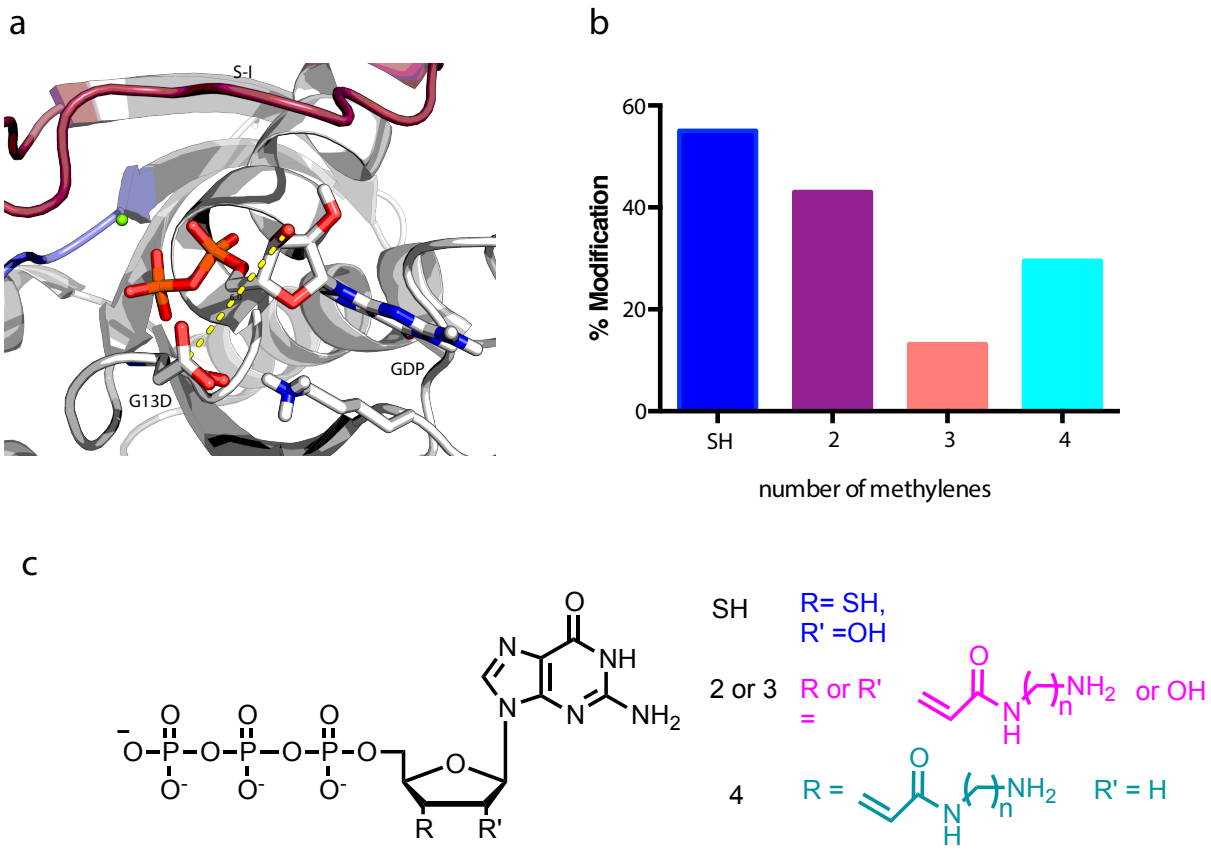

Figure 3.3: **K-Ras(G13C) is amenable to covalent nucleotide labeling** a. Structure of K-Ras^{G13D} (PDB: 4TQA) depicting the nucleotide binding pocket and distance (6.0Å) to 3-OH GDP. b. Percent modification of K-Ras(G13C) with covalent GTP analogues. c. structures of GTP analogues.

3.3 K-Ras(G13C) is more amenable to covalent bond formation via covalent nucleotides

K-Ras(G13C) is structurally closer to the nucleotide binding pocket than G12C, and therefore the possibility of nucleotide inhibition is not precluded (**Figure 3.3a**). Furthermore, given the evidence that K-Ras(G13C) is a destabilizing mutation that may weaken nucleotide affinity, it is likely possible that K-Ras(G13C) can be drugged by a covalent nucleotide analogue. A series of 200uM GTP-analogues were used to treat 4uM K-Ras(G12C) and G13C over 24 hours in the presence of 5mM EDTA and percent modification was monitored via mass spectrometry (**Figure 3.3b-c**). None of the analogues labeled G12C but a few modified G13C partially indicating that G13C is more accessible to covalent capture by nucleotide analogues (**Figure 3.3b-c**). However, cell permeability of nucleotide analogues remains a difficult task to achieve, as seen by prior attempts to drug G12C covalently.

3.4 K-Ras(G13C) is minimally reactive to available K-Ras(G12C) inhibitors

The switch II pocket remains a tractable pocket for K-Ras(G13C) inhibition. K-Ras(G13D) (PDB ID: 4TQA) was aligned to a structure of K-Ras bound to a switch II pocket inhibitor (PDB ID: 4M21) with the inhibitor represented in spheres (slate). From the alignment, one can see that codon 13 is slightly farther away from the switch II pocket. This suggests the necessity for a longer switch II pocket inhibitor to fully occupy the pocket. However, there is a possibility that the switch II pocket series may covalently modify G13C. Twenty four hour treatment of 200uM K-Ras(G12C) inhibitors to G12C and G13C (**Figure 3.4b**) demonstrate that the current series of switch II pocket inhibitors (compounds 1-4: 12, ARS-853, ARS-1620, AMG-510) are minimally able to covalently modify G13C in their current form. This indicates that G12C and G13C are

fundamentally different in either reactivity or orientation to the switch II pocket. Perhaps, linker design of the switch II pocket inhibitors may be necessary in order to reach the switch II pocket from residue 13, which is about 3.3Å further away.

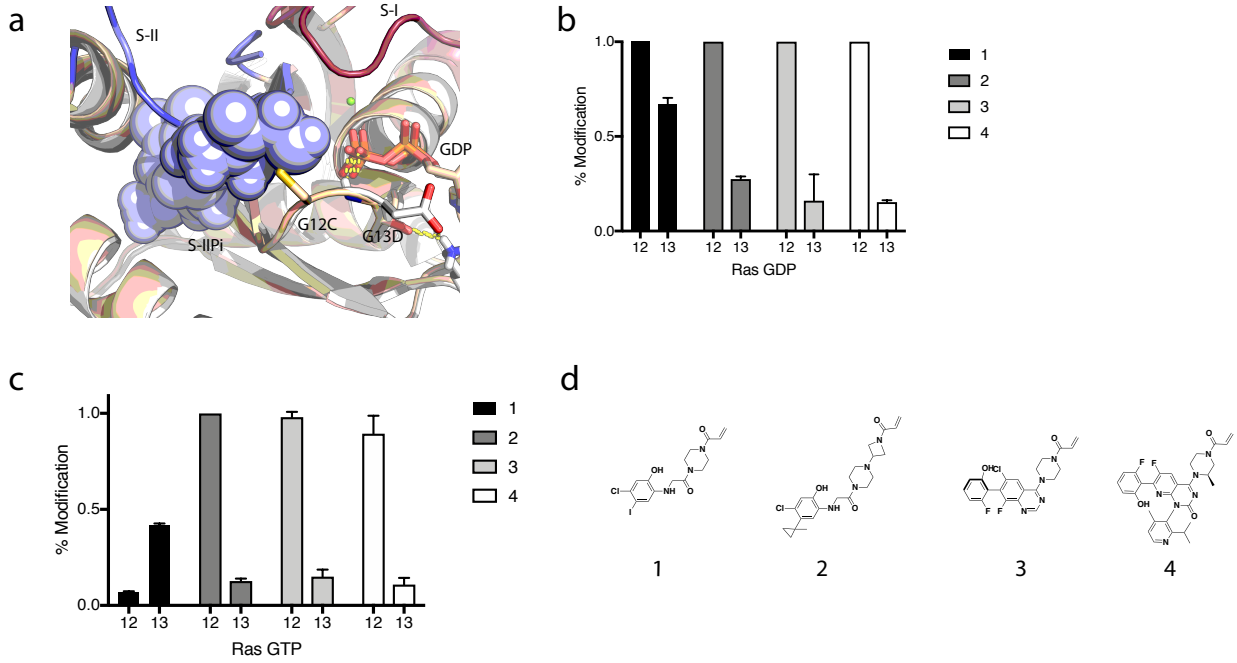

Fig 3.4: K-Ras(G13C) screened with current switch II pocket inhibitors a. Structural alignment of K-Ras(G12C) (yellow, PDB ID: 4M21) bound to a switch II pocket inhibitor (slate) and K-Ras(G13D) (white, PDB ID: 4TQA). B. Percent modification of K-Ras(G12C) inhibitors to K-Ras(G12C) and K-Ras(G13C) by mass spectrometry. C. Percent modification of electrophiles towards K-Ras(G12C) and K-Ras(G13C) d. Chemical structures of select K-Ras inhibitors.

3.5 Optimizing K-Ras(G13C) linker design via covalent docking

In optimizing G12C inhibitors for K-Ras(G13C), one must consider the distance and angle constraints necessary to achieve covalent binding at residue 13, given its further distance from the switch II pocket and potential rotameric differences to G12C. Covalent docking via DOCKOVALENT3.7 was used to achieve this linker design. From a library of 2000 boc-protected

diamines, derivatives of compound 5 were virtually constructed. After pre-generating all protomers and stereoisomers, the virtual library were constrained to only the conformers that achieved a distance criteria of 10.8Å (from the thiol of G13C to the base nitrogen in the piperazine ring) and maintain critical hydrogen bonds to K16, D69, H95. From the 8 compounds that were chosen from covalent docking, only compound 6 labeled G13C via mass spectrometry (**Figure 3.5b**).

After incubation of compounds 5 and 6 on K-Ras for 5 days, the compounds modified Ras partially (**Figure 3.5d**). Upon a thermal stability assay, compound 6 increased stabilization of Ras by 1C **(Figure 3.5c-d).** Structure-activity-relationships around compound 6 to derive compounds 7 and 8 did not improve labeling K-Ras G13C, and in fact abrogated binding, indicating that small molecule recognition is achieved by more than linker length.

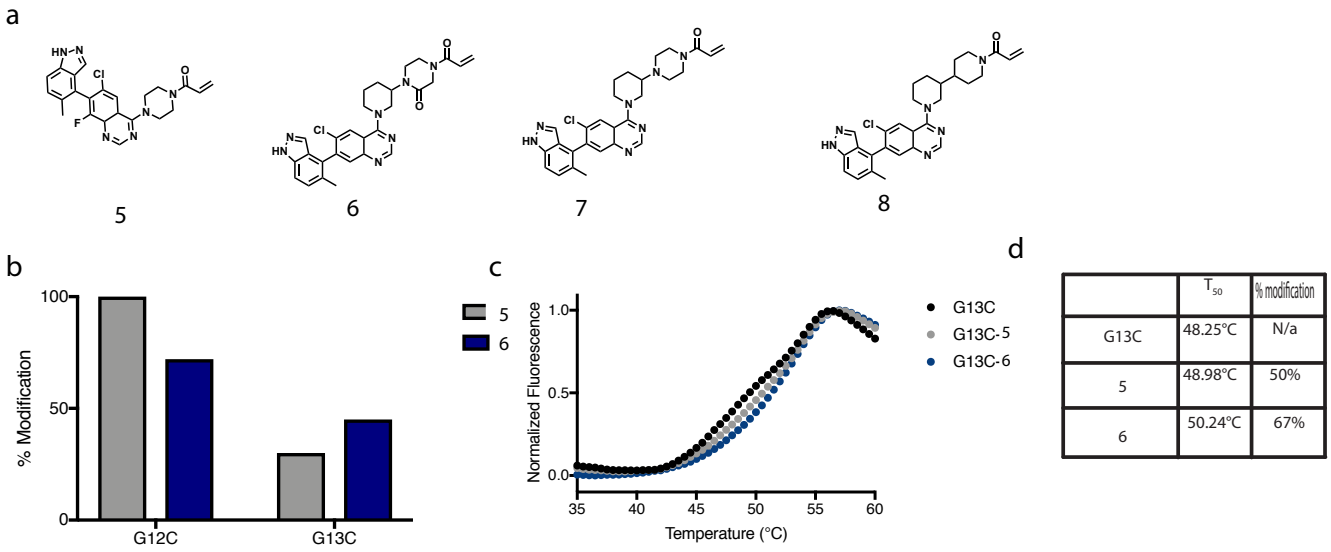

	T_{50}	% modification
G13C	48.25°C	N/a
5	48.98°C	50%
6	50.24°C	67%

Figure 3.5: K-Ras(G13C) screened with covalent docking analogs a. Structure of covalent docking hits and analogues. b. % Modification of compounds 5 and 6 to K-Ras(G12C) and K-Ras(G13C) c. thermal stability of the adducts and d. % modification and melting temperatures.

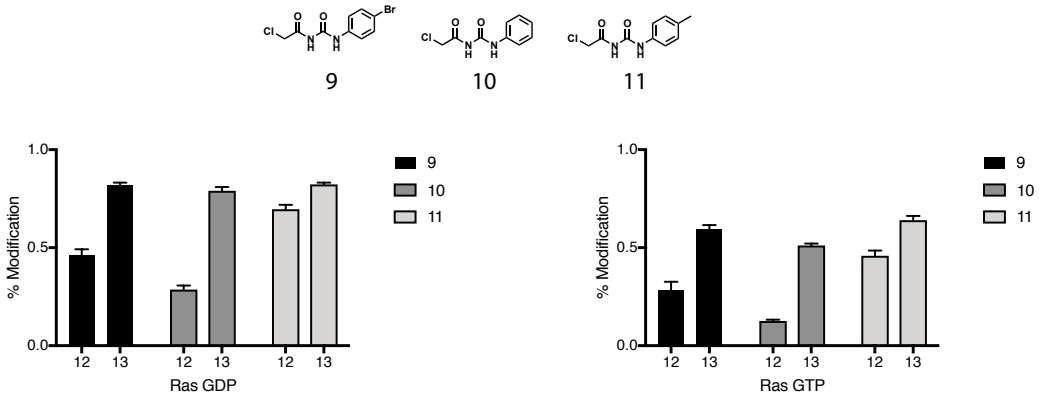

Fig 3.6: Structure-activity-relationships around compound 9. a. Structure of electrophile hits and analogues. % Modification of compounds 9-11 to b. GDP-bound and c. GTP-bound K-Ras(G12C) and K-Ras(G13C)

3.6 Electrophile library screening of G13C reveals new scaffold

4uM K-Ras(G13C) GDP was screened against a library of 993 commercially available acrylamides and cloroacetamides were used to screen at 4C, 24h, 200uM compound, 5mM EDTA. 98 compounds labeled >50% in the primary screen. Since many of the compounds were known promiscuous binders to other targets, 9 compounds were chosen based on their well behaved nature for a follow-up dose response. Compound 9 demonstrated a common motif, a urea linker, that is not frequently seen in hits and was retested against K-Ras(G12C) and G13C in the presence of 1mM $MgCl_2$, at room temperature 24 hours. Compound 9 and its commercially available analogues (10 and 11) both label the GDP-bound version of K-Ras(G13C) more than G12C (**Figure 3.6**), indicating that there is selectivity towards the G13C oncogene. Furthermore, these compounds also label the GTP-bound versions of G12C and G13C. This indicates that this class of compounds may be recognizing an alternative pocket to the GDP-restricted switch II pocket.

3.7 Conclusion

The work presented in this thesis highlights the evolution of K-Ras from an undruggable target to one that can be effectively targeted with mutant-specific covalent drugs. Covalent inhibitors remain a tangible solution to targeting the elusive K-Ras oncogene, given the efficatiousness of K-Ras inhibitors currently in phase I clinical trials. The switch II pocket was discovered to be an allosteric drug binding site that is accessible and stable with covalent tethering from the oncogenic mutation, G12C. Since the switch II pocket has been proven to be

an effective drug pocket for K-Ras(G12C), this opens the avenue for other K-Ras mutants to be treated via modification of existing switch II pocket inhibitors.

K-Ras(G12C) has been shown to be amenable to covalent inhibition via several switch II pocket analogs. This usually works through an allosteric trapping mechanism which traps G12C in a stable inactive, GDP bound state that is resistant to SOS-driven nucleotide exchange. However, covalent binders can also render the protein complex unstable. Therefore, there is a possibility that upon binding, K-Ras is destabilized allowing it to undergo faster SOS-driven nucleotide exchange. The work here shows that the K-Ras mutants are structurally and biochemically distinct and may require several iterations of modification before achieving mutant-specific inhibition seen in G12C.

3.8 Experimental Methods

Protein expression and purification

K-Ras constructs were purified as previously specified.[6] Briefly, His6-tagged recombinant bacterial human K-Ras (isoform 2, residues 1-169), K-Ras Cys-light (isoform 2, residues 1-169, C51S/C80L/C118S), K-Ras (isoform 2, residues 1- 189) were transformed into Escherichia coli (BL21 (DE3)) for expression. K-Ras(G13C) was introduced into each vector using a QuikChange™ PCR protocol. Protein cultures were grown in TB with kanamycin at 37˚C. Upon an optical density (OD_{600}) reached 0.5-0.6, were induced at 18˚C with 120mg IPTG and expressed over 18 hours. The cells were pelleted at 4,5000 rpm, resuspended in lysis buffer (500 mM NaCl, 20 mM TRIS pH 8.0, 5 mM imidazole, 1 tablet of Roche cOmplete EDTA Free protease inhibitor per 50mL lysis buffer), and lysed by microfluidizer at 80psi. The lysate was spun down at 10,000g

and purified by batch binding using TALON beads with elution buffer (500 mM NaCl, 20 mM TRIS pH 8.0, 250 mM imidazole). The His6-tag was cleaved with TEV overnight with cleavage buffer (300 mM NaCl, 20 mM TRIS pH 8.0, 5 mM imidazole, 1 mM DTT, 0.5 mM EDTA). The tag was removed via Nickel NTA beads and the eluate was purified by FPLC using ion exchange (buffer A: 50mM NaCl, 20 mM TRIS pH 8.0, buffer B: 500mM NaCl, 20 mM TRIS pH 8.0). The protein was concentrated to 5-20 mg/ml. If the protein was used for crystallography or hydrogen-deuterium exchange, it was subject to a subsequent size exclusion chromatography (buffer: 20 mM HEPES (pH 7.5), 150 mM NaCl) and concentrated.

Mass Spectrometry Screening

50uL of 4uM K-Ras(G12C) 1-169 (buffer: 20mM HEPES pH 7.5, 150mM NaCl, 1mM $MgCl_2$) was incubated with 200uM compound (4% v/v dimethylsulfoxide respectively) for 24 hours at room temperature. The reaction was quenched with 2uL 10% v/v formic acid to yield 0.4% v/v formic acid final. Mass spectrometry experiments were performed using the Waters Acquity UPLC/ESI-TQD with a 2.1 × 50 mm Acquity UPLC BEH300 C4 column.

Nucleotide Exchange Assay

45uL of K-Ras 1-189 GDP (111nM) was prepared in assay buffer (150mM NaCl, 20mM HEPES, pH 7.5, 2uM $MgCl_2$, 0.01% Triton X-100) was added to a 96 well Costar plate. Exchange was catalyzed by the addition of 5uL of a mixture of 0.5uM EDTA and 5uM incoming nucleotide (500nM final; ThermoFischer™ BODIPY-FL GDP or GTP) and fluorescence intensity was monitored over 1 hour at Ex/Em: 485/520nm using a BioTek H4.

Thermal Stability Assays

The thermal denaturation of K-Ras was monitored using a fluorescence-based differential scanning fluorimetry assay. K-Ras was purified with or without compound for the use of the experiment as previously described. 8uM protein was prepared in assay buffer (150mM NaCl, 20mM Hepes, pH 7.5, 1mM $MgCl_2$) with 1/1000 Sypro Orange. The plate was heated from 25-95°C at a rate of 0.5°C /min. The fluorescence intensity was monitored at Ex/Em: 492/610nm.

Synthetic Methods

All commercial reagents were purchased and used without further purification (Compounds 1-4, 9-11).

Nucleotide analogues A-E were obtained from Roger Goody and Joseph Piccirilli.

A. 3`-BDA-2`-dGTP Acryloyl

B. 2`,3`-EDA-GTP Acryloyl

C. 2`,3`-PDA-GTP Acryloyl

D. 3C-Acryloyl-GTP

E. 4C-Acryloyl-GTP

EDA - Ethylendiamine

PDA - Propylendiamine

BDA - Butylendiamine (all attached to the ribose)

Silica gel chromatography was performed using a Combiflash Rf (Teledyne Isco) with pre-packed 4-24g silica columns and cartridges. Reverse-phase high performance liquid chromatography (RP-HPLC) was performed using a Waters 2545 solvent delivery system equipped with an XBridge prep C18 column. Separation was achieved using a gradient between 5-95% acetonitrile (ACN) in water with 0.1% formic acid unless otherwise specified by monitoring UV absorption (λ=254 nm). ^{1}H NMR were recorded on a Varian Innova 400 MHz or a Bruker DRX 500 MHz spectrometer. ^{1}H chemical shifts are reported in δ (ppm) as s (singlet), d (doublet), dd (doublet of doublets), t (triplet), q (quartet), or m (multiplet) and are referenced to the residual solvent peak. Coupling constants (J) are reported as Hertz.

Compound 5 was synthesized as described.[49]

Compound 6

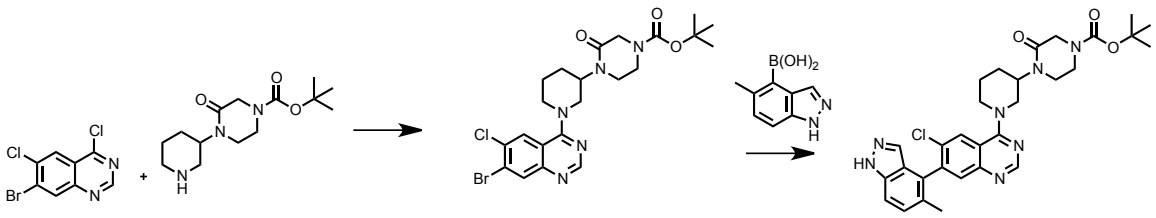

7-bromo-4,6-dichloroquinazoline (50mg, 1 eq, 0.18 mmol) and tert-butyl 3-oxo-4-(piperidin-3-yl)piperazine-1-carboxylate (57mg, 1.1 eq, 0.20 mmol) were dissolved in 2 mL ethanol. DIPEA was added (94uL, 3 eq, 0.54 mmol) at ambient temperature, reaction was stirred and monitored 3.5 hours and then was quenched with 5mL H_2O and extracted with ethyl acetate (5mL x 3). The organic layers were washed with brine (2x5mL) and dried over Na_2SO4. The residue was purified by flash chromatography on silica gel (0-100% hexanes:EtOAc gradient,

followed by 0-10% EtOAc:MeOH) to yield the desired product tert-butyl 4-(1-(7-bromo-6-chloroquinazolin-4-yl)piperidin-3-yl)-3-oxopiperazine-1-carboxylate (32mg, 34% yield).

tert-butyl 4-(1-(7-bromo-6-chloroquinazolin-4-yl)piperidin-3-yl)-3-oxopiperazine-1-carboxylate (32mg, 1 eq, 0.06mmol), 5-methyl-1H-indole-4-boronic acid (43mg, 4 eq, 0.24mmol), Na_2CO_3 (26mg, 4 eq, 0.24mmol), $Pd(PPh_3)_4$ (14mg, 0.2 eq, 0.01mmol) were dissolved in 1,4-dioxane (1 mL) and H_2O (0.2mL) in a septum-topped vial. The solution was sparged with Argon for 10 minutes. The mixture was stirred overnight at 100°C. The mixture was the diluted with 5mL H2O and extracted with ethyl acetate (5mL x 3). The organic layers were washed with brine (2x5mL) and dried over Na_2SO4. The residue was purified by flash chromatography on silica gel ((0-100% hexanes:EtOAc gradient, followed by 0-10% EtOAc:MeOH gradient) to yield the desired product *tert*-butyl 4-(1-(6-chloro-7-(5-methyl-1*H*-indazol-4-yl)quinazolin-4-yl)piperidin-3-yl)-3-oxopiperazine-1-carboxylate (20.2mg, 57.5% yield).

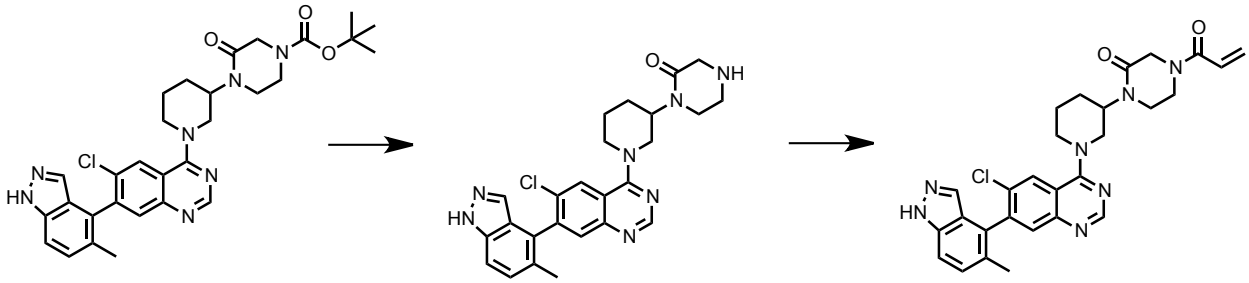

The product was dissolved in 1mL dichloromethane (DCM). The mixture was cooled to 0°C and 500uL trifluoroacetic acid (TFA) was added. After 2 hours, the solvent and excess TFA was removed *in vacuo* with 3x 5mL toluene. The crude product, 1-(1-(6-chloro-7-(5-methyl-1H-indazol-4-yl)quinazolin-4-yl)piperidin-3-yl)piperazin-2-one, was used without further purification as a yellow oil.

1-(1-(6-chloro-7-(5-methyl-1*H*-indazol-4-yl)quinazolin-4-yl)piperidin-3-yl)piperazin-2-one (20.2mg, 1 eq, 0.042mmol), was dissolved in 2mL acetonitrile. TEA (11.8uL, 2eq, 0.084mmol) was added at ambient temperature. The reaction was cooled to 0°C. Acryloyl chloride (3.4uL, 1.1 eq, 0.0424mmol) was added. The reaction was quenched with 5mL saturated NaHCO3 and left stirring for 15 minutes at ambient temperature. The reaction was extracted with ethyl acetate (5mL x 3), dried over Na_2SO4. The compound was purified by HPLC (25-95% acetonitrile:water) to get the desired product (2.8mg, 11.6% yield). ^{1}H NMR (400 MHz, Methanol-d_4) **δ** 8.63 (s, 1H), 8.51 (s, 1H), 8.31 (s, 1H), 7.77(s, 1H), 7.56 (d, J=8.58Hz, 1H), 7.40 (d, J=8.84 Hz, 1H), 6.28 (dd, J=16.81, 1.91 Hz, 1H), 5.81 (J=10.70, 1.68, 1H), 4.69 (m, 1H), 4.48 (t, J=14.866, 2H), 3.96 (m, 1H), 3.85 (m, 2H), 3.57 (m, 2H), 3.39 (t, J=11.74, 2H), 3.22 (t, J=11.86, 2H), 2.22 (s, 3H), 2.02 (m, 4H). NH missing due to exchange with Methanol-d_4.

Compound 7

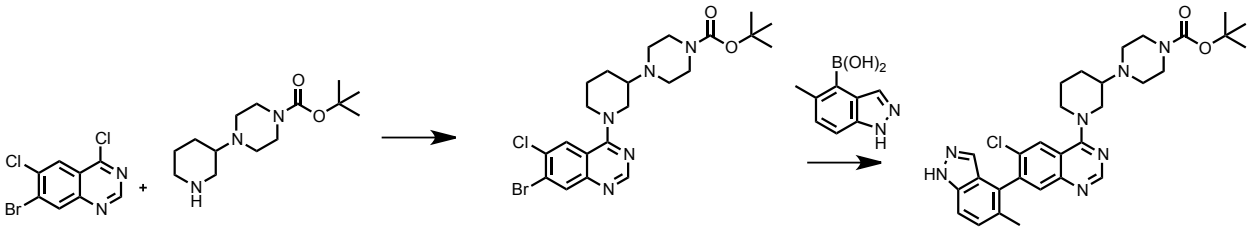

7-bromo-4,6-dichloroquinazoline (50mg, 1 eq, 0.18 mmol) and tert-butyl 4-(3-piperidyl)piperazine-1-carboxylate (53mg, 1.1 eq, 0.20 mmol) were dissolved in 2 mL ethanol. DIPEA was added (94uL, 3 eq, 0.54 mmol) at ambient temperature, reaction was stirred and monitored 3 hours and then was quenched with 5mL H_2O and extracted with ethyl acetate (5mL x 3). The organic layers were washed with brine (2x5mL) and dried over Na_2SO4. The residue was purified by flash chromatography on silica gel (0-15% DCM:MeOH) to yield the

desired product tert-butyl 4-[1-(7-bromo-6-chloro-quinazolin-4-yl)-3-piperidyl]piperazine-1-carboxylate (45mg, 49% yield).

tert-butyl 4-[1-(7-bromo-6-chloro-quinazolin-4-yl)-3-piperidyl]piperazine-1-carboxylate (45mg, 1 eq, 0.087mmol), 5-methyl-1H-indole-4-boronic acid (61mg, 4 eq, 0.35mmol), Na_2CO_3 (37mg, 4 eq, 0.35mmol), $Pd(PPh_3)_4$ (20mg, 0.2 eq, 0.018mmol) were dissolved in 1,4-dioxane (1 mL) and H_2O (0.2mL) in a septum-topped vial. The solution was sparged with Argon for 10 minutes. The mixture was stirred overnight at 100°C. The mixture was the diluted with 5mL H2O and extracted with ethyl acetate (5mL x 3). The organic layers were washed with brine (2x5mL) and dried over Na_2SO4. The residue was purified by flash chromatography on silica gel ((0-100% hexanes:EtOAc gradient, followed by 0-10% EtOAc:MeOH gradient) to yield the desired product tert-butyl 4-[1-[6-chloro-7-(5-methyl-1H-indazol-4-yl)quinazolin-4-yl]-3-piperidyl]piperazine-1-carboxylate (47 mg, 97% yield).

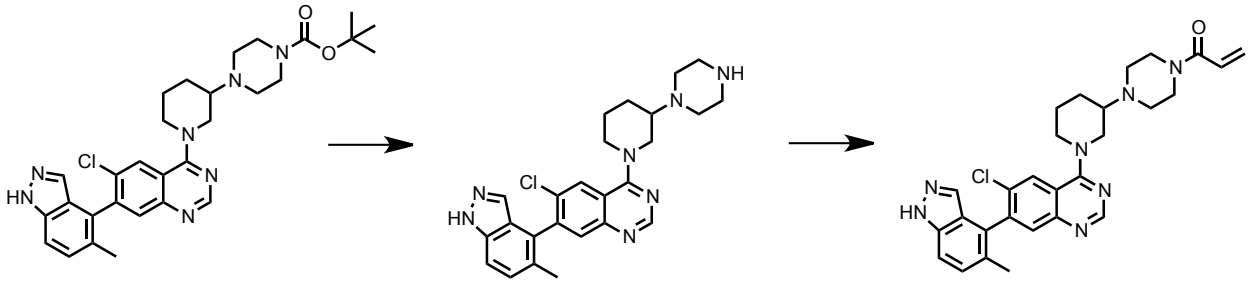

The product was dissolved in 1mL dichloromethane (DCM). The mixture was cooled to 0°C and 500uL trifluoroacetic acid (TFA) was added. After 2 hours, the solvent and excess TFA was removed *in vacuo* with 3x 5mL toluene. The crude product, 6-chloro-7-(5-methyl-1H-indazol-4-yl)-4-(3-piperazin-1-yl-1-piperidyl)quinazoline, was used without further purification.

6-chloro-7-(5-methyl-1H-indazol-4-yl)-4-(3-piperazin-1-yl-1-piperidyl)quinazoline (20.2mg, 1 eq, 0.042mmol), was dissolved in 1mL acetonitrile. TEA (11.8uL, 2eq, 0.084mmol) was added at

ambient temperature. The reaction was cooled to 0°C. Acryloyl chloride (3.4uL, 1.1 eq, 0.0424mmol) was added. The reaction was quenched with 5mL saturated NaHCO3 and left stirring for 15 minutes at ambient temperature. The reaction was extracted with ethyl acetate (5mL x 3), dried over Na_2SO4. The compound was purified by HPLC (25-95 acetonitrile:water) to get the desired product (2.8mg, 11.6% yield). ^{1}H NMR (400 MHz, Methanol-d_4) δ 8.60 (s, 1H), 8.23 (s, 1H), 7.75 (d, *J* = 1.1 Hz, 1H), 7.56 (d, *J* = 8.3 Hz, 1H), 7.50 (d, *J* = 4.0 Hz, 1H), 7.41 (d, *J* = 8.6 Hz, 1H), 6.76 (dd, *J* = 16.7, 10.7 Hz, 1H), 6.20 (dd, *J* = 16.8, 2.0 Hz, 1H), 5.75 (dd, *J* = 10.6, 2.0 Hz, 1H), 4.62 – 4.57 (m, 2H), 3.70 – 3.62 (m, 4H), 2.79 – 2.70 (m, 4H), 2.23 (d, *J* = 3.5 Hz, 3H), 2.19 – 2.10 (m, 1H), 2.04 – 1.97 (m, 1H), 1.80 – 1.69 (m, 2H), 0.95 – 0.84 (m, 2H). 2H missing: (1) NH missing due to exchange with Methanol-d_4, and (2) other hidden under shoulder of solvent residual peak.

Compound 8

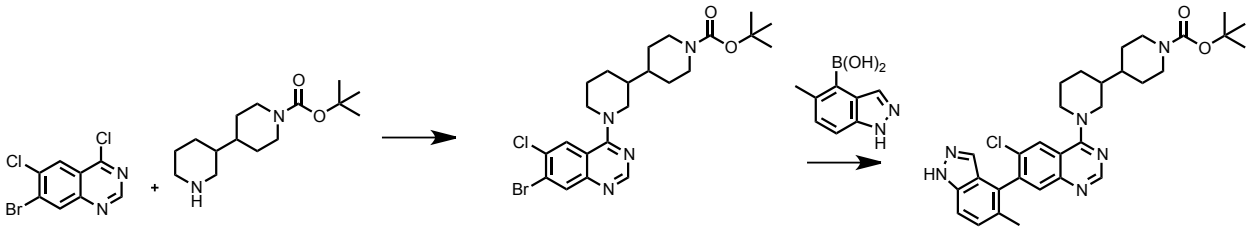

7-bromo-4,6-dichloroquinazoline (50mg, 1 eq, 0.18 mmol) and tert-butyl 4-(3-piperidyl)piperidine-1-carboxylate (53mg, 1.1 eq, 0.20 mmol) were dissolved in 2 mL ethanol. DIPEA was added (94uL, 3 eq, 0.54 mmol) at ambient temperature, reaction was stirred and monitored 3 hours and then was quenched with 5mL H_2O and extracted with ethyl acetate (5mL x 3). The organic layers were washed with brine (2x5mL) and dried over Na_2SO4. The residue was purified by flash chromatography on silica gel (0-15% DCM:MeOH) to yield the

desired product tert-butyl 4-[1-(7-bromo-6-chloro-quinazolin-4-yl)-3-piperidyl]piperidine-1-carboxylate (57mg, 62% yield).

tert-butyl 4-[1-(7-bromo-6-chloro-quinazolin-4-yl)-3-piperidyl]piperidine-1-carboxylate (57mg, 1 eq, 0.11mmol), 5-methyl-1H-indole-4-boronic acid (79mg, 4 eq, 0.45mmol), Na_2CO_3 (47mg, 4 eq, 0.45mmol), $Pd(PPh_3)_4$ (26mg, 0.2 eq, 0.022mmol) were dissolved in 1,4-dioxane (2 mL) and H_2O (0.5mL) in a septum-topped vial. The solution was sparged with Argon for 10 minutes. The mixture was stirred overnight at 100°C. The mixture was the diluted with 5mL H2O and extracted with ethyl acetate (5mL x 3). The organic layers were washed with brine (2x5mL) and dried over Na_2SO4. The residue was purified by flash chromatography on silica gel ((0-100% hexanes:EtOAc gradient, followed by 0-10% EtOAc:MeOH gradient) to yield the desired product *tert*-butyl 4-[1-[6-chloro-7-(5-methyl-1H-indazol-4-yl)quinazolin-4-yl]-3-piperidyl]piperidine-1-carboxylate (59mg, 93% yield).

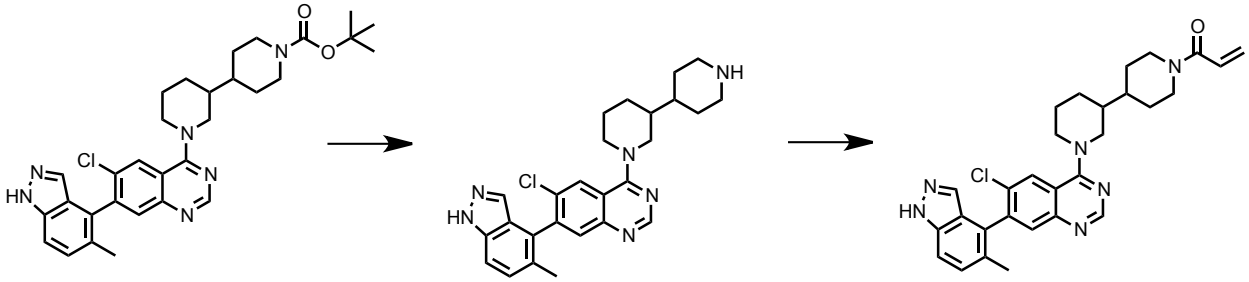

The product was dissolved in 1mL dichloromethane (DCM). The mixture was cooled to 0°C and 500uL trifluoroacetic acid (TFA) was added. After 2 hours, the solvent and excess TFA was removed *in vacuo* with 3x 5mL toluene. The crude product 6-chloro-7-(5-methyl-1H-indazol-4-yl)-4-[3-(4-piperidyl)-1-piperidyl]quinazoline, was used without further purification.

6-chloro-7-(5-methyl-1H-indazol-4-yl)-4-[3-(4-piperidyl)-1-piperidyl]quinazoline (20mg, 1 eq, 0.044mmol), was dissolved in 1mL acetonitrile. TEA (12uL, 2eq, 0.087mmol) was added at

ambient temperature. The reaction was cooled to 0°C. Acryloyl chloride (3.9uL, 1.1 eq, 0.084mmol) was added. The reaction was quenched with 5mL saturated NaHCO3 and left stirring for 15 minutes at ambient temperature. The reaction was extracted with ethyl acetate (5mL x 3), dried over Na_2SO4. The compound was purified by HPLC (25-95% acetonitrile:water) to get the desired product (1.2mg, 5.3% yield). ^{1}H NMR (400 MHz, Methanol-d_4) δ 8.56 (d, *J* = 13.1 Hz, 2H), 8.18 (s, 1H), 7.74 (d, *J* = 1.4 Hz, 1H), 7.56 (d, *J* = 8.6 Hz, 1H), 7.50 (d, *J* = 6.8 Hz, 1H), 7.40 (d, *J* = 8.6 Hz, 1H), 6.84 – 6.70 (m, 1H), 6.17 (d, *J* = 16.8 Hz, 1H), 5.72 (d, *J* = 10.1 Hz, 1H), 4.69 – 4.52 (m, 2H), 4.48 (d, *J* = 13.0 Hz, 1H), 4.18 (d, *J* = 13.1 Hz, 1H), 3.18 – 3.02 (m, 2H), 2.80 – 2.65 (m, 1H), 2.23 (d, *J* = 4.3 Hz, 3H), 2.08 (d, *J* = 13.8 Hz, 1H), 1.95 (d, *J* = 10.3 Hz, 3H), 1.84 – 1.68 (m, 2H), 1.67 – 1.56 (m, 1H), 1.53 – 1.40 (m, 1H), 1.39 – 1.25 (m, 2H). NH missing due to exchange with Methanol-d_4.

Fragment electrophile library

993 covalent fragments - 75% chloroacetamides, 25% acrylamides, all commercially available, were assembled from Enamine. Average molecular weight (of the covalent adduct) is 217 Da.

A full screen of the library was performed using K-Ras G13C (GDP) at 4uM protein, 200uM compound, incubated at 4C for 24h. The primary screens were performed with 5 compounds in each well, and % labeling is assigned based on mass based on the methods in Resnik *et al*.[26]

98 compounds labeled >50% in the primary screen, but many of the compounds were known promiscuous binders. Nine compounds that looked promising based of our knowledge

of the library for follow-up dose response. Three of these turned out to be false positives. Of the remaining 6, three: PCM-0102308, PCM-0102332, PCM-0102705 share a common motif.

Table 3.8 Results of electrophile library screen on K-Ras(G13C) GDP

		200uM	100uM	50uM	10uM
PCM-0102492	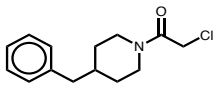	50	30	10	0
PCM-0102366	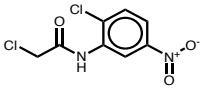	10	5	0	0
PCM-0102308	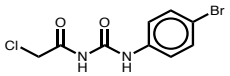	100	95	70	30
PCM-0102332	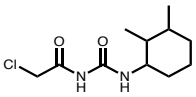	65	60	30	5
PCM-0102813	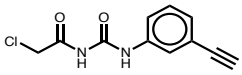	15	5	0	0
PCM-0102705	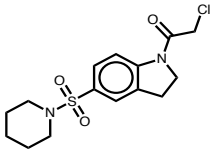	10	0	0	0
Ind1	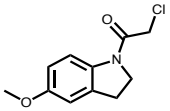	100	90	60	10
Ind2	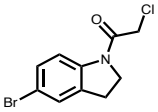	70	80	80	60
Ind3	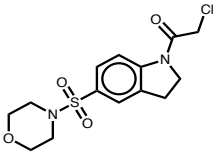	100	100	90	20
PCM-0102690	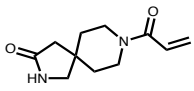	0	0	0	0
PCM-0102923	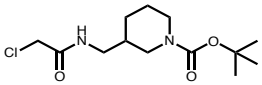	0	0	0	0
PCM-0102804	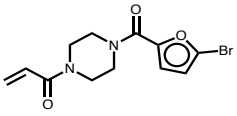	0	0	0	0

For one of the other hits (PCM-0102705) analogues (Ind1-3) showed significant labeling. However, indoline chloroacetamides are very reactive.

Virtual library generation

The cysteine rotamer of G13C was modeled via PyMOL into a crystal structure of K-Ras(G12C) covalently bound to compound 5. The original structure was not deposited in the PDB. The primary docking screen of K-Ras(G13C) was carried out synthesizing a covalent docking library from ~2000 boc-protected amines. To generate the library for the secondary docking screen, we searched Enamine's building block catalogue for boc-protected amines for virtual parallel synthesis according to the scheme shown here.

We selected ~2,000 boc-protected diamine building blocks based on the following criteria: MW of the final product ≤ 350. All pre-generated ligand conformations were built in the reacted form represented by a dummy silicon atom.[25] Protonated and tautomerized conformations were generated by Corina (https://www.mn-am.com/products/corina).

Computational workflow of covalent docking screen

We used DOCKovalent as implemented in DOCK 3.7.[25] For pose reproduction analysis, the sampling parameters of covalent bond length and angle were set according to the value from crystal structures. The bump_rigid and bump_maximum were set to the maximum values and check_clashes was changed from 'yes' to 'no' to improve pose sampling by allowing several steric clashes between protein and ligand. The number_save and

number_write were modified from 1 to 1000 to keep multiple poses for further analysis. Blastermaster.py was used to prepare docking systems, and the parameter margin was changed from the default value of 10Å to 6Å for grid generation. The cysteine rotamer is immobile during the covalent docking. Each conformation of the sampled compound was scored and ranked according to the physics-based scoring function in DOCK3.7 without considering the different conformational energies among the cysteine rotamers.

For the prospective study, the covalent bond parameters were set to a length=1.8Å, bond angles=109.5°±10° (in 2.5° steps).

Post-docking pose analysis

The RMSD values for the ligand heavy atoms between the top-scoring pose and the crystal structure was calculated using an in-house script. The lowest RMSD of top 1,000-scoring poses was saved for minimization refinement, and their RMSD values were also calculated.

For the primary docking screen of G13C, the compounds were selected based on ability to occupy the hydrophobic binding pocket and meet distance criteria of 10.8 Å from the base of the nitrogen in the boc-protected amine to the cysteine of G13C.

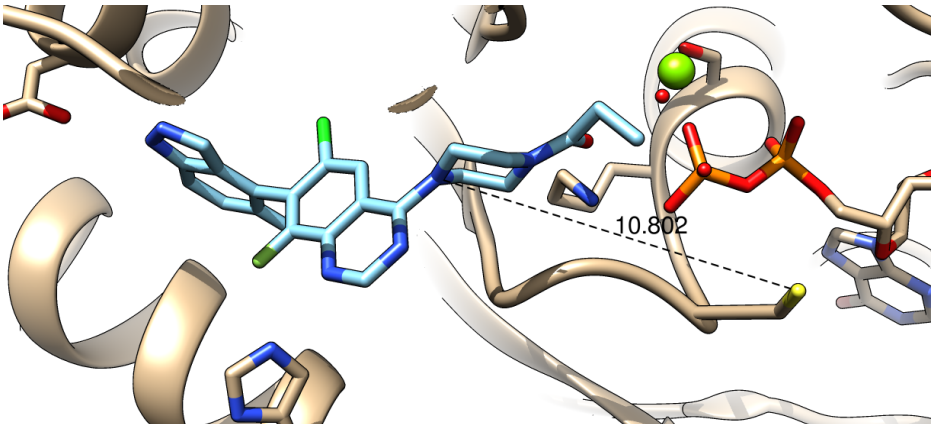

Figure 3.8 Distance constraint parameters demonstrated on crystal structure of K-Ras(G12C) with compound 5. Cysteine 13 and glycine 12 are modeled computationally with Chimera. Distance from cysteine to piperazine nitrogen is 10.8Å.

The top 400 scoring poses for each compound were filtered based on ability to form hydrogen bonds with the side chains of D69, H95 using an automated script. Finally, the top-scoring pose for each compound was selected for minimization and ability to hydrogen bond to K16.

Molecular mechanics-based minimization and MM-GB/SA calculation

We further optimized the geometry of the protein-ligand adducts by energy minimization[6] using AMBER 14.[7] The Antechamber module was used to calculate partial charges using the semi-empirical AM1-BCC method to assign force field parameters and to calculate topology files for the ligand. These files were modified to create a covalent adduct by combining the ligand topology and attached lysine residue. Parameters for the covalent linkage between ligands and Lys residue were assigned by mixing generalized amber force field (GAFF)[8] parameters for the ligand and the Amber force field for the protein. These parameters, located at the borderline between the two force fields, were assigned on the basis of the analogous

parameters available for similar atom types. TLeap was then used to prepare the complex generated from docking for molecular mechanics. We used the sander program to minimize the covalent system. 5,000 steps of minimization were carried out using the Hawkins, Cramer, Truhlar pairwise generalized Born model with harmonic position restraints on all heavy atoms except for the ligand and the attached lysine residue. Snapshots of the receptor, ligand, and receptor-ligand complex (final snapshot after minimization) were analyzed and the binding free energy was calculated by using the molecular mechanics/generalized Born surface area (MM/GBSA) method: $\Delta\Delta G_{bind} = \Delta G_{mmgbsa,complex} - (\Delta G_{mmgbsa,lig} + \Delta G_{mmgbsa,rec})$.

CHAPTER 4

Summary

4. Summary

The field of K-Ras is rapidly expanding to accept that 1. K-Ras mutants behave differently biochemically and may be oncogenic in different ways and 2. That K-Ras might be a druggable oncogene, with the first advances of switch II pocket inhibitors making their way into clinical trials. Here, we describe the ways in which K-Ras(G12C) may be used as a case study to demonstrate that covalent docking is a viable strategy for generating new chemotypes that bind K-Ras. Furthermore we apply the knowledge utilized from KRas G12C to study G13C. Which is seen as a different oncogene, whose oncogenicity may occur from its fast exchanging phenotype. Given that G13C in the cell will be subject to large excesses of GTP, it is feasible that oncogenicity may be purely induced by the disruption of the nucleotide binding pocket by this bulkier residue.

In addition, K-Ras G13C cannot be treated by our current inventory of covalent switch II pocket inhibitors as they do not label G12C even at radically high doses. This necessitates a different strategy to targeting G13C, which may include structure activity relationships around linker modification of G12C inhibitors or screening covalent libraries to find a new chemotype that is G13C specific. The work highlighted in the manuscript indicates that both approaches can yield a G13C binder yet more work needs to be done to characterize the binders that have originated including structure activity relationships and further biochemical characterization and structural characterization.

References

1. Forbes, S. A. *et al.* COSMIC: exploring the world's knowledge of somatic mutations in human cancer. *Nucleic Acids Res.* **43,** D805–11 (2015).

2. Prior, I. A., Lewis, P. D. & Mattos, C. A comprehensive survey of Ras mutations in cancer. *Cancer Res.* **72,** 2457–2467 (2012).

3. Scheffzek, K. *et al.* The Ras-RasGAP complex: structural basis for GTPase activation and its loss in oncogenic Ras mutants. *Science* **277,** 333–338 (1997).

4.Gideon, P. *et al.* Mutational and kinetic analyses of the GTPase-activating protein (GAP)-p21 interaction: the C-terminal domain of GAP is not sufficient for full activity. *Molecular and Cellular Biology* **12,** 2050–2056 (1992).

5. Hunter, J. C. *et al.* Biochemical and Structural Analysis of Common Cancer-Associated KRAS Mutations. *Mol. Cancer Res.* **13,** 1325–1335 (2015).

6. Ostrem, J. M., Peters, U., Sos, M. L., Wells, J. A. & Shokat, K. M. K-Ras(G12C) inhibitors allosterically control GTP affinity and effector interactions. *Nature* **503,** 548–551 (2014).

7. Erlanson, D. A., Wells, J. A. & Braisted, A. C. Tethering: fragment-based drug discovery. *Annu Rev Biophys Biomol Struct* **33,** 199–223 (2004).

8. Patricelli, M. P. *et al.* Selective Inhibition of Oncogenic KRAS Output with Small Molecules Targeting the Inactive State. *Cancer Discovery* 1–38 (2016). doi:10.1158/2159-8290.CD-15-1105

9. Lito, P., Solomon, M., Li, L. S., Hansen, R. & Rosen, N. Allele-specific inhibitors inactivate

mutant KRAS G12C by a trapping mechanism. *Science* 1–9 (2016). doi:10.1126/science.aad6204

10. Janes, Matthew R. et al. Targeting KRAS Mutant Cancers with a Covalent G12C-Specific Inhibitor. Cell, Volume 172, Issue 3, 578 - 589.e17

11. Lipford, JR. Pre-clinical development of AMG 510: the first inhibitor of KRASG12C in clinical testing. Oral presentation at AACR 2019, Atlanta, GA. March 29-April 3, 2019.

12. Visscher, M., Arkin, M. R. & Dansen, T. B. ScienceDirectCovalent targeting of acquired cysteines in cancer. *Current Opinion in Chemical Biology* **30,** 61–67 (2016).

13. Bos, J. L. ras oncogenes in human cancer: a review. *Cancer Res.* **49,** 4682–4689 (1989).

14. Howlader, N., AM, N., Krapcho, M., Garshell, J. & Miller, D. SEER Cancer Statistics Review, 1975-2012, National Cancer Institute. Bethesda, MD. *http://seer.cancer.gov/csr/1975_2012/*

15. Bacher, U., Haferlach, T., Schoch, C., Kern, W. & Schnittger, S. Implications of NRAS mutations in AML: a study of 2502 patients. *Blood* **107,** 3847–3853 (2006).

16. Neumann, J., Zeindl-Eberhart, E., Kirchner, T. & Jung, A. Frequency and type of KRAS mutations in routine diagnostic analysis of metastatic colorectal cancer. *Pathol. Res. Pract.* **205,** 858–862 (2009).

17. Keohavong, P. *et al.* Detection of K-ras mutations in lung carcinomas: relationship to prognosis. *Clinical Cancer Research* **2,** 411–418 (1996).

18. Osumi, H. *et al.* Cetuximab treatment for metastatic colorectal cancer with KRAS p.G13D mutations improves progression-free survival. *mol clin onc* 1–5 (2015). doi:10.3892/mco.2015.602

19. A. K. Ghosh, I. Samanta, A. Mondal, W. R. Liu, *ChemMedChem* **2019**, *14*, 889.

20. Singh, J.; Petter, R. C.; Baillie, T. A.; Whitty, A. The Resurgence of Covalent Drugs. *Nat Rev Drug Discov* **2011**, *10* (4), 307–317.

21. De Cesco, S.; Kurian, J.; Dufresne, C.; Mittermaier, A. K.; Moitessier, N. Covalent Inhibitors Design and Discovery. *Eur J Med Chem* **2017**, *138*, 96–114.

22. Cohen, M. S.; Zhang, C.; Shokat, K. M.; Taunton, J. Structural Bioinformatics-Based Design of Selective, Irreversible Kinase Inhibitors. *Science* **2005**, *308* (5726), 1318–1321.

23. John, J.; Sohmen, R.; Feuerstein, J.; Linke, R.; Wittinghofer, A.; Goody, R. S. Kinetics of Interaction of Nucleotides with Nucleotide-Free H-Ras P21. *Biochemistry* **1990**, *29* (25), 6058–6065.

24. Kathman, S. G.; Xu, Z.; Statsyuk, A. V. A Fragment-Based Method to Discover Irreversible Covalent Inhibitors of Cysteine Proteases. *J. Med. Chem.* **2014**, *57* (11), 4969–4974.

25. London, N.; Miller, R. M.; Krishnan, S.; Uchida, K.; Irwin, J. J.; Eidam, O.; Gibold, L.; Cimermančič, P.; Bonnet, R.; Shoichet, B. K.; Taunton, J. Covalent Docking of Large Libraries for the Discovery of Chemical Probes. *Nature Chemical Biology* **2014**, *10* (12), 1066–1072.

26. Efrat Resnick et al. Rapid Covalent-Probe Discovery by Electrophile-Fragment Screening**.** *Journal of the American Chemical Society* **2019** *141* (22), 8951-8968**.** DOI: 10.1021/jacs.9b02822

27. Fischer, M.; Coleman, R. G.; Fraser, J. S.; Shoichet, B. K. Incorporation of Protein Flexibility and Conformational Energy Penalties in Docking Screens to Improve Ligand Discovery. *Nat Chem* **2014**, *6* (7), 575–583.

28. Fischer, M.; Coleman, R. G.; Fraser, J. S.; Shoichet, B. K. Incorporation of Protein Flexibility and Conformational Energy Penalties in Docking Screens to Improve Ligand Discovery. *Nat Chem* **2014**, *6* (7), 575–583.

29. Teodoro, M. L.; Kavraki, L. E. Conformational Flexibility Models for the Receptor in Structure Based Drug Design. *Curr. Pharm. Des.* **2003**, *9* (20), 1635–1648.

30. Hritz, J.; de Ruiter, A.; Oostenbrink, C. Impact of Plasticity and Flexibility on Docking Results for Cytochrome P450 2D6: a Combined Approach of Molecular Dynamics and Ligand Docking. *J. Med. Chem.* **2008**, *51* (23), 7469–7477.

31. Rueda, M.; Totrov, M.; Abagyan, R. ALiBERO: Evolving a Team of Complementary Pocket Conformations Rather Than a Single Leader. *J Chem Inf Model* **2012**, *52* (10), 2705–2714.

32. Richter, L.; de Graaf, C.; Sieghart, W.; Varagic, Z.; Mörzinger, M.; de Esch, I. J. P.; Ecker, G. F.; Ernst, M. Diazepam-Bound GABAA Receptor Models Identify New Benzodiazepine Binding-Site Ligands. *Nature Chemical Biology* **2012**, *8* (5), 455–464.

33. Corbeil, C. R.; Moitessier, N. Docking Ligands Into Flexible and Solvated Macromolecules. 3. Impact of Input Ligand Conformation, Protein Flexibility, and Water Molecules on the Accuracy of Docking Programs. *J Chem Inf Model* **2009**, *49* (4), 997–1009.

34. Cosconati, S.; Marinelli, L.; Di Leva, F. S.; La Pietra, V.; De Simone, A.; Mancini, F.; Andrisano, V.; Novellino, E.; Goodsell, D. S.; Olson, A. J. Protein Flexibility in Virtual Screening: the BACE-1 Case Study. *J Chem Inf Model* **2012**, *52* (10), 2697–2704.

35. Li, N.; Sun, Z.; Jiang, F. SOFTDOCK Application to Protein-Protein Interaction Benchmark and CAPRI. *Proteins* **2007**, *69* (4), 801–808.

36. Jiang, F.; Lin, W.; Rao, Z. SOFTDOCK: Understanding of Molecular Recognition Through a

Systematic Docking Study. *Protein Eng.* **2002**, *15* (4), 257–263.

37. Bottegoni, G.; Kufareva, I.; Totrov, M.; Abagyan, R. Four-Dimensional Docking: a Fast and Accurate Account of Discrete Receptor Flexibility in Ligand Docking. *J. Med. Chem.* **2009**, *52* (2), 397–406.

38. Armen, R. S.; Chen, J.; Brooks, C. L. An Evaluation of Explicit Receptor Flexibility in Molecular Docking Using Molecular Dynamics and Torsion Angle Molecular Dynamics. *J Chem Theory Comput* **2009**, *5* (10), 2909–2923.

39. Dietzen, M.; Zotenko, E.; Hildebrandt, A.; Lengauer, T. On the Applicability of Elastic Network Normal Modes in Small-Molecule Docking. *J Chem Inf Model* **2012**, *52* (3), 844–856.

40. Vinh, N. B.; Simpson, J. S.; Scammells, P. J.; Chalmers, D. K. Virtual Screening Using a Conformationally Flexible Target Protein: Models for Ligand Binding to P38α MAPK. *J. Comput. Aided Mol. Des.* **2012**, *26* (4), 409–423.

41. Barril, X.; Morley, S. D. Unveiling the Full Potential of Flexible Receptor Docking Using Multiple Crystallographic Structures. *J. Med. Chem.* **2005**, *48* (13), 4432–4443.

42. Nicholls, A. The Character of Molecular Modeling. *J. Comput. Aided Mol. Des.* **2012**, *26* (1), 103–105.

43. Smith, J. M.; Rowley, C. N. Automated Computational Screening of the Thiol Reactivity of Substituted Alkenes. *J. Comput. Aided Mol. Des.* **2015**, *29* (8), 725–735.

44. Flanagan, M. E.; Abramite, J. A.; Anderson, D. P.; Aulabaugh, A.; Dahal, U. P.; Gilbert, A. M.; Li, C.; Montgomery, J.; Oppenheimer, S. R.; Ryder, T.; Schuff, B. P.; Uccello, D. P.; Walker, G. S.; Wu, Y.; Brown, M. F.; Chen, J. M.; Hayward, M. M.; Noe, M. C.; Obach, R. S.;

Philippe, L.; Shanmugasundaram, V.; Shapiro, M. J.; Starr, J.; Stroh, J.; Che, Y. Chemical and Computational Methods for the Characterization of Covalent Reactive Groups for the Prospective Design of Irreversible Inhibitors. *J. Med. Chem.* **2014**, *57* (23), 10072–10079.

45. Carr, R. A. E.; Congreve, M.; Murray, C. W.; Rees, D. C. Fragment-Based Lead Discovery: Leads by Design. *Drug Discov. Today* **2005**, *10* (14), 987–992.

46. Vadas, O.; Burke, J. E. Probing the Dynamic Regulation of Peripheral Membrane Proteins Using Hydrogen Deuterium Exchange-MS (HDX-MS). *Biochem. Soc. Trans.* **2015**, *43* (5), 773–786.

47 Harrison, R. A.; Engen, J. R. Conformational Insight Into Multi-Protein Signaling Assemblies by Hydrogen-Deuterium Exchange Mass Spectrometry. *Curr. Opin. Struct. Biol.* **2016**, *41*, 187–193.

48. Harrison, R. A.; Lu, J.; Carrasco, M.; Hunter, J.; Manandhar, A.; Gondi, S.; Westover, K. D.; Engen, J. R. Structural Dynamics in Ras and Related Proteins Upon Nucleotide Switching. *J. Mol. Biol.* **2016**, *428* (23), 4723–4735.

49. McGregor, L. M.; Jenkins, M. L.; Kerwin, C.; Burke, J. E.; Shokat, K. M. Expanding the Scope of Electrophiles Capable of Targeting K-Ras Oncogenes. *Biochemistry* **2017**.

50. Bateman, L. A.; Nguyen, T. B.; Roberts, A. M.; Miyamoto, D. K.; Ku, W.-M.; Huffman, T. R.; Petri, Y.; Heslin, M. J.; Contreras, C. M.; Skibola, C. F.; Olzmann, J. A.; Nomura, D. K. Chemoproteomics-Enabled Covalent Ligand Screen Reveals a Cysteine Hotspot in Reticulon 4 That Impairs ER Morphology and Cancer Pathogenicity. *Chem. Commun. (Camb.)* **2017**.

51. Roberts, A. M.; Miyamoto, D. K.; Huffman, T. R.; Bateman, L. A.; Ives, A. N.; Akopian, D.;

Heslin, M. J.; Contreras, C. M.; Rape, M.; Skibola, C. F.; Nomura, D. K. Chemoproteomic Screening of Covalent Ligands Reveals UBA5 as a Novel Pancreatic Cancer Target. *ACS Chem. Biol.* **2017**, *12* (4), 899–904.

52. Lennerz, J. K. & Stenzinger, A. Allelic ratio of KRAS mutations in pancreatic cancer. *Oncologist* 20, e8–9 (2015).

53. Riely, G. J. *et al.* Frequency and distinctive spectrum of KRAS mutations in never smokers with lung adenocarcinoma. *Clinical Cancer Research* 14, 5731–5734 (2008).

54. Westcott, P. M. K. *et al.* The mutational landscapes of genetic and chemical models of Kras-driven lung cancer. *Nature* 517, 489–492 (2015).

55. Atreya, C. E., Ostrem, J. M. & Kelley, R. K. KRAS and Colorectal Cancer: Shades of Gray. *Personalized Medicine in Oncology* **6,** 1–10 (2012).

56. Siegel, R. L., Miller, K. D. & Jemal, A. Cancer statistics, 2016. *CA Cancer J Clin* **66,** 7–30 (2016).

57. Gideon, P. *et al.* Mutational and kinetic analyses of the GTPase-activating protein (GAP)-p21 interaction: the C-terminal domain of GAP is not sufficient for full activity. *Molecular and Cellular Biology* **12,** 2050–2056 (1992).

58. Seeburg, P. H., Colby, W. W., Capon, D. J., Goeddel, D. V. & Levinson, A. D. Biological properties of human c-Ha-ras1 genes mutated at codon 12. *Nature* **312,** 71–75 (1984).

59. Bos, J. L. *et al.* Amino-acid substitutions at codon 13 of the N-ras oncogene in human acute myeloid leukaemia. *Nature* **315,** 726–730 (1985).

60. Osumi, H. *et al.* Cetuximab treatment for metastatic colorectal cancer with KRAS p.G13D mutations improves progression-free survival. *mol clin onc* 1–5 (2015). doi:10.3892/mco.2015.602

Publishing Agreement

It is the policy of the University to encourage the distribution of all theses, dissertations, and manuscripts. Copies of all UCSF theses, dissertations, and manuscripts will be routed to the library via the Graduate Division. The library will make all theses, dissertations, and manuscripts accessible to the public and will preserve these to the best of their abilities, in perpetuity.

Please sign the following statement:

I hereby grant permission to the Graduate Division of the University of California, San Francisco to release copies of my thesis, dissertation, or manuscript to the Campus Library to provide access and preservation, in whole or in part, in perpetuity.

DocuSigned by:
797F5C2C267240B...

Author Signature

12/18/2019

Date